OPTICAL AND ELECTRONIC CORRELATION EFFECTS IN SEMICONDUCTOR NANOSTRUCTURES

WITH EMPHASIS ON SILICON NANOSTRUCTURE

A Dissertation Submitted to the Department of Physics Addis Ababa University

In Partial Fulfillment of the Requirement of the Degree of Doctor of Philosophy in Physics

By:Mekonnen Abebe Gebru

April 2011

Addis Ababa, Ethiopia

OPTICAL AND ELECTRONIC CORRELATION EFFECTS IN SEMICONDUCTOR NANOSTRUCTURES

WITH EMPHASIS ON SILICON NANOSTRUCTURE

A Dissertation Submitted to the Department of

Physics Addis Ababa University

Approved by the Examination Committee

Dr. Gizaw Mengistu, Chairman, _____

Prof. P. Singh, Advisor, _____

Prof. K. N. Pathak, External Examiner, _____

Prof. V. Mal'nev , Internal Examiner, _____

Acknowledgement

The beginning to my Ph. D. studies was at the same period where I have been through the most difficult part of my life; my wife Zenash has passed during the first semester of my Ph. D studies. Many people have cooperated, encouraged and helped me in all respects so that this works to be possible. I am very grateful to all of you.

This thesis work was not performed in isolation. Rather, it was the culmination of many fruitful and fortunate opportunities, discussions, interactions, and collaborations with the professors in the department of physics in Addis Ababa University (AAU), all my colleagues in the Defence Engineering College (DEC) and elsewhere. First and foremost, I would like to thank my supervisor professor P.Singh who has stood by my side in the very challenging moment of my work when it become difficult to find some one that could help me in dealing over the research problem. His patience and understanding coupled with his research and teaching experience has contributed immensely to the successful completion of my studies.

I would like to express my deep gratitude to Colonel Halefom Ejigu commandant of the DEC for his support and encouragement during my PhD research work and for maintaining an academic environment profoundly motivating for continuous research in the college. I thank Tewoldebrhan Kifle, Dean of Research and Graduate Studies in the DEC who shared me much of his time for frequent discussions on advanced manufacturing techniques. Yesegat Asaye, Hailu G/ tsadik, Fessha Haile, Dereje Shebeshi , Anteneh Fisseha, and Tiret Endale are also thanked for their willingness and initiatives in searching reference materials, reading the manuscript and producing print outs at all stages of my work.

Also, a great debt of gratitude is owed to Neafe and all staffs in the department of Information Communication Technology (ICT): You have helped me with your out smarting technical skills and in creating an enjoyable working environment. I would like also to acknowledge Dr Stopa Michael of the Nano

research director in Harvard for his advice to continue working on this problem which he mentioned it as the current and challenging research issue.

A special kind of thanks goes to my kids Bereket and Blen Mekonnen for their patience and the many efforts they made to make me use all my time on the work.

Table of Contents

List of Figures and Tables

Figures

Tables

Abstract

In this thesis we theoretically investigated static and dynamic correlation effects in semiconductor nanostructures. Structural inhomogneity and confinement quantization effects make this class of materials exhibit exotic properties under different experimental conditions. Time dependent coupling of the local states under time dependent perturbations and the fluctuation of the proximity couplings in the length scale of tunneling give rise to dynamical correlations that put their signature in the optical and transport properties. Based on the Orbital Free Local Density Approximation (OF-LDA), the exchange and correlation contribution to the orbital energy and the size dependent nature of the threshold for optical absorption are studied. The effects of dynamical correlations between the states in a single nanostructure and the effects of dynamical correlations between the states in proximity coupled configurations are investigated with the Non Equilibrium Green Function Formalism (NEGF) as the theoretical frame work.

The theoretical formulation of the non equilibrium dynamical analysis is used to describe the coherent regime optical and transport phenomena in semiconductor nanostructures. The results demonstrate that the presence of strong coupling between electronic states in semiconductor nanostructures leads to the formation of d states. First we have shown the emergence of collapse and revival phenomenon during the coherent regime absorption in a single dot. We presented qualitative and quantitative description of the Rabi oscillation. The dependence on the mean photon number and on the strength of the couplings between electronic states is demonstrated. We found that similar phenomenon in a wide range of many body system could be satisfactorily described assuming entanglement of the lower levels. Secondly, we theoretically investigated correlation effects in tunnel coupled nanostructures. The quantum blockade phenomenon in wide experimental samples is

explored. The appearance of double dot structures as a time shared entangler is predicted. It is also found that the presence of a transparent boundary between quantum dots lead to the formation of local entangled states that are too difficult for experimental demonstration. Lastly the possible technological value of a double dot –in series configuration is presented. Its operation as electron-spin polarization is discussed and its potential for application as IR detector is proposed.

1

Introduction

Electronic correlation interactions and the interplay of correlations and coherence have become central research issues in all areas where the molecular level controlling of properties becomes significant. These include Single Electron Transistors (SETs) based devices such as single electron logic, single electron memory, high precision electrometer, and the development of qubits in quantum computing and communications [1-4]. In the last few years great achievements have been made in the synthesization, characterization and as well as in structural patterning of nano solids for device fabrication [5-8]. However, consistent insight into the mechanism behind the nano solid tunability remains yet at infancy [9, 10].

In this work we investigated theoretically both static and dynamical correlation effects in nano silicon and in silicon based nano device cells. The static correlation together with the kinetic and electrostatic contributions to the total electronic energies at the ground state condition of the sample is approximated in the framework of the Local Density Approximation (LDA) in the Density Functional Theory (DFT). This is supplemented by the Poisson's equation and the Ewald's potential summation rule for determining the charge density and electrostatic potential distribution in a self consistent calculation. Instead of solving for the Kohn-Sham orbitals we made the computation on the basis of the Orbital-Free DFT (OF-DFT) which recently found wide acceptance for its level of accuracy, efficiency and cost [11].

In the remaining parts of the work, emphasis is laid on the dynamical correlation effects which are the basic elements of this work. The effects of the dynamic correlations are accessible to experimental observation for observation time within the time scale of the coherent regime. This lies in

practice within the initial temporal regime of the phenomena under short pulse field perturbations. The interplay of dynamic correlation and coherence which is vital for quantum electro-optic applications is a short lived phenomena the application and monitoring of which require fast techniques. We studied dynamical correlation effects in semiconductor nanostructures and assemblies of these based on the ubiquitous Non Equilibrium Green Function (NEGF) formalism. Introduction to the mathematical frame work of this formalism is presented in chapter 3. Our investigation of dynamical correlation is guided by classifying the correlations on the basis of the length scale of the couplings the fluctuation of which are responsible for the observed phenomena. The consequences of quantum indistinguishability, quantum interference and entanglement are reviewed in chapter 5. The mathematical frame work for our analysis of the non equilibrium dynamics and the conceptual frame work on quantum indistinguishability and entanglement reviewed at this early step constitute the ground work for our dynamical studies of the dynamical correlation effects in semiconductor nanostructure and the modeling of semiconductor based nano devices in the remaining parts of this thesis.

The emergence of correlated inter- and intra-band electronic states under the action of short light pulse in a single nano solid is studied and this is presented in chapter 6. In this, semiconductor nanostructures of dimension in the quantum confinement regime are considered. The equal time limit correlation functions of the optically coupled states are computed by starting from the Dyson's equation. The coherent regime temporal evolution of the occupation probabilities of the coupled states is then described using the formulation.

Chapters 7-9 are devoted to the correlation effects in proximity coupled nanostructures. In these chapters correlation effects associated to the fluctuation in electronic and spin polarization exchange couplings are explored. Different coupled structures: Semiconductor nanostructure with metallic contacts and semiconductor double dot configurations with the

length scale of their spacing in the tunneling regime are considered. Through our dynamical analysis of the perturbed system, equations are developed linking the correlation effects with the charge-spin polarization current, which is the observable. In chapter 7, the phenomena in a voltage triggered coupled structure are studied. Our theoretical investigation of optically triggered correlation effects in proximity coupled structures with transparent boundaries are presented in chapter 8. Chapter 9 demonstrates the efficiency the formulation through application to model an electron-spin entangler device. Lastly, the summary of the work is presented.

2

Problem Review

Nanostructures are low dimensional systems, with size in the order of the De Broglie wavelength of electrons, and exhibit distinct optical and transport properties than their bulk counterparts. Nanometer size Si particles (quantum dots), quantum wires, nanoscale Si-MOSFETS are examples of semiconductor based quantum structures. Besides being ideal for the realization of ultimate compactness in device technology [1-5], they exhibit novel electro-optic properties which make them promising candidates for various applications. Contrary to the bulk crystalline silicon which doesn't show luminescence, the nanoscale counterparts for example exhibit electro- as well as photo- luminescence at wavelengths ranging from the ultraviolet to the infrared [12-14] depending upon the size of nanostructures and show a blue-shifted photoluminescence [14,15]. Nanoscale condensed matter systems in general show various optical and transport properties that could never be explained by the theories formulated for bulk materials: -Polarization dependent photoluminescence [16,17]; Quantum and polarization beats observed in optical experiments [18,20]; Quantum Confined Stark Effect, QCSE,[21]; Geometrical confinement and in-built field induced quantization of conductance [22,23] are among the exotic phenomena.

The exotic optical and transport properties of nano-sized semiconductors coupled with their dimension makes them highly important for applications to fast switching electro optical devices, optical logic gates, and optical bistable etalons, in photochemical catalysts and in the realization of a single-photon-on demand device. They have also great demand for quantum cryptography, secured data transfer technology, in the making of arrays of active nano wire devices and field emission arrays

or photonic band gap structures [24, 25]. From the wealth of information that still continued being added to the catalogue of optical and transport phenomena in nanostructures there is now emerging a consensus that surface effects, lack of long range ordering, quantum confinement, the high surface to volume ratio and scaling are among the factors contributing to the exotic properties in these classes of materials.

The presence of unsaturated and broken bonds at the surface is quite the inevitable at the layer where the solid structure is terminating. The presence of dangling bonds is normally controlled by passivating the specimen in an appropriate environment. The passivation process makes the surface atoms to form bonding with atoms of different chemical species and there by reduces the concentration of dangling orbitals. Hydrogenated Si nano-clusters, SiO2 coated Si nano crystals are examples of a passivated nano-structure in the silicon based technology. The effectiveness of the passivation process depends on the temperature and as well on the nature and concentration of the passivating material. In the process where the passivation is administered with sufficient concentration of the passivating atomic species at the temperature required for the particular process, very high percent of the unsatisfied bonds will get removed. This could not however totally resolve the variation of the atomic environment with distance from the surface. The inter-atomic bonding at positions close to the outer surface and in the inner most regions are not the same since the atomic environment at the two positions is different. The structural fluctuation decreases with distance from the outer surface and practically ceases at atomic sites where the bulk property is recovered. The later is so when the dimension of the particular system is sufficient to support the approach to the long range ordering. It is believed that the fluctuation extends to the order of about 6-7 atomic layers.

The structural relaxation is, of course, the common feature for both nanostructures and their bulk counterparts. It is not the occurrence of the structural fluctuation but rather the degree to which the fluctuation

influences the properties that distinguishes nanostructures from their bulk counter parts. In nanostructures where the surface to volume ratio is relatively higher the effect of the structural fluctuation will become prominent. Nanostructures are, in general, where long range ordering is lacking. This structural inhomogneity of nanostructures becomes crucially important for two reasons; removal of the spatial degeneracy of electronic energies and secondly its significance in creating the atomic environment appropriate for build up of dynamical correlations when the atomic states are coupled under time dependent perturbations.

The motion of an electron in a solid is controlled by all the other electrons in the material system. The time evolution of the dynamical states of the electrons has characteristic interdependence. It is well known that such electronic correlation effects become more significant near impurity sites, defect and in general in regions where symmetry is broken. In nanostructures where there is a structural variation and also where the fraction of the total electron within the structurally inhomogeneous region is large or comparable with the concentration in the inner most region where the bulk properties are to be restored, electronic correlation will be in the order where it becomes significant in influencing the material properties. Because of this and of course since the dimension of nano materials is in the order where finding small scale (length, time energy scales) is a challenge, suppressing the correlation effects would no longer be a valid approximation. Both static and dynamic correlation effects play vital role in determining the properties that make nanostructures the possible candidates for applications in wider areas; Quantum computation and communications, manufacturing of multifunctional artificial atoms for various photonic and optoelectronic applications.

Correlation is a very challenging issue both from theoretical and experimental perspectives. This is primarily because it is a quantum many-body problem for which obtaining exact solution to the Schrödinger wave equation is unlikely. The second point and which is specifically relevant for

correlation is that it is an interaction for which there is so far no clear understanding in its interrelationship with other dynamical quantities. Sometimes correlations are classified under two major categories: Dynamical correlations and non-dynamical or static correlations [26,27]. Static correlation refers to the electronic correlations, exchange and coulomb correlations that contribute to the electronic energy.

Dynamical correlations follow when different electronic states of a material or the electronic states in different materials are coupled with an impressed time dependent perturbation. In nanostructures where the energy of electronic states at a site differs only slightly from the electronic energies at the neighboring regions, a time dependent perturbation may lead to the formation of correlated states the evolution of which is governed by the coupling between the two states. Intra band and inter band state correlations in a single nanostructure or between the interfacial states in two closely spaced materials belong to this class. The states couple strongly under exchange of photons [28-30] or electronic and spin polarization waves [31-34]

There have been numerous theoretical approaches that have been introduced for studying the electronic energies and the contributions of the various interactions to the total energies. First principles calculations of band structures of crystals are usually based on one-particle theories where the electrons are assumed to move in some effective potential that reflect the presence of long range periodicity which is difficult to accept for low dimensional structures. Many other computational approaches have been known generating quantitative explanations with variable degree of accuracy. The Hartree and the Hartree-Fock theories are among the pioneering theories widely used in the ground state characterization of solids including semiconductor materials [35,36]. The Hartree-method does not, however, account for any amount of electron correlation. The Hartree-Fock theory on the other hand includes the correlation between electrons of similar spin. However, the molecular orbitals of the Hartree-Fock method

are optimized by evaluating the energy of an electron in each molecular orbital moving in the mean field of all other electrons, rather than including the instantaneous repulsion between electrons.

The other approach which has been established as one of the most widely used first-principles method is the Density Functional Theory (DFT). The introduction of the method is due to the theories of Kohn and Sham [37,38] and was developed by many researchers. There are now varieties of computational techniques for making calculations in the frame work of the DFT theory; The Local Density Approximation (LDA) [38], the gradient Wave Approximation (GWA), the Pseudo Potential Approximations (PPA) are among the numerical options popular in the application of the DFT theory [38-41].

As it is the case in any material system in general, the effects of coupling with the external perturbation are as well determined by the coupling parameters and the electronic states and the distribution of the electrons in the various dynamical states in the material. One obvious consequence of the coupling with external perturbations is a shift in the electronic energies which incorporates the shifts in the contributions of the various interactions to the total electronic energies. When a nano structure is subjected to a system that maintains a constant potential difference across the end points, it results in a shift in the electronic levels at each site. For a semiconductor nanostructure at the ground state, the application of a small potential difference could alter the valence and the conduction electronic levels differently and the level displacement of the levels in the valence states will be dependent of position. This is typical of a situation leading to the quantum stark effect. One other obvious outcome of a fixed external field is that it's tuning of the system by the modification the energies of the electronic states that determine the properties of the material.

In the special case when the perturbation is time dependent, the effect will be beyond what could be described in the sense it is done for the

coupling under a constant field. One direct consequence of a time dependent perturbation is the time dependent shift it possibly results on the energy contributions to the total electronic energies of the atomic orbital. This in principle includes the time dependent variations in the electronic correlation contributions to the total energy. A time dependent perturbation however brings about not only a time dependent level shift but as well other correlation effects which one could not find traces of their existence in the remote past and as well in the remote future. This second variety, dynamical correlation, is at the heart of every measurement process and device applications of materials. This is because it is the situation by which the information distributed among the various quantum states of the electrons in one region is mapped over the electronic states in the other; the underlying mechanism in quantum computations and communications.

The dynamical correlations in nanostructures are understood to be responsible for the longer lived coherence in nanostructures. The dynamical correlation effects have no patience to wait the approach toward equilibrium [42-45]. The window appropriate for direct observation of these correlation effects is the coherent regime response. This is a temporal regime where the application of ultra fast techniques for experimental observation of the phenomena and a non equilibrium dynamical theory for interpreting the observation will become quite indispensable. The issue is therefore on a non equilibrium quantum many-body problem which will be more challenging both from experimental and theoretical perspectives. The limitations on experimental investigation of dynamic correlations have begun finding solutions following the technological achievements that contributed to the explosion of diverse ultra-fast experimental techniques [46,49]. Hand in hand to these developments there have been numerous theoretical studies that have furnished theoretical frame works for explaining the dynamical correlation effects in a specific experimental range. Just to indicate some of the methods, we found theoretical approaches formulated on the basis of the

reduced density matrix method ranging from mainly analytical up to direct integration of the Liouville equation [50,51]; The Feynman path integral methods [52]; the density matrix method [53,54]; the method of Time Dependent DFT (TD-DFT) [55,56]; the method of Green function [57,60]. The Non Equilibrium Green Function (NEGF) formalism are among the approaches used in the last method.

The ubiquitous Non Equilibrium Green Function is theoretical frame work of our choice for studying the dynamic correlation effects in nanostructures. With the NEGF as theoretical formalism, we made theoretical investigations on the evolution of nearest neighbor scale correlations in a single nanostructure and proximity correlations in between coupled units. The rich physics and broad application potential of a multi component nano system arises from the "proximity" between the materials with characteristic distribution and occupancy of electronic states. The proximity effect results in the generation of electronic correlations in the neighboring materials. These correlations typically decay on a nm-scale and therefore can be studied and exploited in multi component hybrid nano systems. Finding quantitative descriptions for the signatures of electronic correlation effects over wide experimental range and methods for monitoring the correlations are the prime motives for our concern in multi-component nanostructures. Hence is the potential contribution of the work to the development of nano-electronics, quantum computing and quantum communication processing.

3

Mathematical Formulations

Device application of low dimensional structures in general involves the interaction of the material systems with one another and with an external perturbing parameter or field. Property investigations of the material structure and various optoelectronic applications are where the information distributed in the various quantum states of one are to be transferred and mapped in the other material system, probe, which is coupled to the first. This is realized by bringing the coupled system such that the atomic states in the materials are correlated under the stimulating perturbation. This dynamical correlation requires the presence of states slightly different in energy and a time dependent coupling. The task is in general to prepare states that tend to the formation of correlation and a time dependent coupling.. Thus the preparation of the testing ground for dynamical correlation effects is the problem of preparing the structures with the required ground state properties. Hence the problem becomes typical of that where adequate mathematical formulations for the ground state property investigation and for analyzing the time dependent dynamical interactions will become necessary. In this chapter we therefore present the mathematical frame works employed for the ground state characterization and for the short time scale dynamical analysis in sequence. The` mathematical frame work for the ground state property analysis is the LDA of the DFT theory. The non equilibrium dynamical investigation on the other hand is made on the basis of the Non Equilibrium Green Function (NEGF) formalism. The mathematical frame work of both formalisms is presented in the following two sections of this unit.

3.1 Orbital Free Local Density Approximation (OF-LDA)

The Local Density Approximation (LDA) is basically an extension of the Density Functional Theory (DFT) which has its ground from the theorems due to Hohenberg and Kohn [37]. The later asserts that there exists a functional F of the density, independent of the external potential V such that the electronic density of the ground state of the n-electron problem with the external potential V is a solution of

$$F(\rho) + \int_{R^3} \rho V d^3 r \Big|_{\min imum} \tag{3.1a}$$

$$\int_{R^3} \rho d^3 r = n \tag{3.1b}$$

The extension of the theory for local property approximation is based on the use of the formulation to describe the energy per particle at the ground state condition of an atom at a given atomic site: The local total energy over the unit cell could be written as functional of the local density [38, 39] as

$$E_T(\rho, r) = \frac{1}{2}\int_{cell} d^3 r \rho(r) V_C(\rho, r) + T(\rho) + E^{xc}(\rho, r) \tag{3.2a}$$

The terms $T(\rho)$ and $E^{XC}(\rho)$ in this equation respectively represent the kinetic and the exchange-correlation contributions to the total local energy and $V_C(\rho, r)$ is the Coulomb potential. The integral term, in eq. 3.2a, which is representing the Coulomb contribution to the total energy is evaluated over the unit cell volume. The corresponding local energy at the surface atomic site is

$$E_T(\rho, r_s) = \frac{1}{2}\int_{cell(s)} d^3 r \rho(r) V_C(\rho, r) + T(\rho_s) + E^{xc}(\rho_s, r_s) \tag{3.2b}$$

The variation from the bulk value is associated to the variation in the local density and potential. Consequently, we find the variation of the local energy from the bulk value, $\delta E_T(\rho)$ resulted upon forming the layer at position $r > r_b$ to be approximated by

$$\delta E_T(\rho, r) = \frac{1}{2}\int_{cell} d^3r(\rho(r_b) + \delta\rho(r))[V_C(\rho_b, r_b) + \delta V_C]$$
$$- \frac{1}{2}\int_{cell} d^3r\rho(r_b)V_C(\rho_b, r_b)$$
$$+[T(\rho_b + \delta\rho) - T(\rho_b)] + [E^{xc}(\rho_b + \delta\rho, r) - E^{xc}(\rho_b, r_b)] \qquad (3.3)$$

However, from the definition for the potential at a point due to changes of density ρ, one could easily come to write

$$\int_{cell} d^3r\delta\rho(r)V_C(\rho, r) = \int_{cell} d^3r\rho(r)\delta V_C(\rho, r) \qquad (3.4)$$

Using eq.3.4 and the minimization for the local energy given by eq.3.3 one finds

$$V^{XC}(\rho, r) = \mu + V_C(\rho, r) + \frac{\partial}{\partial\rho}T(\rho) \qquad (3.5)$$

Clearly, the hope for obtaining a meaningful result from the computation is only if all the functionals in eqs.3.2-3.5 are known in terms of density. There are so far two well known basic approaches introduced to tackle the problem; the orbital based and Orbital free models.

In the orbital based approach, such as the Kohn-Sham model, the computation of the kinetic energy functional for a system of N electrons requires to carry the calculation for the *N non*-interacting electron orbitals. The problem therefore becomes 3N dimensional, without involving the spin variables. This makes the computation practically much difficult and prohibitively expensive. On the other hand it is a well recognized fact that electrons are indistinguishable. This naturally leads one intuitively expect

the properties of a material system to be described from a knowledge of the electron density and probability of finding the electron in any given region of space. It is the motive in the OF-DFT to find a systematic approach that could help in obtaining results that we could relied on for quantitative analysis with the kinetic energy approximated by a functional of the density alone, free of orbitals.

Use of orbital free models reduces the dimensionality of the problem from 3N to 3. Because the formulations made via the orbital free approaches have no orbital dependence, the complication and cost associated with orbital manipulation are practically avoided. Shortly, the quantum mechanical calculation for the many body system is drastically simplified in the non orbital based approaches. One very simple model and perhaps historically the first kinetic energy density functional (KEDF) is the Thomas-Fermi (TF) model [37, 38]. Since the TF model is derived from the local implementation of a uniform free electron gas approximation, its effectiveness is limited only for approximating the properties in simple metals. Since the first introduction of this orbital free approach great many efforts have been made in search of a numerically applicable and transferable KEDF models. These efforts have lead to the formulation of kinetic energy functional that enabled in obtaining promising results for a wider class of materials. These formulations are presented with the Von Weisäzker gradient approximation and the linear response behavior enforcing functional are incorporated as the first and second correction terms for the TF KEDF [142,143];

$$T_S(\rho) = T_{TF}(\rho) + T_{VW}(\rho) + T_x(\rho) \qquad (3.6a)$$

$$T_{TF}(\rho) = \int_{R^3} \rho t(\rho) d^3 r_j = \frac{3\hbar^2}{10m} \int_{R^3} \rho (3\pi^2 \rho)^{2/3} d^3 r_j \qquad (3.6b)$$

$$T_{VW}(\rho) = C_{VW} \int_{R^3} \frac{1}{\rho^2} \left| \vec{\nabla} \rho \right|^2 d^3 r_j \qquad (3.6c)$$

The approach in this work is based in extending the DFT to the Local approximation without losing the information on the interactions that become responsible for the exotic properties in nanostructures. We have the belief that the kinetic energy could be represented in the same form as the in the TF-KEDF model but with the possible corrections to the drawbacks of the TF model are structurally built in the formulation. To make this real, we choose an approach that allows in incorporating the information on the local number of particles, the symmetry of the sample, the exponential decay of charge density away from atomic sites, and the modification by factors that alter the atomic environment at each region in to the density itself. This has to be made, of course, along with preserving the realities on the electrostatic contributions to the total energy of the local atoms. Therefore, approximating the contributions of the density and potential variations on the local atomic energies will be one central element of the task. We believe it will be worth if the poisons equation is solved by introducing boundary requirements that accommodate the features mentioned.

The issue we have to step on next as the logical sequence of the computational development is the Poisson's equations:

$$-\nabla^2 V = 4\pi\rho \qquad (3.7)$$

Both the Coulomb potential and the local density are to be approximated from a self consistent calculation. Solving this seemingly simple equation is, however, tricky when it comes to the application for insulating type materials at low temperature. First of all we require a solution that reflects the realistic situation in the sample. We require the charge neutrality condition to be preserved. Also, the solutions determined both for the local density and the potential have to converge to the respective values at the

inner most points. The values at these inner most points are considered to be represented by the bulk values of the respective quantities when the dimension of the material is in the order that could support bulk phenomena. For points at the outer layer the convergence of the solutions is to values that closely agree with experimental results such as the values determined in the surface core level spectroscopy. More over, it will be required both the potential and charge density functions to reflect the exponential decay, with distance from atomic centers, and the periodic properties over regions where long range ordering still prevails. In our calculation, periodicity of charge and potential over atomic layers is assumed. This simplifying assumption is believed reasonable especially for nanostructures of spherical symmetry, spherical dots, and thin films of thickness at the nanoscale. We then solved the Poisson's equation following a technique similar to the Edwald's summation of potential [61] and imposing the requirements mentioned. The result we found is in the form

$$V(r+r_j) = V_b \frac{[1-erf(\frac{r}{r_b}\sqrt{\lambda})]}{[1-erf(\sqrt{\lambda})]} e^{-\chi r_j^2} e^{-ik_{11}r_{11}} \qquad (3,8a)$$

$$\rho(r+r_j) = \frac{\rho_b}{1-\lambda}[\frac{r_b^2 - r^2\lambda}{rr_b}] e^{-\lambda[(\frac{r}{r_b})^2-1]} e^{-\chi r_j^2} e^{-ik_{11}r_{11}} \qquad (3.8b)$$

Where the subscript b in V_b and ρ_b refers that these are the bulk values. This is an important issue we need to come back over few steps later. Here, r_j measures the radial distance from the center of the atom and the role of the Gausian term $\exp(-\chi r_j^2)$ is to limit the distribution of particle density and potential within the atomic sphere. On the other hand, r_{11} is the length measure from the atomic site along (parallel to) the atomic layer. The complex exponential term in eqs.3.8, thus attends the periodicity of the potential and charge distributions over the atomic layer.

The parameters λ and χ are quantities embodying information on the decay or else spatial dispersion of the property. The parameter λ has the nature to be identified with the coefficients of the Slater's hopping or coulomb integral, matrices [62, 63]. Since the coefficients are understood to depend on the bonding parameters in a complicated way, it requires consulting experimental facts in the course of the iteration. The coupled equations are basically oscillatory functions augmented by a Gaussian distribution. The later is instrumental for checking the fast convergence to the bulk values, at the inner most points, and to the surface properties at the outer most sites. The instrumentality of the result in eq.3.8 is of course beyond the usual purpose of formulating the relation between the Coulomb potential and the charge density. It is an equation that sheds light to our hope of incorporating the spatial fluctuation nature of the density and the potentials.

The local density averaged energy is compared with the local energy determined from summing the contribution of the local atomic orbital which itself is to be computed from self consistent calculation with the requirement to converge to the values at the surface and the bulk region. The resulting equation could be used to approximate the exchange and correlation potential in the sample.

3.2 Quantum Kinetic Formulation

The theoretical frame work used in dealing with the short time phenomena in nanostructures in this work is the NEGF formalism. The ground for the choice for this approach is due to the advantages it offers for investigation. The dynamical problem, in this approach, is formulated in the form of equations of motion for the class of time ordered Green functions; the lesser $G^{<}$, the greater $G^{>}$, the retarded G^{r} and the advanced G^{a} Green functions. As will be demonstrated shortly, these are interrelated

functions. More importantly each of these functions is that we could directly link with observables. Moreover, the functions are satisfying the same dynamical equation as the particles' wave function and convenient for systematic application of perturbation approximations. Encouraged by these features, the formalism has been used by a number of workers who studied optical and transport phenomena in low dimensional systems.

3.2 .1 The Contour Ordered Green Function

The one particle contour ordered Green function, which in the present case is the Green function for an orbital electron, for a thermodynamically equilibrium system at low temperature (T→ 0) is defined as

$$G(r,t;r',t') = \frac{-i}{\hbar}\left\{\left\langle \phi(t_o)\right| T_C[\psi_H(t)\psi_H^{\dagger}(t')]\left|\phi(t_o)\right\rangle\right\} \qquad (3.9)$$

Where, ψ_H and $\psi_H^{\dagger}$ are respectively the annihilation and creation fermionic field operators; $|\phi(t_o)\rangle$ is the eigen ket at the ground state of the interacting system of electrons; T_C is the chronological ordering operator. The time ordering parameter T_C is such that

$$T_C[\psi_H(t)\psi_H^{\dagger}(t')] = \theta(t-t')\psi_H(t)\psi_H^{\dagger}(t') - \theta(t'-t)\psi_H^{\dagger}(t')\psi_H(t) \qquad (3.10)$$

For a system at finite temperature, the averaging of an observable involves both quantum averaging and Gibbs averaging. Thus, the average of an observable with corresponding quantum mechanical operator $\hat{A}$ is given by

$$\left\langle \hat{A}(t)\right\rangle = \left\langle n\right|\rho_H \hat{A}_H(t)\left|n\right\rangle \qquad (3.11)$$

Where, ρ_H is the density operator related with the partition function Z as

$$\rho_H = e^{-\beta(H-\mu N)}/Z \qquad (3.12a)$$

With the partition function Z is given by

$$Z = \sum e^{-\beta(H-\mu N)} \tag{3.12b}$$

when the thermodynamic response of the system does not instantly follow the change in the Hamiltonian that resulted from external perturbation, the density matrix could be approximated by the ground state equilibrium value as

$$\rho_H \approx \rho_{H_o} = \frac{e^{-\beta(H_o-\mu_0 N_o)}}{Z(H_o,\mu_o,N_o,T)} \tag{3.12c}$$

The substitution of the expression in eq.3.10 for the time ordered product in eq.3.9 in this case then results

$$G(r,t;r',t') = -\frac{i}{\hbar}\{\theta(t-t')\left\langle\varphi(t_o)\right|\rho_{H_o}\psi_H(t)\psi_H^{\dagger}(t')\left|\varphi(t_o)\right\rangle$$

$$-\theta(t'-t)\left\langle\phi(t_o)\right|\rho_{H_o}\psi_H^{\dagger}(t')\psi_H(t)\left|\phi(t_o)\right\rangle\} \tag{3.13}$$

It is now time to define other forms of Green functions that we could use in the future steps depending on whether the interest is prior or after some event. The greater and lesser Green functions are defined as

$$G^{>}(r,t;r',t') = -\frac{i}{\hbar}[\left\langle\phi(t_o)\right|\rho_H\psi_H(t)\psi_H^{\dagger}(t')\left|\phi(t_o)\right\rangle] \tag{3.14a}$$

$$G^{<}(r,t;r',t') = -\frac{i}{\hbar}[\left\langle\varphi(t_o)\right|\rho_H\psi_H^{\dagger}(t')\psi_H(t)\left|\varphi(t_o)\right\rangle] \tag{3.14b}$$

Accordingly,

$$G(r,t;r't') = \theta(t-t')G^{>}(r,t;r't') - \theta(t'-t)G^{<}(r,t;r't') \tag{3.14c}$$

Two other types of Green functions with a structure designed to carry information on the propagation characteristic are the retarded, $G^r(r,t;r't')$, and advanced, $G^a(r,t;r't')$, Green functions which respectively defined as

$$G^r(r,t;r't') = \theta(t-t')[G^>(r,t;r't') - G^<(r,t;r't')] \quad (3.14d)$$

$$G^a(r,t;r't') = \theta(t'-t)[G^<(r,t;r't') - G^>(r,t;r't')] \quad (3.14e)$$

The Green functions expressed so far in the preceding steps are according to the representation in the Heisenberg picture where state kets are frozen and operators vary in time with their time evolution determined by the total Hamiltonian, H. That is,

$$\left|\phi\ (t)\right\rangle_H = \left|\phi\ (t_o)\right\rangle_H = \left|\phi\ (t_o)\right\rangle_S \quad (3.15a)$$

$$\psi_S(t) = e^{i\frac{H(t-t_o)}{\hbar}}\psi_S(t_o)e^{-i\frac{H(t-t_o)}{\hbar}} = U_H(t,t_o)\psi_S(t_o)U_H(t,t_o) \quad (3.15b)$$

$$\psi_H^\dagger(t') = e^{\frac{i}{\hbar}H(t'-t_o)}\psi_S^\dagger(t_o)e^{-\frac{i}{\hbar}H(t'-t_o)} = U_H^\dagger(t',t_o)\psi_S^\dagger(t_o)U_H(t',t_o) \quad (3.15c)$$

Where, the U_H's are the unitary operators carrying the information how a state in the remote past ψ evolve dynamically under the interaction represented by the total Hamiltonian:

$$U_H(t,t_o) = e^{-\frac{i}{\hbar}H(t-t_o)} \quad (3.16a)$$

$$U_H^\dagger(t,t_o) = e^{\frac{i}{\hbar}H(t-t_o)} \quad (3.16b)$$

For a system under coupling with the external; which in general may include interactions with photons, phonons, impressed static fields, the total Hamiltonian incorporates the dynamical contributions of the particles of the system at the ground state condition and the contributions that

follow the coupling with the external perturbation. The later in general include the contribution associated with direct couplings of the system with the perturbing field, interaction induced effects and couplings with the local environment. The contribution to the total Hamiltonian due to interaction induced effects such as the inter- and intra-band polarization fluctuations, the exchange and correlation contributions associated with the fluctuation in the local density and potential distributions, the interaction with the local environment via phonon exchanging couplings, and the like will make the interaction Hamiltonian too difficult to handle. On the other hand in nanostructures under time dependent perturbations, these effects would be in the order that could underlie the properties of the system. It may be useful in many cases to put the total Hamiltonian as the sum of contributions from two parts; the easy to solve and the difficult.

$$H(t) = h + \int_{t_o}^{t} V_I(\tau) d\tau \tag{3.17}$$

This is the interaction picture representation of the Hamiltonian. In this representation the complicated part of the Hamiltonian is defined to be time dependent whether or not it explicitly depends on time. This is made using unitary transformations such that the field operator $\psi_I(t, t_o)$ and the interaction term $V_I(t)$ in the interaction picture, are linked with the corresponding expressions $\psi_s(t_o)$ and $V_S(t)$ in the Schrödinger picture by the unitary operator $U_h(t, t_o)$

$$\psi_I(t, t_o) = U_h(t, t_o)\psi_s(t_o) \tag{3.18}$$

$$V_I(t) = U_h^{\dagger} V_S(t) U_h \tag{3.19}$$

Where the unitary operator carrying information on the evolution of the state from the remote past under the simple or time independent Hamiltonian satisfies the Schrödinger equation

$$i\hbar \frac{\partial}{\partial t} U_h = \varepsilon U_h \qquad (3.20a)$$

That is, it is evolving according to

$$U_h(t, t_o) = e^{-\frac{i}{\hbar}\varepsilon(t-t_o)} \qquad (3.20b)$$

The dynamical evolution of the basis ket in this picture, $\left|\phi(t)\right\rangle_I$, is governed by the interaction part of the Hamiltonian and is related with the corresponding value at t_o.

$$\left|\phi(t)\right\rangle_I = U_I(t, t_o)\left|\phi(t_o)\right\rangle_I \qquad (3.21)$$

Where, similarly to U_h in eq.3.20, the unitary operator U_I also satisfies the Schrödinger equation:

$$i\hbar \frac{\partial}{\partial t} U_I = V_I U_I \qquad (3.22a)$$

That is,

$$U_I(t, t_o) = e^{-\frac{i}{\hbar}\int_{t_o}^{t} V(\tau) d\tau} \qquad (3.22b)$$

Using the expressions in eqs3.18-3.22 and the definition in eqs.3.14, it will be now easy to determine the interaction picture representation of the Green function. We next consider the operator product $\psi_H(t)\psi_H^{\dagger}(t')$,

$$\psi_H(t)\psi_H^{\dagger}(t') = e^{\frac{i}{\hbar}\int_{t_o}^{t} V_I(\tau) d\tau} \psi_I(t) e^{-\frac{i}{\hbar}\int_{t_o}^{t} V_I(\tau) d\tau} e^{\frac{i}{\hbar}\int_{t_o}^{t'} V_I(\tau) d\tau} \psi_I^{\dagger}(t') e^{-\frac{i}{\hbar}\int_{t_o}^{t'} V_I(\tau) d\tau} \qquad (3.23)$$

Accordingly, the lesser and greater Green functions in eqs.3.14 are found to be rewritten in the representation of the interaction picture as

$$G^{<}(r,t;r',t') = \frac{i}{\hbar}\{_I \left\langle \varphi(t_o,t') \middle| \psi_I^{\dagger}(t') e^{\frac{-i}{\hbar}\int_{t}^{t'} V_I(\tau)d\tau} \psi_I(t) \middle| \varphi(t_o,t) \right\rangle_I \} \qquad (3.24a)$$

$$G^{>}(r,t;r',t') = -\frac{i}{\hbar}\{_I \left\langle \varphi(t_o,t) \middle| \psi_I(t) e^{\frac{-i}{\hbar}\int_{t'}^{t} V_I(\tau)d\tau} \psi_I^{\dagger}(t') \middle| \varphi(t_o,t') \right\rangle_I \} \qquad (3.24b)$$

From inspection of these two equations one could easily notice also that,

$$G(r,t;r't') = \theta(t-t')G^{>}(r,t;r't') - \theta(t'-t)G^{<}(r,t;r't') \qquad (3.24c)$$

From comparing the relations in eq.3.14 one could easily notice that eq.3.24c can also be given in terms of the advanced and retarded Green functions as

$$G(r,t;r't') = G^{r}(r,t;r't') - G^{a}(r,t;r't') \qquad (3.24d)$$

3.2.2 The Dyson Equation

For studying the non equilibrium dynamics in such an inhomogeneous system where quantum effects will be significant the Non Equilibrium Green Function Formalism is a powerful candidate since it is structured in the way that brings the problem in a manner amenable for perturbation expansion and enables the formulation in terms of quantities to be linked with observables directly. The formulation uses the Dyson equation and the Kadanoff-Baym anstaz as the fundamental theoretical frame work. The starting point in the analytical development of the formulation is the Dyson equation [64]. The integro-differential form of the Dyson's equation in terms of the contour variables is

$$[i\mathrm{h}\frac{\partial}{\partial\tau}-\{-\frac{\mathrm{h}^2}{2\mu}\nabla_{\chi}^{2}+U(\chi,\tau)\}]G(\chi,\tau;\chi',\tau')=\delta(\chi'-\mathrm{X})\delta(\tau'-\tau)$$

$$+\int_c d\bar{\tau}\int d^3\bar{\chi}\Sigma(\chi,\tau;\bar{\chi},\bar{\tau})G(\bar{\chi},\bar{\tau};\chi',\tau') \quad (3.25)$$

Where, C is the contour over which the integral has to be evaluated and the Greek alphabets representing contour variables. The use of the other parameters is such that μ is the reduced mass of an electron in the sample; U is the electron potential energy at the contour variable specified and Σ is the self energy referring the irreducible interaction terms. Based on the contour ordered structure of G and the anti commutation relations of fermionic field operators it is well known eq.3.25 to be reformulated in terms of other forms of the Green functions; $G^{<}$, $G^{>}$ and the advanced and retarded Green functions G^{a} and G^{r}. Formulating the problem as the equations of motions of such functions which could be linked directly with experimentally relevant quantities is of course an advantage.

$$\Sigma_{\alpha\beta}(\tau,\tau')=\Sigma^{s}_{\alpha\beta}(\tau,\tau')\delta(\tau'-\tau)+\theta(\tau-\tau')\Sigma^{r}_{\alpha\beta}(\tau,\tau')+\theta(\tau'-\tau)\Sigma^{a}_{\alpha\beta}(\tau,\tau') \quad (3.26)$$

Where,

$$\theta(\tau_1-\tau_2)=\begin{cases}1 & for\,\tau_1>\tau_2\\ 0 & for\,\tau_2>\tau_1\end{cases} \quad (3.27)$$

To put the Green function in a usable form we then employed the Dyson's series expansion and the Langareth theorem [65, 66].

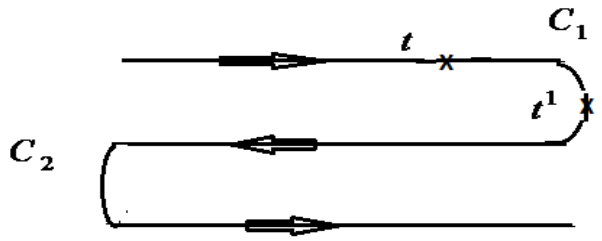

Fig.3.1: *Contour for evaluating terms consisting product of two time ordered operators*

Evaluation of the contour integral in eq.3.25 using the Langareth theorem [66] and transforming in to the real space-time representation leads to the formulation of the equations of motion for the correlation function, $G^{<}$, in a component matrix form, in the primed and unprimed coordinate basis respectively as

$$i\hbar \frac{\partial}{\partial t} G^{<}_{\alpha\beta}(t,t') = \delta(t-t') + \varepsilon_{\alpha} G^{<}_{\alpha\beta}(t,t') + \sum_{m} \Sigma^{S}_{\alpha m}(t) G^{<}_{m\beta}(t,t')$$

$$+ \sum_{m} \{ \int_{t_o}^{t} d\bar{t}\, \Sigma^{>}_{\alpha m}(t,\bar{t}) G^{<}_{m\beta}(\bar{t},t') + \int_{t}^{\infty} d\bar{t}\, \Sigma^{<}_{\alpha m}(t,\bar{t}) G^{>}_{m\beta}(\bar{t},t') \} \quad (3.28a)$$

$$-i\hbar \frac{\partial}{\partial t'} G^{<}_{\alpha\beta}(t,t') = \delta(t'-t) + \varepsilon_{\beta} G^{<}_{\alpha\beta}(t,t') + \sum_{m} G^{<}_{\alpha m}(t,t') \Sigma^{S}_{m\beta}(t')$$

$$+ \sum_{m} \{ \int_{t_o}^{t'} d\bar{t} G^{<}_{\alpha m}(\bar{t},t') \Sigma^{>}_{m\beta}(t,\bar{t}) + \int_{t'}^{\infty} d\bar{t} G^{>}_{\alpha m}(\bar{t},t') \Sigma^{<}_{m\beta}(t,\bar{t}) \} \quad (3.28b)$$

Where, α, β, n, m, are energy state indices. The energy, say $\varepsilon_{\alpha}(r,t)$, refers to the energy of electron at the level α of the atom of the solid at position r in the ground state condition of the system irrespectively of whether the particular state is occupied or it is empty. The pair equations

of motion for the advanced Green function, in the two coordinate variables, obtained using the same procedure are

$$i\hbar \frac{\partial}{\partial t} G^a_{\alpha\beta}(t,t') = \delta(t'-t) + \varepsilon_\alpha G^a_{\alpha\beta}(t,t') + \frac{1}{2}\sum_m \Sigma^S_{\alpha m}(t) G^a_{m\beta}(t,t')$$

$$+ \sum_m \int_{t_o}^{\infty} d\bar{t}\, \Sigma^a_{\alpha m}(t,\bar{t}) G^a_{m\beta}(\bar{t},t') \qquad (3.29a)$$

$$-i\hbar \frac{\partial}{\partial t'} G^a_{\alpha\beta}(t,t') = \delta(t'-t) + \varepsilon_\beta G^a_{\alpha\beta}(t,t') + \frac{1}{2}\sum_m G^a_{\alpha m}(t,t') \Sigma^S_{m\beta}(t')$$

$$+ \sum_m \int_{t_o}^{\infty} d\bar{t}\, G^a_{\alpha m}(\bar{t},t') \Sigma^a_{m\beta}(t,\bar{t}) \qquad (3.29b)$$

4

Static Correlation Effects and the Ground State Property Characterization

The making of a device material for specific application is naturally a step where the material is engineered such that the quantum states of the later are prepared in a way it strongly correlates with the electronic states in the subject material. The characterization and tailoring of the ground state electronic state distribution is therefore a crucial and common starting point in designing dynamic correlations as well.

The static correlation of a ground state system represents a fraction of the total electronic energy. The coupling of different materials by contacts modifies the electronic structure at the positions at least closer to the interface. On the other hand the application of a constant potential difference possibly results in position dependent change on the potential distribution in the material. Such a position dependent change of the potential distribution becomes an additional element for its influence in introducing changes on the symmetry condition. Our emphasis in this chapter is on the structural characterization of a nanostructure where the contribution of the electronic correlation is to be explored. Our particular emphasis is on the silicon nanostructure at equilibrium. The investigation is made with the OF-DFT [67,68] as the theoretical framework.

4.1 Characterization of the Ground State Properties of Semiconductor Nanostructures (With Emphasis on Si Nanostructure)

In works where the prime interest is on investigating the dynamical correlation effects or exploiting these for technological applications, the issue of whether the material structure qualifies for supporting pointer states for particular application is among the issues to be raised at the primary step. This basically demands understanding the energy distributions of the various states of the atomic system constituting the particular specimen.

At the surface of the solid structures there are some unpaired bonds, dangling bonds, with the corresponding atomic orbitals is in the fundamental gap of the crystalline structure. The interaction between dangling bonds on neighboring atomic sites at the surface leads to a broadening of the surface state level and forms the surface state band. In addition to this formation of band gap states or surface bands within the fundamental gap is that the surfaces relax and in most cases reconstruct giving rise to variations in the angle between the bonds. This could be controlled by using passivants so that the dangling bonds to be paired with the passivant. This subsequently drives the surface states out from the fundamental gap. The center of gravity and broadening energy corresponding to the paired orbital of the atoms of the semiconductor and the passivants depend on the two atomic species and the interaction with orbital at the neighboring sites. For single bonded passivants such as the case in a hydrogenated silicon, the states are pushed to the bottom of the valence band [67,68] and contributes very small in the optical absorption. On the other hand, for double bonded passivants, such as the atomic oxygen, the bonding thus formed interact leading to the formation of bonding and anti-bonding states and reduces the band gap by about 1 eV.

The emphasis in this work is on the hydrogen terminated silicon nanostructure where the surface atomic states now involve orbital levels at energies at about the bottom of the valence band. The passivant obviously modifies the atomic environment at the surfaces altering the surface potential distribution and the local density of states. The effect of this together with the relaxation and reconstruction of the structure propagates in to the interior region at a rate that decays with distance from the outer surface. Our investigation of the ground state condition energy structure in the nanostructure has to be made, therefore, with this structural fluctuation taken in to account.

In performing the computation we started from the results found from the energy minimization in the LDA approximation and with the expressions for the charge density and potential functions determined using the Ewald's potential summation rule (eq.3.3, eq.3.8). We made this with the electronic contribution to the energy of the local atom is represented by the sum of the spatial dependent values of the energies of the electrons at all the levels occupied at the ground state. This choice of representation is because of the technical advantages we possibly benefit in our steps. One of the main advantages is that the boundary values, the level energies at the surface and most inner points, are more convenient to access in measurements. Results of surface spectroscopy studies and the knowledge on the bulk material are elemental resources for the respective boundary values. Secondly, the level energies are characteristic parameters which most of our theories link with macroscopic properties of the material. With this in mind we now proceed with the electronic contribution to the total energy of a local atom represented as

$$E_T(r) = \sum_j \varepsilon_j(r) \tag{4.1}$$

Applying the minimization requirement by assuming equal level shift in the orbitals, we found

$$\delta E_T(\rho, r) = \delta \sum_j \varepsilon_j(r) = 2\ell \Delta\varepsilon(r) = \mu[\rho(r) - \rho_b]V_{cell}(r) \qquad (4.2a)$$

Where, ℓ is the atomic orbital degeneracy which is $\ell = 4$ for silicon. Rearranging eq.4.2a,

$$\Delta\varepsilon(r) = \frac{\mu}{2\ell}[\rho(r) - \rho_b]V_{cell}(r) \qquad (4.2b)$$

Using this, the equation for the exchange-correlation potential (eq.3.5) will give

$$V^{xc}(\rho, r) = V_C(\rho, r) + \frac{\partial}{\partial\rho}T(\rho) + \frac{2\ell\Delta\varepsilon(r)}{[\rho(r) - \rho_b]V_{cell}(r)} \qquad (4.3)$$

Hence,

$$\varepsilon^{xc}(\rho, r) = V_C(\rho, r)\rho(r) + \rho(r)\frac{\partial}{\partial\rho}T(\rho) + \frac{2\rho(r)\ell\Delta\varepsilon(r)}{[\rho(r) - \rho_b]V_{cell}(r)} \qquad (4.4)$$

The contribution of the last term in the equation, eq. 4.4, is easily noticed to depend on a number of parameters characteristic of the structure and the chemical species of the constituents. More over this term has signs that depend on whether the local density is less or greater than the bulk value.

The expression (eq4.2.) indicates the level shift in atomic orbitals to be due to complicated changes in the energy values contributing for the molecular orbital energy. The rapid decrease, with increasing distance from the interior and in regions within few atomic layers deep from the surfaces, is accompanied with a decrease in the kinetic term and an increase in the exchange-correlation contribution. The exchange and correlation contributions are of course negative but it becomes less negative tending toward the situation where it could no more be accounted as the energy lowering factor.

The fitting parameters in eq.4.4 are three. The two are the same parameters accounting to the variations of density and potential toward the surface and the distribution parameter associated to the spread about the core atoms. The third is the shift of energy levels $\Delta_{\varepsilon}(r)$. From a glance, it seems it will be sufficient to make the computation through a onetime adjustment. Of course the shift in energy levels primarily has to match experimental realities. The expression in eq 4.2 also shows that this has to be compared with the chemical potential, the total number of atomic orbital, 2ℓ, and the other terms which are functional of density. Since the later forms the group determined from self consistent solutions, this will be an additional testing tool as the result reflects the realities. It in particular aids in explaining the property variation among nanostructures of different surface passivation.

In making the computation, we determine first the adjustable parameters λ and χ in eqs.3.8. Here, the critical radius r_b is considered to be at the order seven times the plane spacing (~7.43Å). We made the calculation using the results of surface core level spectral shift in [68, 69] as the boundary values for the level shift. From a series of iterations we found the expressions for the charge and potential distribution rapidly converge for the values of the parameters $\lambda \approx 0.01-0.05$ depending on the surface preparation of the sample (Table 4.2) and $\chi \approx 7R_a^{-2}$, R_a being the atomic radius. The spatial dependent Coulomb potential we determined using this result is shown in Fig.4.1a. This potential curve is representing the normalized electrostatic potential, normalized to the bulk value, at the position of atomic sites over the layers indicated by the layer indices (Fig. 4.1a). It is noticed to demonstrate the spatial dependent nature of the Coulomb potential as predicted by the model. As it is suggested by the result depicted in the diagram (Fig. 4.1a), the electrostatic potential tends decreasing toward the surface. The prediction is in good agreement with the results in other independent studies [70].

The curve in Fig.4.1b on the other hand shows the exchange and correlation potential predicted by eq.4.4. The curve is drawn using the results we found for λ and χ in the previous steps. The calculation that led to the result depicted in Fig. 4.1b is made with the kinetic term in eq.4.4 is replaced by the kinetic function in eq.3.6. The result shows that the exchange and correlation contribution increases the more the atomic site is closer to the surface. When the surface is approached from the interior, the exchange-correlation contribution builds up as opposed to the case of the electrostatic contribution which is decaying to smaller values. This is a feature similar to the prediction by the exchange and correlation energy relations due to Perdew and Zunger [71,72].

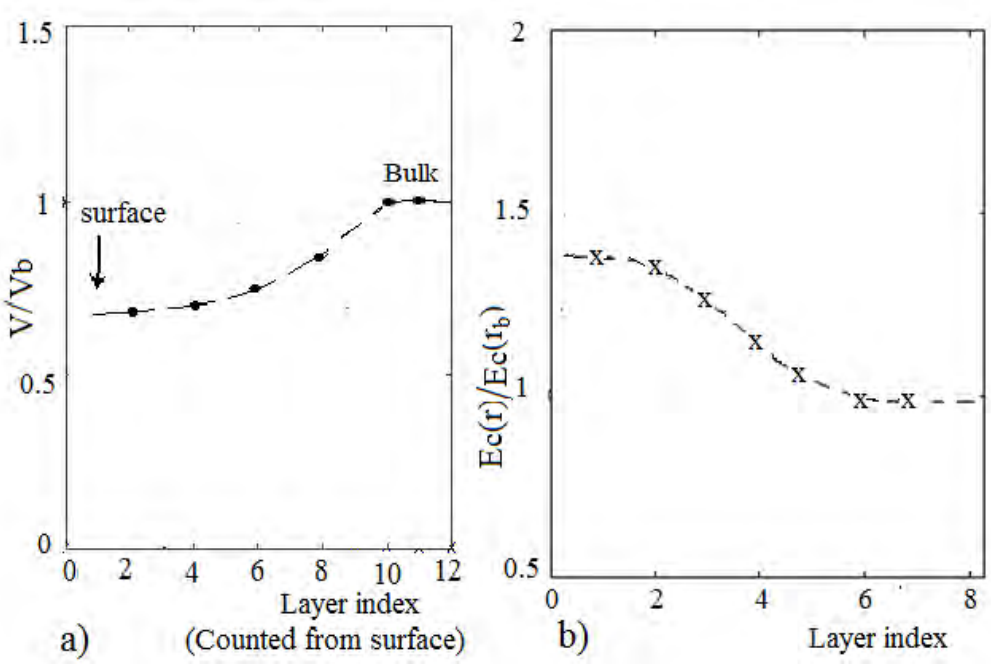

Fig.4.1: *Spatial variation of (a) the Coulomb and (b) the correlation potentials in nano silicon.*

The expressions in eq.4.3 and eq.4.4 predict the buildup of the exchange and correlation term associated to the structural fluctuation. This term explicitly suggests the direction for structural tuning of the sample in such a way that it favors the preparation of pointer states for a particular application. It could be noted from the expression that this involves

selection of the chemical species of the passivant, the size and geometry of the sample. The later, though not explicitly appear in the expression the role is embodied within the size and geometry dependence of the local density. The dynamic correlation effects taking place under time dependent perturbations depend on the spatial dependent level shift of atomic orbitals in the material system. As it will be described at later stages, the dynamical correlations tend to vanish at long times and do not converge to the exchange and correlation contributions to the ground state energy at the remote past. The result is therefore sufficient to aid the steps both in the theoretical investigations and design of device materials. To investigate the importance of structural tailoring in preparing a sample, it is important rather to investigate the distribution of the HUMO-LOMO gap. This is the subject in the following section of this chapter.

Table 4.1 *parameters of silicon used in the calculations*

Parameter	Value
Lattice constant of ***Si (a)***	0.52 nm
Coordination number **(ℓ)**	
Bulk band gap($(\varepsilon_{co}^{b} - \varepsilon_{Vo}^{b})$	1.2 eV
Mass of electron Longitudinal Transverse	$0{,}92m_e$ $0.19m_e$
Dielectric constant $(\in_r = \in / \in_o)$	11.7
$r_b = 7a$	3.64 nm
$z = \chi R_a^2$	7

Table 4.2: *Values of the parameter λ, for nano silicon of different surface preparation condition.*

Surface preparation condition	***Values of λ***
Non passivated silicon	*0.01*
Hydrogenated Silicon	*0.04-0.05*
Oxygenated Silicon	*0.032*

4.2 Threshold for optical absorption transition

As it is pointed out in the preceding section, the atoms in the nano-structured sample are not in an identically interacting environment. Following the Born-Openheimer approximation, the energy of the electronic state $|\alpha\rangle$ in the valance band of an atom i in the nanostructure at equilibrium is

$$E_{\alpha i} = E^{C}_{\alpha i} + E^{k}_{\alpha i} + E^{XC}_{\alpha i} \; - \sum \varepsilon' \qquad \alpha \in V \qquad (4.5a)$$

The first term in the right hand side is the contribution due to the Coulomb interaction with the electrons and the nuclei, the second term refers to the kinetic contribution and the third term is the exchange-correlation contribution to the total one electron energy. In reality all microstructures are inhomogeneous. Thus, the energy of the atomic levels shows a spatial dependent nature leading to the broadening of levels. Allowing the equation contain the information we can rewrite eq.4.5a for the level at a position r_ℓ as

$$E_{\alpha}(r_\ell) = E^{C}_{\alpha}(r_\ell) + E^{k}_{\alpha}(r_\ell) + E^{XC}_{\alpha}(r_\ell) \; - \sum \varepsilon' \qquad \alpha \in V \qquad (4.5b)$$

The electronic energy at a conduction level in the ground state material on the other hand could be described by

$$E_\beta = E_\beta^{inp} - E^b = E_c^o + E_\beta^{ex} \qquad \beta \in C \qquad (4.5c)$$

Where, the term E_β^{inp} refers to the input energy that is required to result the transition. The term E^b in eq.4.5c represents the binding energy of the exciton if such a bound electron-hole pair is formed. For the samples that could be well characterized by confinement quantization effects $E^b = 0$ and

$$E_\beta^{ex} = E_{\beta n}^{con} = \frac{\hbar^2}{2m_e} K_n^2 \qquad \text{n=1, 2, 3} \qquad (4.6)$$

For the ground state condition of the system, the confinement energy for a nanostructure of spherical geometry is easily computed to be in the form

$$\varepsilon_\ell^c = \varepsilon_c^o + \frac{\hbar^2}{2m_e}\frac{\gamma_\ell^2}{R^2} \qquad (4.7)$$

Where γ_{ci} is the zero of the Bessel function that has to be determined from the requirement of a wave function that vanishes at the surface; $J_{\frac{1}{2}}(k_{ci}R) \approx 0$.

Under the situation when excitons are predominant, $E^b \neq 0$ and the system is modeled by excitonic effects such that the corresponding approximation becomes

$$E_{n\beta}^{ex} = E_{\beta n}^{e-h} = \frac{\hbar^2}{2\mu_{\beta e}} K_{\beta n}^2 \qquad (4.8)$$

Where, m_e and μ_e in the preceding two equations refer the effective mass of the electron and the reduced mass of the e-h pair in the material respectively. Whether it is the quantum confinement or the excitonic formation that determines the dynamics of the particles in a particular system is an issue to be decided by the competition between the two mechanisms. The dimension of the samples considered in our investigations is in the order where quantum confinement effects will be the predominating mechanism. The selection of the range for the dimensions of the samples is made from comparing the energy requirement for the two quantization processes. If the confining potential at the boundary is assumed as infinite, it will be easy to see that the comparison between the energy required for the two quantization processes lead to an inequality of the form

$$\frac{\hbar^2 \gamma_\ell^2}{2m_j R^2} > \frac{\hbar^2}{2\mu_r a_B^2} \qquad (4.9)$$

Where, m_j is the mass of electron or hole; μ_r is the reduced mass of the electron-hole system; R is the sample dimension; and a_B is the Bohr radius which is related with permittivity $\in$ of the material and the reduced mass μ_r as

$$a_B = \frac{4\pi \in \mathrm{h}^2}{\mu_r e^2} \qquad (4.10)$$

Clearly, the confinement will become more prominent than the formation of excitons when $R < 2a_B$ and the reverse for the situations where $R \geq 4a_B$. When $2a_B < R < 4a_B$, it will be important to take into account the contributions of both mechanisms.

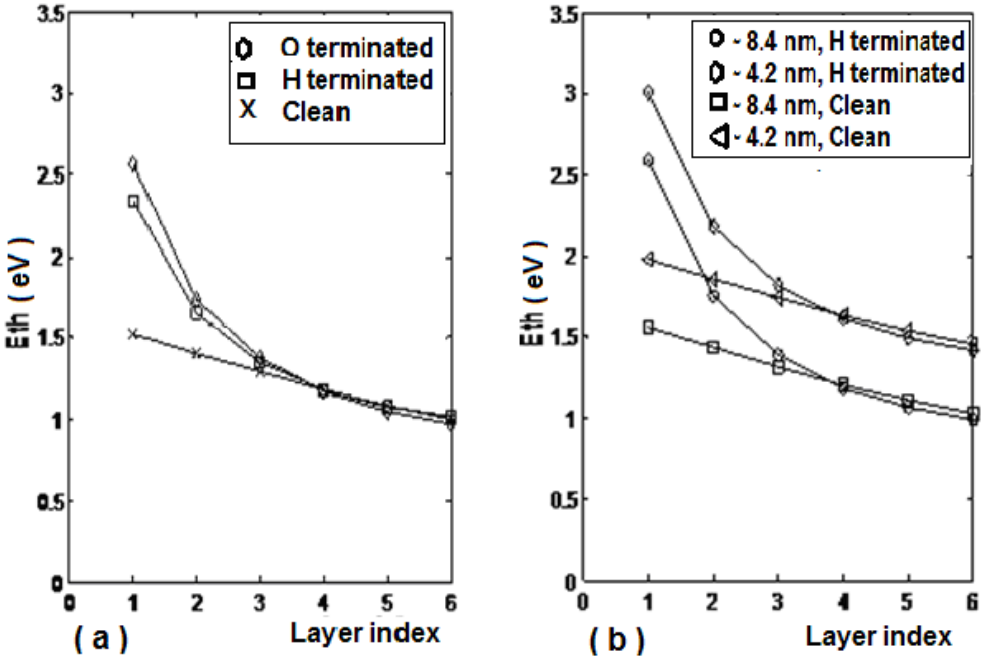

Fig. 4.2: *The dependence on **(a)** surface termination condition **(b)** both size and surface passivation of the absorption threshold in nano-Silicon.*

The curves in Fig.4.2 are illustrating the dependence on the sizing and surface termination conditions of the absorption threshold in Si nano structure. The change in size of the structures modifies the threshold by introducing a non local shift on the quantized level energy. The two nearly straight lines in Fig.4.2b are illustrating this prediction. The surface passivation could alter the threshold conditions magnificently at the atomic sites that are much closer to the surface. The modification by the passivation is mainly due to the change in the local density and interaction potential the different atomic environment in chemical environment at the surface. This change of chemical environment subsequently results in a level shift that decays with distance from the surface.

In arriving at the predictions illustrated by the non straight curves in Fig.4.2, we allowed changes both in the density and chemical potential at the surface and the changes brought by these modifications decays to zero

over six atomic layer steps. As represented by the characteristic relations in eq.4.2 and eq.4.4, terminations bringing about reduction in the surface local density have positive contributions while terminations increasing surface density modifying in the opposite sense. We can notice from comparing the two non straight curves in Fig.4.2b that termination with oxygen introducing states in the gap and thereby reducing the threshold for absorption. Contrarily, termination by hydrogen pushes away the gap states down in to the valance band edge and thereby opening the gap wider. This later case is leading to a situation where the near threshold absorption in hydrogen terminated solids to be prominently linked with the under layer atoms. This understanding is consistent with experimental investigations reported in [70,73] and the results of recent studies in [144]. The graph in Fig4.3 provides the summary of the result reported for silicon in [144-146].

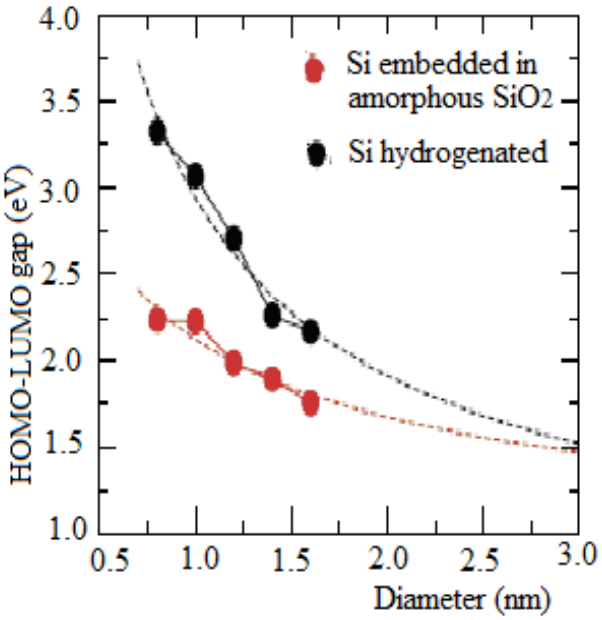

Fig. 4.3: *HOMO-LUMO gap in nano silicon as a function of size [144].*

5

Dynamical Correlations and Quantum Indistinguishability

Our understanding of the properties of the many atoms system has recourse to our analysis of the dynamical behaviors of the electrons of the constituent atoms: The dynamical evolution of the constituent particles is computed and the overall system response is determined by statistical averaging of the contributions of the many particles. In mesoscopic systems and bulk counter parts the interaction between the particles is too strong to be analyzed independently of the other particles and the number of particles is too huge for direct computation. The general trend is to approximate the system by outer orbital electrons of the constituent atoms, analyze the dynamical behavior of these electrons and statistically average their contributions. However the number of particles to be considered under this approximation is also too large to be involved in direct calculations. The general line of approach is to take advantage of some properties of the system and the interacting environments that make use of some approximation techniques adequate. The results obtained from using the Bloch theorem for bulk materials, assuming long range ordering, provided a frame work where the analysis could be made on a unit cell basis. But the same approach has failed to be equally useful for mesoscopic systems.

The spatial dependent energy shift in the low orbital levels and quantum confinement effects together with Pauli's exclusion principle make dynamical correlation, quantum interference and indistinguishability prominently influence the short time responses of mesoscopic materials. The structural inhomogneity plaguing mesoscopic materials in general,

makes the atomic sites at different regions of the sample become a different atomic environment for electrons. The energies of the filled levels show local characteristic while the unoccupied quantized levels are non local. The number of states at a given quantized level is limited to a value that depends on its quantization order. Hence it is only with a limited number of states that a given atomic state could entertain the particle exchanging couplings at given instant. Moreover, the spatial dependent relative detuning between the lower, initially filled, levels may increase, decrease and it may even vanish when a time dependent perturbation is impressed on the system.

Dynamical analysis that based in describing a physical observable by the superposition of the contributions from the localized particles could not serve to describe the observation. Such an approach is limited to taking in to account the first order correlation effects. However, this alone could neither make the particular formalism to be a quantum approach and to the effect even classical waves do interfere. Investigating of the phenomena in the context of quantum mechanics need to include also the quantum statistics of the constituents and quantum indistinguishability which believed to reflect their role in the coherent regime dynamical behaviors of mesoscopics.

5.1 Quantum Indistinguishability and Interference

In the sense of classical mechanics, identical particles do not lose their "individuality". That is, at any instant the particles of a many body system can be identified and their evolution can be tracked irrespective of whether or not they are identical in properties. But, the understanding in quantum mechanics is totally different. According to the Heisenberg uncertainty principle in quantum mechanics the path of particle evolution could have no meaning. There is in principle no possibility of separately tracking the evolution of each one of the similar particles in a many body system. Even

the particles of a many body system that could be regarded as distinguishable at one earlier instant may turn out to be indistinguishable at later time when the system is under an impressed perturbation. We consider for instance a many body system of total energy E and a total number, N, of quantum particles, the eigen function ψ and the Hamiltonian operator H of the system obeys the equation

$$H\psi = E\psi \tag{5.1}$$

Suppose the operator H and the function ψ could be labeled by the position, r_j, and spin ,σ_j, of the particles such that $H \equiv H(r_j,\sigma_j)$ and $\psi \equiv \psi(r_j,\sigma_j)$. Where, j labels the j^{th} particle in the system. For a system where the particles energy is functional of position, such as the case of nanostructures in general, this could be rewritten as $H \equiv H(\varepsilon_j,\sigma_j)$ and $\psi \equiv \psi(\varepsilon_j,\sigma_j)$. The state of the composite system is represented by tensor product of the individual states; For N particles at states $(\varepsilon_1,\sigma_1),(\varepsilon_2,\sigma_2),...(\varepsilon_N,\sigma_N)$, the state of the composite system could be represented for instance as

$$\left|\psi\right\rangle \equiv \left|\psi_{1,}(\varepsilon_{1,}\sigma_1)\right\rangle \otimes \left|\psi_{2,}(\varepsilon_2,\sigma_2)\right\rangle \otimes .... \otimes \left|\psi_{N,}(\varepsilon_N,\sigma_N)\right\rangle \tag{5.2a}$$

or

$$\left|\psi\right\rangle \equiv \left|\psi_{1,}(\varepsilon_{1,}\sigma_1)\right\rangle \left|\psi_{2,}(\varepsilon_2,\sigma_2)\right\rangle ... \left|\psi_{N,}(\varepsilon_N,\sigma_N)\right\rangle \tag{5.2b}$$

Where, $\otimes$ is to indicate that it is a tensor product. This is however only one of the possible ways the system could be represented. If the particles are identical, the properties of the system will remain invariant under permutations. In the particular case of a system of two particles with opposite spin polarizations, both $\left|\psi\right\rangle \equiv \left|\psi_1;\varepsilon_1,\uparrow\right\rangle \left|\psi_2;\varepsilon_2,\downarrow\right\rangle$ and

$|\psi'\rangle \equiv |\psi_1;\varepsilon_2,\downarrow\rangle|\psi_2;\varepsilon_1,\uparrow\rangle$ represent the two particle composite system. One will become unable to distinctly specify the state of the particular constituent quantum particle. One may of course tempt to view the phenomenon as interference between the individual states. The states represented by each of the permuted products are inaccessible by experimental measurements. The interference is lost before making any measurements which is essentially quantum interference. The fact that it becomes unlikely to specify the states of the constituents reveals one important feature of quantum many body systems, indistinguishability. This is a feature leading to the entanglement of the constituent particles.

5.2 Quantum Mechanical Representation of Physical States

The dynamical state of quantum particles is described using the set of quantum numbers; energy, angular momentum and spin quantum numbers. A composite system is described from combining the quantum labels of the constituents by applying the superposition principle. To do this one could use either the Hilbert space (first quantization) notation or quantized field operator (second quantization) notation. It will not be difficult also to switch from one notation to the other if that is handled with the appropriate use of symmetrization (anti-symmetrization) postulates. In this short review of the effects of quantum indistinguishability in measurements we use the first quantization notation. For a composite system constituted from a particle A in a quantum state ϕ , $|\phi;A\rangle$, and a particle B in state θ , $|\theta;B\rangle$, the state of the composite system at subsequent times evolves in to a superposition

$$|\psi\rangle = |\phi;A\rangle \otimes |\theta;B\rangle = |\phi_A\rangle \otimes |\theta_B\rangle \qquad (5.3)$$

Where, the last expression is only due to a choice for alternative way of writing in a compact form. The superposition is described by products of the particle states with each state has a particle labeling. That is not of course the only way the system could be represented. The forms we could get from permuting under particle labeling are also possible representation each tracking one specific path of the evolution of the wave function describing the system and constitute the state-space vector. For a single composite system consisting of N particle states, there are $N!$ state-space vectors. The state space degeneracy is lifted using the symetrization postulate and the particle spin statistics [74].

Fermions (bosons) have half-integer (integral) spins and are anti symmetric (symmetric) under exchange of particle labeling. One could start from one arbitrary state-space representation, also called the first term, and all the permuted representations are determined in such a way that for every step of interchanging the particle labeling of two consecutive terms in the product picks a negative sign. The physical state is then represented by the normalized sum of the complete set of the state-space vectors. For a system of two particles A and B, and particle states $|\phi\rangle$ and $|\theta\rangle$, the two state-space representations are

$$|\psi_1\rangle = |\phi_A\rangle|\theta_B\rangle \tag{5.4a}$$

$$|\psi_2\rangle = -|\phi_B\rangle|\theta_A\rangle = -|\theta_A\rangle|\phi_B\rangle] \tag{5.4b}$$

Where, the change in the ordering in eq.5.4b follows since the first quantization notation is independent of the state ordering. The physical state of the two particle composite system is therefore represented by

$$|\psi\rangle = \frac{1}{\sqrt{2!}}[|\phi_A\rangle|\theta_B\rangle - |\theta_A\rangle|\phi_B\rangle] \tag{5.5a}$$

$$\left|\psi\right\rangle = \frac{1}{\sqrt{2!}}\begin{vmatrix}\left|\phi_A\right\rangle & \left|\theta_A\right\rangle \\ \left|\phi_B\right\rangle & \left|\theta_B\right\rangle\end{vmatrix} \qquad (5.5b)$$

This can be generalized for an arbitrary number of particles. The physical state representation of a composite system consisting of N particles in particle states $\left|\varphi(\alpha_1)\right\rangle, \left|\varphi(\alpha_2)\right\rangle, \ldots\ldots \left|\varphi(\alpha_N)\right\rangle$ is

$$\left|\psi\right\rangle = \frac{1}{\sqrt{N!}}\begin{vmatrix}\left|\varphi_1(\alpha_1)\right\rangle & . & . & \left|\varphi_1(\alpha_N)\right\rangle \\ . & . & . & . \\ . & . & . & . \\ \left|\varphi_N(\alpha_1)\right\rangle & . & . & \left|\varphi_N(\alpha_N)\right\rangle\end{vmatrix} \qquad (5.6)$$

One could also arrive to the same understanding using the second quantization notation. In the second quantization notation the particle states are represented by field operators; the creation $\hat{a}^\dagger$ and annihilation $\hat{a}$ operators. A particle state $\left|\phi\right\rangle$, in this notation, is taken as a state created from a vacuum state $\left|0\right\rangle$ under the action of the creation operator $\hat{a}_\phi^\dagger$;

$$\left|\phi\right\rangle = \hat{a}_\phi^\dagger\left|0\right\rangle \qquad (2^{nd}\text{quantization}) \qquad (5.7)$$

The degeneracy in the state space representation for a fermionic (bosonic) composite system is lifted upon using the anti-commutation (commutation) relations. In contrast to the first quantization notation, the expressions in the second quantization notation are sensitive to ordering of the field operators. For a system of two particles in states $\left|\phi\right\rangle$ and $\left|\theta\right\rangle$, the state of the composite system is

$$\left|\psi\right\rangle = \hat{a}_\phi^\dagger\hat{a}_\theta^\dagger\left|0\right\rangle = \pm\hat{a}_\theta^\dagger\hat{a}_\phi^\dagger\left|0\right\rangle \qquad (5.8)$$

Where, the " $+$ " sign is applied for bosons and the " $-$ " for fermions.

In representing the state of a composite system, one first requires to uniquely specify the quantum states of the constituents. This is to be achieved with the use of a set of quantum numbers, such as the energy and spin quantum numbers. In the first quantization notation, the state of a particle can be represented with the orbital and spin parts, for each particle , are combined in a product form. For a particle A of spin σ at energy state α , the state vector is given by

$$\left|\phi_A\right\rangle = \left|\alpha_A;\sigma,A\right\rangle = \left|\alpha_A\right\rangle\left|\sigma,A\right\rangle \qquad (1^{st}\text{quantization}) \qquad (5.9a)$$

In the notation of the second quantization, the same particle state is represented as

$$\left|\phi\right\rangle = \left|\alpha,\sigma\right\rangle = \hat{a}^{\dagger}_{\alpha\sigma}\left|0\right\rangle \qquad (2^{nd}\text{quantization}) \qquad (5.9b)$$

The second quantization notation is also noticed in common use for describing the injection or generation of excited electrons at a given spatial location in material media. The state of a spin σ electron that is injected to the state at energy ε_C , in the right contact "R" of a unit device is described by

$$\left|\psi_C\right\rangle = \hat{a}^{\dagger}_{R\sigma}(\varepsilon_C)\left|\psi_o\right\rangle \qquad (5.9c)$$

The operator $\hat{a}^{\dagger}_{R\sigma}(\varepsilon_C)$ is identified as an operator creating electron state at the energy ε_C in the right contact and $\left|\psi_o\right\rangle$ is the reference state.

From the product form notations in eqs.5.9 we can notice that the physical state of a system with two electrons of opposite spin polarizations σ and $\overline{\sigma} = -\sigma$ in states α and β, can be described by two distinct state vectors. Accordingly, the physical

state of the system, in the first and second quantization notation respectively, is described by the normalized sum of the state vectors:

$$\left|\psi_{\pm}\right\rangle_{1^{st}\,quan.} = \frac{1}{\sqrt{2}}[\left|\alpha_A\right\rangle\left|\beta_B\right\rangle \pm \left|\alpha_B\right\rangle\left|\beta_A\right\rangle][\left|\sigma,A\right\rangle\left|\bar{\sigma},B\right\rangle \mp \left|\bar{\sigma},A\right\rangle\left|\sigma,B\right\rangle] \quad (5.10a)$$

$$\left|\psi_{\mp}\right\rangle_{2^{nd}\,quan} = \frac{1}{\sqrt{2}}[\hat{a}^{\dagger}_{\alpha\sigma}\hat{a}^{\dagger}_{\beta\bar{\sigma}} \mp \hat{a}^{\dagger}_{\alpha\bar{\sigma}}\hat{a}^{\dagger}_{\beta\sigma}]\left|0\right\rangle \quad (5.10b)$$

5.3 Entangled EPR Type States

Clearily, the expressions in eq.5.10 are in a form where the state vector of the individual particles can not be factored out. The evolution of composite system in such a manner where the state of the constituent cannot be factored out, is when the particles are entangled. The expression in eq.5.10 is noted to be in a form of the product of state vectors in two subspaces; the orbital sub space and the spin sub space. The overall symmetry is that fermions are anti-symmetric while bosons are symmetric. The spin sub space symmetry is established by nomenclature. Of the spin sub spaces, the spin singlet sub space is anti symmetric. It follows there fore that the orbital sub space for the spin singlet need to be symmetric so that the overall anti-symmetric nature of the fermionic state to be preserved. Similarly, the orbital sub space for the triplets has to be anti-symmetric. Consequently one will come across the representation of fermions singlet, $\left|\psi_s\right\rangle$, and triplet , $\left|\psi_t\right\rangle$,states respectively as

$$\left|\psi_s\right\rangle = \frac{1}{\sqrt{2}}[\left|\alpha_A\right\rangle\left|\beta_B\right\rangle + \left|\beta_A\right\rangle\left|\alpha_B\right\rangle][\left|\sigma,A\right\rangle\left|\bar{\sigma},B\right\rangle - \left|\bar{\sigma},A\right\rangle\left|\sigma,B\right\rangle] \quad (5.11a)$$

$$\left|\psi_t\right\rangle = \frac{1}{\sqrt{2}}[\left|\alpha_A\right\rangle\left|\beta_B\right\rangle - \left|\beta_A\right\rangle\left|\alpha_B\right\rangle][\left|\sigma,A\right\rangle\left|\bar{\sigma},B\right\rangle + \left|\bar{\sigma},A\right\rangle\left|\sigma,B\right\rangle] \quad (5.11b)$$

$$\left|\psi_S\right\rangle_{2nd\ quan.} = \frac{1}{\sqrt{2}}[\hat{a}^{\dagger}_{\alpha\uparrow}\hat{a}^{\dagger}_{\beta\downarrow} - \hat{a}^{\dagger}_{\alpha\downarrow}\hat{a}^{\dagger}_{\beta\uparrow}]\left|0\right\rangle \qquad (5.12a)$$

$$\left|\psi_t\right\rangle_{2nd\ quan.} = \frac{1}{\sqrt{2}}[\hat{a}^{\dagger}_{\alpha\uparrow}\hat{a}^{\dagger}_{\beta\downarrow} + \hat{a}^{\dagger}_{\alpha\downarrow}\hat{a}^{\dagger}_{\beta\uparrow}]\left|0\right\rangle \qquad (5.12b)$$

These are the EPR (Einstein- Podolsky-Rosen) type [75] entangled fermion states. The entangled states in eqs.5.11-12 are also often referred as the Bell's singlet and triplet states for fermions [76,77] A violation of Bell's inequalities in correlation measurements of the constituents indicates the presence of entanglement.

Quantum entanglement represents the nature of quantum many body system where the state of the system can not be decomposed as direct products of single-particle states. The phenomenon is non local and noted taking place in a correlated system with multiple degrees of freedom. This non locality is an important scenario against the notion of the so called single−site entanglement.

5.4 *Detection of Entanglement*

Experimental demonstrations of solid state entanglement involve steps very much challenging to put it in practice in a solid state system. First, two (or more) particles must be made to interact to form an entangled pair. Then the entangled pair is needed to be separated from each other and from the environment they are created in without changing the state of the entangled pair [78-80]. It is however extremely hard to spatially separate electrons in solids in a controlled manner without causing decoherence.

. As a matter of fact it is a natural phenomenon and no exception for the electron in solids also to entangle [81-83]. However direct demonstration of entanglement has so far been limited mostly to experiments involving photons because it is easier to generate and detect entangled photons

[84,85] . The problem in observing entanglement in solids is not because it is too little to influence the observed but rather because it is too much to spatially separate them and extract the information without causing a decoherence [81,86] in order to observe entangled correlations within the pair is very difficult, if not impossible.

Analyzing this quantum mechanical phenomenon is quite useful not only for understanding the process itself, but also for its value both in technology and quantum mechanics:-for possible use in secure quantum communication protocols, quantum information processing [[87-90], and of course in the fundamental tests of quantum mechanics [78].

The consequences of entanglement and the way the effects manifested in the phenomena observed in nanostructures is one of the key issue that has to be considered in the course of investigating the coherent regime phenomenon in nanostructures. Lack of experimental demonstrations on the generation of entanglement in solid state system is not justifications for the absence. Rather, entanglement in these material systems is a rule but not an exception. This makes it important for the dynamical analysis to take in to account entanglement effects if the result has to reflect the realities on the coherent regime interactions in nanostructures. Therefore is the attempt.

6

Dynamical Correlations in a Single Nanostructure-Photon system

6.1 Background

The spatial dependent level shift pledging nanostructures as a result of their inherent structural inhomogneity removes the degeneracy of the occupied levels. This gives rise to the existence of occupied states with very small energy difference that is dependent of the nature of the termination at the surface and the distance of the atom from the surface. This provides a physical environment for generating dynamical correlation between intra-band local atoms when impressed by time dependent perturbation. When the length scale is in the quantum confined range, the spacing in the unoccupied states will be large and excitation to higher states will become less likely to happen. As a result, a radiation with a frequency close to the threshold frequency for absorption effectively leads to the transition from the few HOMO states to the LUMO state in the semiconductor nanostructure.

Indeed the transition from the level at close resonance with the perturbing radiation frequency is accompanied with the change in the local density and potential. This results a time dependent level shift in the neighboring atomic sites [91]. The level shift is obviously in the same sense for all local atomic sites. However, the effect with regard to the tuning of the local atomic states depends on the signs of the detuning of the states: the effect on the states with positive detuning is such as to increase the detuning and for states

When the magnitude of the relative detuning between the neighboring atomic sites is very small or close to the induced level shift, the local atoms may evolve in such a way that it become difficult to factor out the individual atomic states from the composite system. This is a situation where the states are said to be entangled. Explaining the phenomenon observed under this situation in light of the resonance coupling between the bare states which we probably have some information about their strong coupling at the beginning will then become doubtful.

To study the role dynamical correlation and entanglement play in mesoscopic systems we need primarily to explore what physically measurable consequences these could have and which temporal regime to be the appropriate time window to observe the effects. The number density of carriers in a given band is perhaps the key dynamical parameter. It is the strategic parameter firstly because its dynamic evolution carries the information on the interaction with the perturbing field and the inter-orbital correlation effects. Secondly, the number density is a parameter which is directly connected to the many experimentally measured properties. Observation of the effects associated to dynamical correlation and entanglement is only possible before the coherence of the system is lost. Therefore, one needs a pulsed coherent radiation field of very short pulse width and ultra fast techniques to make the observation. This undoubtedly brings us to dealing with the well known phenomenon, the Rabi oscillation. There is nothing to surprise if, just as the case for entanglement .in solids, most of the available information in this respect too is for radiation-two level atomic system interaction [92-94]

6.2 Short Time Scale Dynamical Evolution of the Equal Time Limit Correlation Function

Our objective in this chapter is to analyze the dynamical equation for the atomic states coupled under the perturbing radiation by taking in to account the statistics in the photon distribution, interference and quantum entanglement. As a step in filtering the contributions we considered, the occupation of a given level of an excited state as the superposition of the occupation probabilities of the electrons excited to that level from indistinguishable orbital states. This is of course highly complex to deal with. However it is believed to be less challenging for atomic system with only single excited level. Nanostructures of dimension in the quantum confined regime are ideal for such purpose. For excitation with frequency close to the HOMO-LUMO transition frequency, the process will become practically a two electron transition. This is in effect a dynamical process which mainly involves the strong couplings of the LUMO level to a maximum of two lower levels that contribute electrons of opposite spin polarization through absorbing photons at the same energy.

6.3 Calculation of the Equal Time Limit Correlation Function for Atomic states in a Nanostructure

The local threshold frequency for transition can be determined from the knowledge of the ground state condition energy structure of the system. This information is in fact helpful for a preliminary analysis of the modification in the LDOS of the atoms at the neighboring sites in the course of time. More relevant information on the temporal fluctuations is however possible through the investigation of the dynamic interactions. In the particular case when the interest is on the interactions responsible for the exotic properties that are signatures of a time dependent quantum

mechanical interactions, the short time response will become the focal point.

The starting point in the analytical development of the formulation is the Dyson equation, eq.3.25. The equations of motion for the correlation function in the real space - time representations is, eq.3.28,

$$i\hbar \frac{\partial}{\partial t} G^{<}_{\alpha\beta}(t,t') = \delta(r'-r)\delta(t-t') + \varepsilon_{\alpha} G^{<}_{\alpha\beta}(t,t') + \sum_{m} \Sigma^{S}_{\alpha m}(t) G^{<}_{m\beta}(t,t')$$

$$+ \sum_{m} \{ \int_{t_o}^{t} d\bar{t} \Sigma^{<}_{\alpha m}(t,\bar{t}) G^{>}_{m\beta}(\bar{t},t') + \int_{t}^{\infty} d\bar{t} \Sigma^{>}_{\alpha m}(t,\bar{t}) G^{<}_{m\beta}(\bar{t},t') \} \qquad (61a)$$

$$-i\hbar \frac{\partial}{\partial t'} G^{<}_{\alpha\beta}(t;t') = \delta(r'-r)\delta(t'-t) + \varepsilon_{\beta} G^{<}_{\alpha\beta}(t,t') + \sum_{m} G^{<}_{\alpha m}(t,t') \Sigma^{S}_{m\beta}(t')$$

$$+ \sum_{m} \{ \int_{t_o}^{t'} d\bar{t} G^{<}_{\alpha m}(\bar{t},t') \Sigma^{>}_{m\beta}(t,\bar{t}) + \int_{t'}^{\infty} d\bar{t} G^{>}_{\alpha m}(\bar{t},t') \Sigma^{<}_{m\beta}(t,\bar{t}) \} \qquad (6.1b)$$

Where, α, β, n, m, are energy state indices. The task of solving the matrix equations basically involve formulation of an expression for the self energy matrix components appearing in the equations. With no ambiguity this energy term can be thought as consisting of the contribution due to the interaction of particles with the radiation field, Σ^{F} , and the contribution from the interaction of the particles of the system, Σ^{eff} . That is,

$$\Sigma^{S}_{\alpha m}(t) = \Sigma^{F}_{\alpha m}(t) + \Sigma^{eff}_{\alpha m}(t) \qquad (6.2a)$$

The light field contribution to the self energy can be described following the dipolar approximation as

$$\Sigma^{F}_{\alpha m}(t) = -dE(t) = -\tfrac{1}{2} e d E_{o}(t) [e^{i(\omega t+\varphi)} + e^{-i(\omega t+\varphi)}](1-\delta_{\alpha m}) \qquad (6.2b)$$

Where, the parameters E_o , ω , and φ are the amplitude, frequency and phase parameters of the radiation field respectively with the remaining

quantities, e and d, represent the electronic charge and the dipole length. The self energy corresponding to the internal interaction is the result of inter and intra state interactions that accounts for the Coulomb interaction and as well the exchange and correlation effects.

$$\Sigma^{eff}_{\alpha m}(t) = V^{eff}(t)\rho_{\alpha m}(t) \qquad (6.3a)$$

Where, the effective potential is the sum of the total electrostatic potential $V^{tot}(t)$ which satisfies the Poisson's equation at the local scale and the potential associated to the exchange and correlation interactions $V^{XC}(t)$:

$$V^{eff}(t) = V^{tot}(t) + V^{XC}(t) \qquad (6.3b)$$

It is known of course that obtaining exact solution to the non equilibrium quantum many body dynamics is very difficult. One very popular approach is perhaps to use the Fourier transformation. However, this is doubtful when it comes to an inhomogeneous low dimensional system. In such a system separating position and energy is a difficulty. Also since the spatial inhomogneity in real space leads to non locality in the momentum space, there is not advantage in using it [95, 96]. Rather we deal with the real space coordinate basis so that we could directly associate with the structural features of the sample.

Subtracting the second equation in eq.6.1 from the first and taking the limit $t^1 \to t$ leads to an equation of motion for the equal time limit value of $G^<$;

$$\left[\frac{\partial}{\partial t} + \frac{i}{\hbar}\{\varepsilon_\alpha - \varepsilon_\beta\}\right]G^<_{\alpha\beta}(t,t) = -\frac{i}{\hbar}\sum_m [\Sigma^S_{\alpha m}(t)G^<_{m\beta}(t,t) - G^<_{\alpha m}(t,t)\Sigma^S_{m\beta}(t)] + \frac{\partial}{\partial t}\Gamma^<_{\alpha\beta} \qquad (6.4a)$$

Where, $\Gamma^<_{\alpha\beta}$ represents the scattering contributions;

$$\Gamma^{<}_{\alpha\beta}(t) = \frac{-i}{\hbar}\sum_{m}\{\int_{t_o}^{t} d\bar{t}[\Sigma^{>}_{\alpha m}(t,\bar{t})G^{<}_{m\beta}(\bar{t},t) + \Sigma^{<}_{\alpha m}(t,\bar{t})G^{<}_{m\beta}(\bar{t},t) - [G^{>}_{\alpha m}(t,\bar{t})\Sigma^{<}_{m\beta}(\bar{t},t) + G^{<}_{\alpha m}(t,\bar{t})\Sigma^{>}_{m\beta}(\bar{t},t)]\} \quad (6.4b)$$

Here, our interest is in the coherent regime absorption when the system is under very short radiation pulse. In practice, the pulse width of the exciting radiation pulse has to be well below the dephasing time τ_d which is characteristic of the system. For observation under a coherent pulse radiation of very short pulse width, in the femto second scale, the coulomb scattering and screening effects can be suppressed [97]. I*n* addition we limit our investigations to the low temperature experimental condition where the effects of phonon couplings are sufficiently suppressed. Then, it will be a reasonable approximation if the scattering term in eqs 5.4 is neglected. Also it is considered that at the ground state condition of the semiconductor nano material, all the valence levels are filled and all the higher levels are empty. For a clean sample with good geometrical perfection and where the effects of dangling orbital are restructured by passivation under appropriate atmospheric condition, the influence of mid gap states will be greatly reduced. When the sample prepared with the set requirements is under a short coherent radiation pulse of frequency ω which corresponds to the HUMO-LOMO energy separation in the sample, the states with energy difference close to this value will strongly couple with the radiation. For excitation by radiation of frequency at about the threshold for absorption and where the spectral width is narrow enough so that the strong coupling is limited to a value that does not exceed the level difference between nearest neighbor states, the absorption phenomenon could be analyzed using the local approximation. The equations of motion for the diagonal and off diagonal components of the equal time limit correlation function could be written therefore, from eq.3.26 and based on the arguments in the preceding paragraph, as

$$\frac{\partial}{\partial t} G^{<}_{vjcl}(t,t) = \frac{i}{\hbar}[\varepsilon_{cl}(t) - \varepsilon_{vj}(t)]G^{<}_{vjcl}(t,t) + \frac{i}{\hbar}[G^{<}_{vjvj}(t,t)\Sigma^{s}_{vjcl}(t) - \Sigma^{s}_{vjcl}(t)G^{<}_{clcl}(t,t)] \quad (6.5a)$$

$$\frac{\partial}{\partial t} G^{<}_{clvj}(t,t) = -\frac{i}{\hbar}[\varepsilon_{cl}(t) - \varepsilon_{vj}(t)]G^{<}_{clvj}(t,t) - \frac{i}{\hbar}[\Sigma^{s}_{clvj}(t)G^{<}_{vjvj}(t,t) - G^{<}_{clcl}(t,t)\Sigma^{s}_{clvj}(t)] \quad (6.5b)$$

Similarly the diagonal lesser Green functions could be obtained as

$$\frac{\partial}{\partial t} G^{<}_{vjvj}(t,t) = -\frac{i}{\hbar}[\Sigma^{S}_{vjcl}(t,t)G^{<}_{clvj}(t,t) - G^{<}_{vjcl}(t,t)\Sigma^{<}_{clvj}(t,t)] \quad (6.6)$$

$$\frac{\partial}{\partial t} G^{<}_{C,C}(t,t) = -\frac{i}{\hbar}[\Sigma^{<}_{CVj}(t,t)G^{<}_{VjC}(t,t) - G^{<}_{CVj}(t,t)\Sigma^{<}_{VjC}(t,t)] \quad (6.7)$$

Where,

$$\varepsilon_{cl}(t) = \varepsilon^{o}_{cl} + \Sigma^{S}_{clcl}(t) \quad (6.8a)$$

$$\varepsilon_{Vj}(t) = \varepsilon^{o}_{Vj} + \Sigma^{S}_{VjVJ}(t) \quad (6.8b)$$

and the diagonal self energy components are given as

$$\Sigma^{S}_{clcl}(t) = V_{eff}(r,t)\rho_{cl}(r,t) \quad (6.9a)$$

$$\Sigma^{S}_{VjVJ}(t) = V_{eff}(r,t)\rho_{Vj}(r,t) \quad (6.9b)$$

The off diagonal self energies as determined based on the Jaynes-cummings [98] representation of the radiation field and using the non rotating approximation, A8-A9, are

$$\Sigma^{S}_{vjcl}(t) = -e^{i(\omega t+\varphi)}[\tfrac{1}{2}dE_0(t)\hat{b}^{\dagger} + V_{eff}\rho_{vjcl}(t)e^{-i(\omega t+\varphi)}] = -\Omega^{\dagger}_{R}(t)e^{i(\omega t+\varphi)} \quad (6.10a)$$

$$\Sigma^{S}_{CVj}(t) = -e^{-i(\omega t+\varphi)}[\frac{1}{2}dE_0(t)\hat{b} + V_{eff}\rho_{CVj}(t)e^{i(\omega t+\varphi)}] = -\Omega_R e^{-i(\omega t+\varphi)} \qquad (6.10b)$$

The role of the diagonal and off-diagonal components of the singular self energy matrices now becomes apparent; the diagonal components go to renormalize the carriers' energy and the off-diagonal components renormalize the Rabi frequency. The off-diagonal components therefore appear as the natural modification of the field.

To get a result that we could easily associate with observables, it will require us to solve for the correlation functions in eq.6.5 and eq.6.6. From combining the sets of equations as it is demonstrated by the steps that led to A17 (Appendix A), we find that the time evolution of the diagonal components of the equal time limit correlation functions describing the system is in the Lindblad form [99]. That is,

$$\frac{d}{dt}G^{<}_{VjVj}(t,t) = \frac{i}{\hbar}[\frac{\Omega^{\dagger}_R(t)\Omega_R(t)}{\Delta_{\varepsilon}(t)}, G^{<}_{VjVj}(t,t)] \qquad (6.11)$$

Where, $\Delta_{\varepsilon}(t)$ is the time dependent detuning;

$$\Delta_{\varepsilon}(t) = \varepsilon_C(t) - \varepsilon_V(t) - \hbar\omega \qquad (6.12)$$

This is an equation of motion with solution in the form, A20,

$$\rho_{Vj}(t) = \rho_{Vj}(t_o)\exp[\frac{i}{\hbar}\int_{t_o}^{t} d\bar{t}\,\frac{\Omega^{\dagger}_R(\bar{t})\Omega_R(\bar{t})}{\Delta_{\varepsilon}(\bar{t})}] \qquad (6.13)$$

Obviously, the integral at the exponent of the term in the right hand side of this equation has points of singularities at time values that correspond to the condition of resonance coupling the radiation. Depending on the length of observation time but still within the coherent regime, the integration up to the observation time t, may involve a number of

singularities (at τ_i's). Firstly, the integral at each singularity in general has two contributions; the Lorenzian term and the principal integral. The former renormalizing the amplitude term whiles the later the frequency and the phase. For the range of time that covers a number of such singularities, the solution appears containing the accumulation of the contributions from the integrals about all these points. This is suggesting the Markovian nature of the dynamical process. Eq.6.13, therefore, takes the form (A.25)

$$\rho_{Vj}(t) = \rho_{Vj}(\tau_c)\exp\{\frac{i}{\hbar}P\int_{\tau_c}^{t} d\bar{t}\,\frac{\Omega_R^{\dagger}(t)\Omega_R(t)}{\Delta_{\varepsilon}(t)} - \frac{\pi}{\hbar}\sum_{i=1}\frac{\Omega_R^{\dagger}(\tau_i)\Omega_R(\tau_i)}{\dot{\Delta}_{\varepsilon}(\tau_i)}\} \quad (6.14)$$

Where, τ_c is the characteristic time which marks the build up of dynamically correlated states. Clearly the first exponential term renormalizes the phase and sets the frequency of oscillation while the second goes to modify the amplitude. The total phase introduced in the processes and as well the amplitude are dependent of the number of turns the system approaches to the resonance condition and the normalizing factor introduced at each time segment. Based on this understanding the occupation probability of the level Vj at time t: $\tau_\ell < t < \tau_{\ell+1}$, are found to be given by (A27)

$$\rho_{Vj}(t) = \mathrm{Re}[e^{-A_\ell}e^{i[\omega_R^{\ell}t+\tilde{\varphi}_\ell]}\rho_{Vj}(\tau_c)] \quad (6.15)$$

As could be noticed from eq.6.14 the term A_ℓ attending the amplitude renormalization is given by

$$A_\ell = \sum_{i=1}^{\ell}\frac{\pi}{\hbar}\frac{\Omega_R^{\dagger}(\tau_i)\Omega_R(\tau_i)}{\dot{\Delta}_{\varepsilon}(\tau_i)} \quad (6.16a)$$

The frequency of oscillation ω_R^ℓ and the phase $\widetilde{\phi}_\ell$, on the otherhand, are determind from a short time scale averaging of the integral in eq.6.14 using the steps that led to eq. B10. This leads the two quantities ω_R^ℓ and $\widetilde{\phi}_\ell$, to be given respectively by (eqs.A27-A29).

$$\omega_R^\ell = \left\langle \frac{\Omega_R^\dagger(\tau^\ell)\Omega_R(\tau^\ell)}{2\hbar\left|\Delta_\varepsilon(\tau^\ell)\right|} \right\rangle = \left\langle \frac{\left|\Omega_R(\tau^\ell)\right|^2}{2\hbar\left|\Delta_\varepsilon(\tau^\ell)\right|} \right\rangle \qquad (6.16b)$$

$$\widetilde{\phi}_\ell = \phi_\ell - \omega_R^\ell \tau_\ell \qquad (6.16c)$$

$$\phi_\ell = \sum_{i=1}^{\ell-1} \left\langle \frac{\left|\Omega_R(\tau^i)\right|^2}{2\hbar\left|\Delta_\varepsilon(\tau^i)\right|} \right\rangle (\tau_{i+1} - \tau_i) = \sum_{i=1}^{\ell-1} \omega_R^i (\tau_{i+1} - \tau_i) \qquad (6.16d)$$

Here, $2\tau^\ell < \tau_{\ell+1} - \tau_\ell$ refers the time interval, centered at the time of interest t: $\tau_\ell < t < \tau_{\ell+1}$, over which the frequency term is averaged.

After the occupation probability at either of the coupled energies is determined it will be easier to compute for the other from using the conservation of probabilities;

$$\rho_c(t) = \rho_{V_j}(t_o) - \rho_{V_j}(t) \qquad (6.17a)$$

$$\rho_C(t) = [\rho_{V_j}(t_o) - \rho_{V_j}(\tau_c) e^{-A_\ell} Cos(\omega_R^\ell t + \widetilde{\varphi}_\ell)] \qquad (6.17b)$$

This expression represents the evolution of the excited state population in a correlated system. It therefore describes the phenomenon taking place after the build up of correlation between the states of the system. When it

becomes the interest to include the temporal region $t < \tau_c$ the behavior is described by the usual exponentially decaying relation, with decay parameter κ .The result is

$$\rho_C(t) = \rho_{Vj}(t_o)[1 - e^{-\kappa t}] \qquad t < \tau_c \quad (6.18)$$

$$\frac{\rho_C(t)}{\rho_{Vj}(t_o)} = [1 - e^{-[\kappa\tau_c + A_\ell]} Cos(\omega_R^\ell t + \tilde{\varphi}_\ell)] \qquad t > \tau_c \quad (6.19)$$

This expression suggests the oscillation of the coherent regime transition probability at the renormalized Rabi frequency and with a renormalized amplitude and phase as given in eqs.6.16.

6.4 Locality and Orbital Entanglement at Lower Energy States

Features that are associated with size and structural inhomogneity, the time dependence of the energy levels in the local atoms together with the very quantum mechanical nature play characteristic role in determining the system response for a perturbing radiation field. The structural condition determines the distribution, in energy, of the filled states and the spatial dependent relative detuning. The time dependence of the levels appears as a means of monitoring the tuning and detuning between the coupled levels. The size of the samples being in the confinement regime, leads to the emergence of non local and widely separated quantized levels and quantum number dependent density of states. There is a limitation in the maximum number of electrons a given level could accommodate. However, the filling of the levels has to respect the Pauli's exclusion principle.

For excitation by radiation at energy close to the HOMO-LUMO gap, for instance, there are only two electronic states to be filled at the LUMO level. Electrons of opposite spin polarizations could make transition by absorbing

photons at the same energy. Since the transition of an electron from a site modifies the local atomic environment the maximum probability for transition at any particular moment is from a level with energy closer to resonance energy for absorption transition. The atomic orbitals contributing electrons of opposite spin polarization could be labeled, depending on the spin polarization of the electron undergoing transition from the respective atomic sites, using their position or alternatively the energies of their outer orbital electron states; $\left|\psi(\varepsilon_V(\vec{r},t));\uparrow\right\rangle$ ($\left|\psi(\varepsilon_V(\vec{r},t));\downarrow\right\rangle$) and $\left|\psi(\varepsilon_V(\vec{r}^{\,1},t));\downarrow\right\rangle$ ($\left|\psi(\varepsilon_V(\vec{r}^{\,1},t));\uparrow\right\rangle$) Where, the time and spatial dependent level energies, as given by eq.6.8 and eq.6.9, are

$$\varepsilon_V(\vec{r},t) = \varepsilon_V^o(\vec{r}) - \Sigma_V^S(\vec{r},t) \qquad (6.20a)$$

and

$$\varepsilon_V(\vec{r}^{\,1},t) = \varepsilon_V^o(\vec{r}^{\,1}) - \Sigma_V^S(\vec{r}^{\,1},t) \qquad (6.20b)$$

The orbitals tuned to strongly couple with the excited state contribute electrons of opposite spin polarization to the conduction state have similar energy and therefore

$$\varepsilon_V(\vec{r},t) = \varepsilon_V(\vec{r}^{\,1},t) \qquad (6.21)$$

There is a common view that two adjacent atoms in a semiconductor material such as silicon are bonded by sharing two electrons of opposite spin polarizations. The transition of an electron of either spin polarization then makes the other electron to be strongly held by the atoms lowering its energy. This makes the atoms with overlapping orbitals not to contribute further for the transition by the same photon energy. That is the two atoms must be distant by an order exceeding the mean atomic spacing, say **a**, in the material.

$$\left|\vec{r}^{\,1} - \vec{r}\right| > \boldsymbol{a} \qquad (6.22)$$

There are now two possibilities for this. One obvious case is the situation where the time dependent level shift induced on atomic orbitals following the transition of electrons from the neighboring atoms is insufficient to compensate the relative detuning between the levels. In this case the transition will be limited to involve orbital states with the same ground state energy. The spin degenerate excited state is coupled with HOMO levels of the same energy with the transition from either is negligibly small to tune the other. In this case each strongly coupled region separated by a distance exceeding the nearest neighbor separation could be regarded to form a photon coupled system;

$$\alpha\left|\psi(\varepsilon_V^o(\vec{r})\right\rangle\left|n\right\rangle \pm i\beta\left|\psi(\varepsilon_C\right\rangle\left|n-1\right\rangle \qquad (6.23)$$

(α and β being constant parameters). The time evolution of the excited carriers due to the couplings at all the equivalent atomic sites is determined by solving a single equation. The overall response of the system is then computed from the superposition of the contributions from these sites. The result in this case appears in suggesting Rabi oscillations with amplitude that carries information on the interference between the contributions from the bare states.

Another interesting case comes when the time dependent level shift induced on atomic levels due to transitions from the neighboring sites is sufficient to compensate the relative detuning between levels at different sites. Since the time dependent level shift is in the same sense for all sites the effect will bring the levels with negative initial detuning toward resonance while it shifts the other levels more away from resonance. This leads to the emergence of states where the fluctuation in the occupation

probability of one tunes the energy of the other at close resonance for absorption and detunes through time.

When an electron of one spin polarization makes an absorption transition from one site, an electron of opposite spin polarization from another site copies the change in the local environment and responds by undergoing transition (Fig.6.1). This then leads the subsystem to become indistinguishable. The emerging pair atomic orbitals in the HOMO sub band (Fig.6.1) could be represented, following the result in eq.5.9, as

$$\left|\psi_V(\vec{r};\vec{r}^{\,1},t)\right\rangle = \left|\psi_V(\vec{r},t)\right\rangle\left|\psi_V(\vec{r}^{\,1},t)\right\rangle[\left|\uparrow\vec{r}\right\rangle\left|\downarrow\vec{r}^{\,1}\right\rangle - \left|\downarrow\vec{r}\right\rangle\left|\uparrow\vec{r}^{\,1}\right\rangle] \qquad (6.24)$$

The dynamics in this case could be studied from analyzing the temporal evolution of the entangled orbital states. The concept local in this case need to be modified to cover all the points at radial positions $\Delta\vec{r} = \vec{r}^{\,1} - \vec{r}$ for which the condition

$$\Sigma_V^S(\vec{r} \pm \Delta\vec{r}, t) \geq \varepsilon_V^o(\vec{r} \pm \Delta\vec{r}) - \varepsilon_V^o(\vec{r}) \qquad (6.25)$$

is satisfied. This is determined, in general, by the atomic energy dispersion and the spectral distribution of the photons in the radiation.

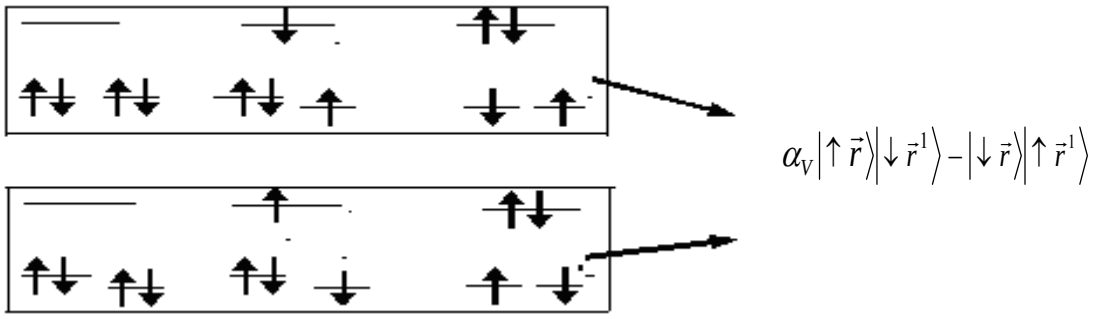

Fig. 6.1: *Illustration for the formation of entangled lower orbital states.*

Equation 6.24 shows that the atoms contributing their electrons to the excited level are dynamically correlated in such a way that it will be difficult to factor out the contribution of either from the composite state. The atomic orbitals are entangled. The entangled lower level orbitals disentangle upon photon emission and entangled again if photon is absorbed at the subsequent steps. In short, the HOMO levels entangle and disentangle in sequence. On the basis of the foregoing arguments, the fluctuation in one half cycles is such as to increase the coupling and in the other it is in the opposite sense. Consequently, the quantity $\dot{\Delta}_{\varepsilon}$ in the equations takes different sign alternatively. Then, the exponential commutation relation for the the two consecutive terms that appear at the exponent of the amplitude factor in eq.6.14 under this approximation will turn out to be related as

$$A_{\ell} = \frac{\pi}{\hbar}[(\frac{\left|\Omega_R(\tau_1)\right|}{\left|\dot{\Delta}_{\varepsilon}(\tau_1)\right|} - \frac{\left|\Omega_R(\tau_2)\right|}{\left|\dot{\Delta}_{\varepsilon}(\tau_2)\right|}) + \ldots + (\frac{\left|\Omega_R(\tau_{\ell-1})\right|}{\left|\dot{\Delta}_{\varepsilon}(\tau_{\ell-1})\right|} - \frac{\left|\Omega_R(\tau_{\ell})\right|}{\left|\dot{\Delta}_{\varepsilon}(\tau_{\ell})\right|})] \quad (\ell \text{ even}) \quad (6.26a)$$

$$A_{\ell} = \frac{\pi}{\hbar}[(\frac{\left|\Omega_R(\tau_1)\right|}{\left|\dot{\Delta}_{\varepsilon}(\tau_1)\right|} - \frac{\left|\Omega_R(\tau_2)\right|}{\left|\dot{\Delta}_{\varepsilon}(\tau_2)\right|}) + \ldots + \frac{\left|\Omega_R(\tau_{\ell})\right|}{\left|\dot{\Delta}_{\varepsilon}(\tau_{\ell})\right|}] \quad (\ell \text{ odd}) \quad (6.26b)$$

From the relation in eq.6.26 we shall notice that the change in amplitude that is taking place at one pont of singularity is tending to recover the change introduced at the preceeded singularity point. In the special case when the radiation is of fixed mean photon number, the summation in eq.6.16a and thus the exponent term A_{ℓ} reduce to a very simple form;

$$A_{\ell} \to 0 \quad (\ell \text{ even}) \quad (6.27a)$$

$$A_{\ell} \approx \frac{\pi}{\hbar} \frac{\left|\Omega_R\right|^2}{\left|\dot{\Delta}_{\varepsilon}\right|} \quad (\ell \text{ odd}) \quad (6.27b)$$

The amplitude renormalization as prescribed by eqs.6.28 is schematically represented in Fig6.2b.

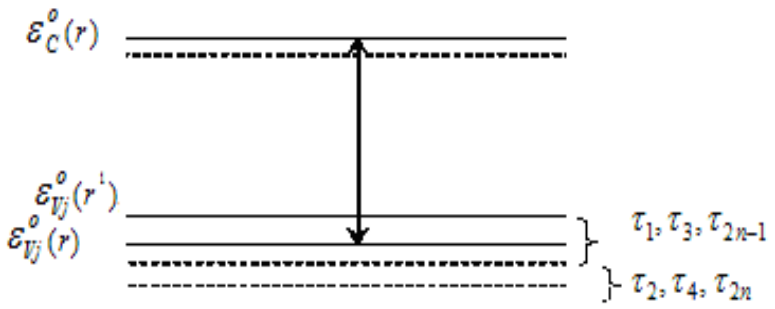

(a)

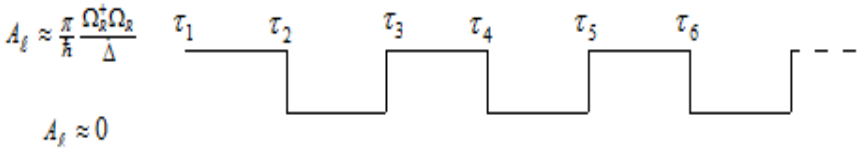

(b)

Fig. 6.2: *Schematic diagram for illustrating evolution of low-energy states entanglement* **(a)** *the width over which the energy of the low- energy entangled state is fluctuating.* **(b)** *Amplitude renormalizing factor picked at instances of changes of sign in the rate of fluctuation in the coupling.*

Considering the expressions in eq.6.16c and eq.6.16d and rearranging, one can easily show that the phase term $\widetilde{\phi}_\ell$ could be represented alternatively as

$$\widetilde{\phi}_\ell = \sum_{i=1}^{\ell} (\omega_R^i - \omega_R^{i+1})\tau_{i+1} - \omega_R^1 \tau_1 \qquad (6.28a)$$

$$\widetilde{\phi}_\ell = -\omega_R^1 \tau_1 \qquad \text{For } \omega_R^i \text{ constant} \qquad (6.28b)$$

Probability oscillation of fixed Rabi frequeny is of special interest. In this particular case, the probability oscillates with nearily constant phase that is introduced during the build up of the coupling at the initial stage.

6.5 Interpretation of the Occupation Probability Oscillation

We shall easily notice from the results in eq.6.16 and eq.6.19 that the model predicts the oscillation of the excited state occupation probability. The occupation probabilities versus time graphs shown in Figs.6.3 are drawn assuming fixed number of photon flux. This implies that there is occupation probability oscillation even when the photon flux in the radiation is fixed. It is of course true that the modified Rabi frequency in eq.6.16b suggests constant frequency of oscillations for fixed mean photon number. More clear vision of the phenomenon, however, requires close inspection of the modified Rabi oscillation ω_R^{ℓ} since it consists of information which may intrigue our conception of the phenomenon. Primarily, ω_R^{ℓ} is determined by photon number correlation in the incoming radiation flux, the intra and inter band local correlations that couple the states via exchange of electron and spin polarizations and lastly by the correlation between these. In absence of correlation between the photon flux, $\omega_R^{\ell} = 0$. That is, for the phenomena under discussion to take place the incoming radiation needs to be initially coherent and the predicted oscillation of occupation probabilities is non existent if the radiation is incoherent.

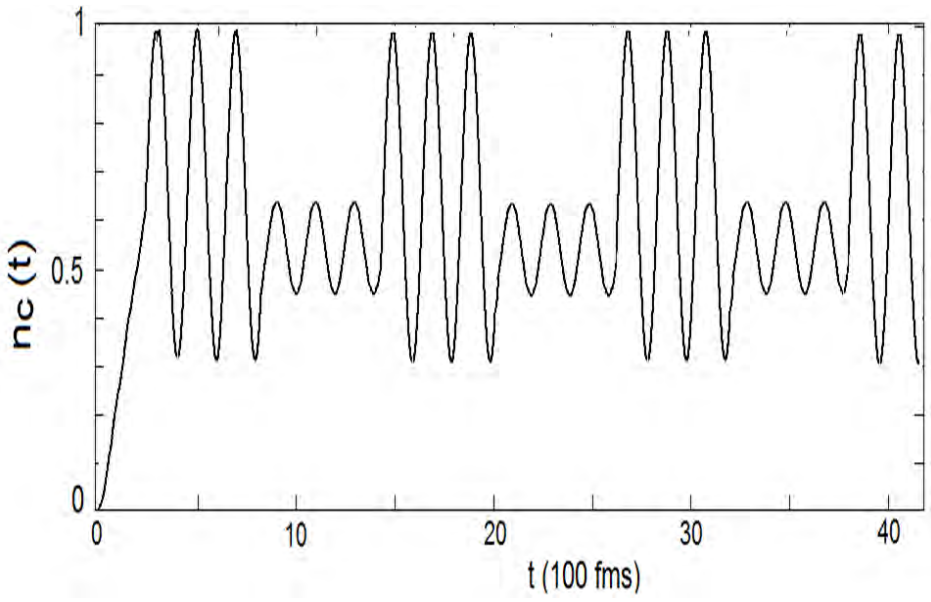

Fig. 6.3: *Evolution of the excited state population under radiation field of fixed mean photon number predicted by the model*

The predicted temporal evolution of the occupation probability in a photo-excited semiconductor nanostructure, Fig.6.3, shows amplitude fluctuation. The number density of excited electrons oscillates with amplitude that decays, collapses, and then revives repetitively (Fig.6.3a); Collapse and revival phenomenon as often referred in quantum optics. According to the understanding that leads to the result in eq.6.28, the collapse and revival is expected to take place even when the photon flux in the incoming radiation is considered fixed. The fluctuation in the photon number rather manifests itself by local bumps on the probability curve. The periodic amplitude fluctuation in the occupation probability is understood in this model as to be the signatures of many body effects in the nanostructure. That is, there must be the many body effect that is responsible for the correlated exchange of photon between the entangled orbital and the photon flux. The collapse is when the entangled atoms given out the stored energy at the moment of disentangling. The revival is when the energy stored in the atomic orbital builds up following the entanglement.

The predicted oscillatory behavior in Fig.6.3 shows qualitative agreement with the Rabi oscillations that have been reported for other systems [100-106]. This can be deduced easily from comparing the present result with the evolution of the occupation probabilities of two quite different systems included in Fig.6.4 and Fig.6.5, for the purpose. The diagram in Fig.6.4 shows the collapse and revival phenomenon of a two level atom in a cavity mode [100,101] where as the diagram in Fig.6.5 depicts the occupation probability oscillation in a solid structure recently reported in [102].In fact this later diagram (Fig.6.5) is illustrating the occupation probability population evolution in the Josephson junction under a resonant photon mode in a cavity [102]. The population evolution curves reported for semiconductor nanostructures are also structurally similar to this result [103-106].

It is of course true that in all cases the experimental condition is where the atomic electrons undergoing transitions as a result of interaction with the photon flux. This interaction is between particles that obey different statistics; The Bose-Einstein statistics for the photons and the Fermi-Dirac statistics for the electrons. However, the atomic flux entering and leaving a cavity and solid state systems are quite different as far as the many body effects are concerned. It is also the expectation the pronounced quantum mechanical interaction between the particles in the solid leaves its signature on the short time evolution of the electrons.

The behavioral similarities between the population evolution curves messages that the oscillation of excited state population and the collapse and revival phenomenon are the common characteristic features in photon coupled atomic systems and the solid structures considered. It is not proper, however, to account a similar physical origin for the observed phenomenon based on this mere visual inspection of the probability evolution graphs (Figs.6.3-5). Finding an explanation to the observation requires further steps of testing the results with respect to the

characteristic dependence of the phenomenon on the parameters of the material and the radiation field.

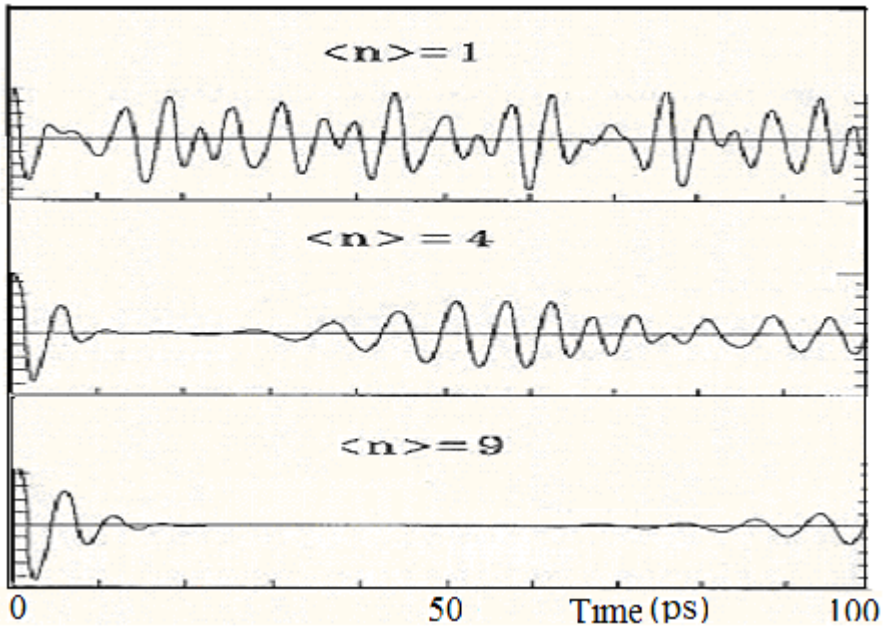

Fig.6.4: *Evolution of the excited state population of a two level atom interacting with a single mode cavity field for different values of mean photon number.[100].*

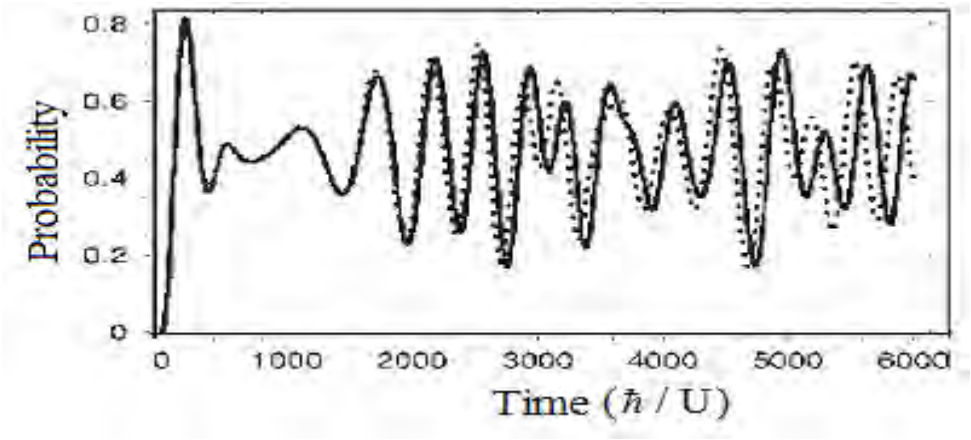

Fig.6.5: Rabi oscillation in the Josephson junction under a resonant photon mode in a cavity [102].

The dependence on the photon number and inter-atomic interaction of the Rabi frequency, the period of revival and collapse, the probability amplitude

are among the key aspects we need to explore. To aid the purpose it will be more convenient to represent the electric field of the radiation in the Jaynes Cummings model

$$\vec{E}(t) = i(\hbar\omega / 2 \in_o V)^{\frac{1}{2}} \hat{e}[\hat{b}\exp(-i\omega t) - \hat{b}^{\dagger}\exp(i\omega t)] \qquad (6.29)$$

Where ω is the radiation frequency, $\hat{b}(\hat{b}^{\dagger})$ the annihilation (creation) operator for the photon field, $\hat{e}$ is the unit polarization vector, $\in$ the permittivity and V is the photon confining volume. Using this in the expression for the Rabi operator (eq.6.16b) and for the exponent in the amplitude term (eq.6.28), we can easily identify that

$$\omega_R^{\ell} = \left\langle \frac{\Omega^{\dagger}\Omega}{2\hbar\Delta_{\varepsilon}} \right\rangle = \frac{\omega d_e^2 \tilde{n}_{ph}}{2 \in V \Delta_{\varepsilon}} \qquad (6.30)$$

$$A_{\ell} \approx \frac{\pi}{\hbar} \frac{\Omega_R^{\dagger}\Omega_R}{\dot{\Delta}} = \frac{\pi\omega d_e^2 \tilde{n}_{ph}}{2 \in V \dot{\Delta}} \qquad (6.31)$$

Clearly, the expression in eq.6.30 suggests a mean photon number dependent occupation probability oscillation. There is in fact nothing unfamiliar in that even though the common Rabi oscillation for a free atom-photon system doesn't fall under this characteristic class. For systems far to be considered ideal, this is rather a widely anticipated notion. Several experimental and theoretical studies that have been devoted in dealing on the quantum Rabi oscillations of atoms in real atomic beams [107-110] and solid structures [103-106] interacting with photon modes have reported the photon number dependent nature of the oscillations.

The occupation probability predicted by our model is noticed in consisting of information, other than the photon number dependence, on the inter-atomic coupling parameter that contributes to the emergence of the observed phenomenon. The expression (eq.6.30) is identical with the results found on similar investigations that have been made on the

evolution dynamics of excited electrons where the quantum mechanical interaction between the particles of the system leave noticeable signatures on the observed phenomenon. There is a striking similarity for instance between the expression in eq.6.30 and the results determined for photon coupled trapped ions that lead to the observation of non classical states such as the generation of Schrödinger cat and anti bunching in resonance fluorescence [111]. The comparison with the results in [111] suggest the interaction energy of the trapped ion to be given by $\mathcal{E}_{\ell} = \hbar\omega_R^{\ell}$, with ω_R^{ℓ} is as given by eq.6.30. Interestingly, the result also reproduces the interaction energy of cooper pairs in a photon-cooper pair entangled states [102]. In all the above mentioned cases the observed phenomenon is described to be the outcome of a continuous exchange of energy between the correlated lower levels and the photon in the radiations. This is the same understanding the modeling in this thesis report also shares.

Close inspection of eq.6.30 also shows the applicability of the result for general application. To show this we only require putting the expression in a form convenient to relate with the frequency of Rabi oscillation, ω_R^o, of atoms coupled with a cavity mode;

$$\omega_R^{\ell} = g\omega_R^o \tag{6.32}$$

Where,

$$g = \frac{\Omega}{2|\Delta_{\mathcal{E}}|} \tag{6.33}$$

The modified Rabi oscillation here appears as a product of two terms; the Rabi frequency of atoms in a photon-atom entangled state and a parameter that represents the strength of the photon-atom coupling in the scale of the dynamic coupling between the particles of the system. According to this scheme, the Rabi oscillation of the free atom is a particular situation that could be viewed as the dynamical process which the same expression in

eq.6.30 represents as a limiting case of balanced interaction. That is $\omega_R^{\ell} \approx \omega_R^{o}$, as $g \to 1$. Similarly, the frequency of oscillation will be large and becomes difficult to observe when $g \to \infty$ $(\omega_R^{\ell} \to \infty)$. This is when $\Delta \to 0$ and thus corresponds to the situation where quantum indistinguishability appears to play a prominent role. The result therefore reflects the challenge in observing the Rabi oscillation in solid structures where the entanglement between the lower levels is too much to observe.

So far we only mentioned the general fact that the quantum Rabi frequency depends on the number of photons. This is what the expression in eq.6.30 also predicts. There is a danger of losing the information on the phenomenon unless eq. 6.30 is analyzed without taking in to account the physical situation which the equation is intended to describe. The expressions are to describe the phenomenon in the presence of many body interactions and in the temporal regime where the interacting states are evolving in a correlated manner. For the phenomenon predicted by the equation to take place, the entanglement of the non overlapping HOMO levels need to take place. This requires a characteristic minimum number of photons. That is, investigating the prediction of the mathematical results by arbitrarily varying the photon number to a range lower than the threshold value can not have validity from physical points of view. Secondly, the probability oscillation is a likely physical consequence even without the many body effects or when these are negligibly small to be considered. The oscillation in this case is determined by the life time of the excitation with respect to stimulated emission. The presence of the inter-atomic interaction now creates an atomic environment where the time scales for the different atoms are synchronized by the computation between the interactions persisting in the system.

The graph in Fig.6.6 shows the predicted photon number dependence of the Rabi oscillation that follows from optical coupling of the HOMO levels with the spin degenerate LUMO level. The initial rise portion of the curves

and the shift in position of the characteristic time τ_c in Fig.6.6 is describing the frequency dependent nature of the phenomenon. With other conditions remain fixed, the initial rise portion will be steeper and the position of τ_c on the time axis shifts toward the origin with increasing photon number and the reverse upon lowering it. When the radiation strength is very low, τ_c will be very large implying that the interaction is unlikely to result a population inversion when its strength is below a characteristic minimum. The oscillating part of the curves also carries similar information on the radiation intensity dependence. Further increase in the photon number, in the situation when operating by photon number above threshold, leads to a reduction in amplitude and an increase in the frequency of the probability oscillation.

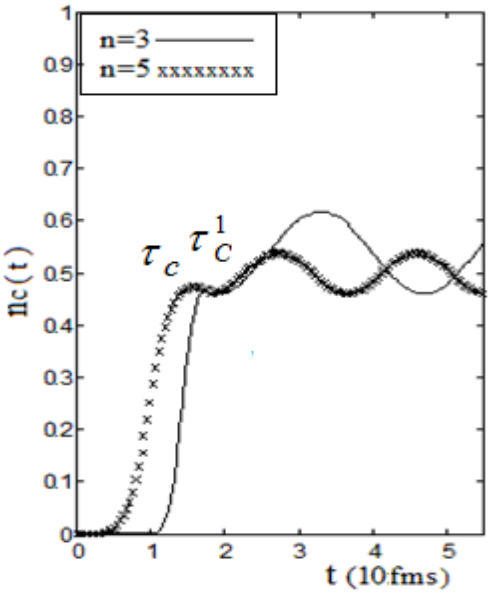

Fig. 6.6: *Photon number dependence of Rabi oscillation in nanostructure*

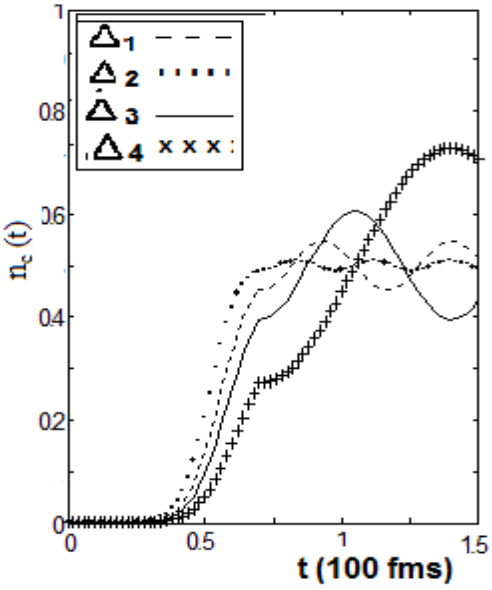

Fig. 6.7*: Dependence of Rabi oscillation on relative detuning at fixed photon number*

The curves in Fig.6.7 are showing the predicted population evolution characteristics under constant mean photon number but different rates of detuning. The smaller the oscillation frequency of the transition probability

is implying a higher detuning rate. The inter-atomic correlation shows the tendency to reverse the change induced by the action of the field. For the correlation to build up and lead to the entanglement of inter atomic orbital states, the change in the detuning has to be in the order that could compensate the relative detuning between the atomic orbitals to be coupled via their interactions with the excited state. This characteristic dependence on the relative detuning between the interacting non degenerate HOMO levels is manifestly the dependence on the sample structure of the phenomenon. When the relative detuning is very large and also when the inter-atomic coupling is very small, the entanglement may not take place. This characteristic dependence has a practical importance in the step toward monitoring the entanglement and hence a practical value in technology

6.6 Interpretation from the Perspective of the Quantum Theories of a Continuous Measurement

In our current study the observable is the occupation number density of atomic orbitals. The dynamic environment is monitored by pumping the material with radiation. Just following the pulse arrival, the electron strongly driven by the radiation undergoes a transition leaving behind a charged core with an unpaired spin electron. This process modifies the atomic environment leading to a strong coupling of the second electron with a spin polarization opposite from the former. This leads to induced dynamical interactions that control the occupation of the orbital levels coupled under the perturbing radiation. The temporal evolution of the occupation number density of atomic states is a resourceful dynamical character for studying the interactions and the material response under the monitored external conditions.

To study the dynamic correlation effects, it is however the coherent regime that will be the appropriate time window. This is so, primarily, since

the relevant information on the dynamical correlation effects will get lost as the coherence deteriorates. The focus is therefore on the dynamical history taking place within a bounded time continuum. To fix ideas, the interest is on the dynamical events that take place from the moment of the first entry of the photons in to the material, t_o , up to the time $t = t_o + \tau_{coh}$ where the coherence in the system is lost. The curves in Fig.6.3 represent the occupation probability of the coupled orbital states for this temporal regime. The occupation probability oscillates with a photon number dependent Rabi frequency, eq.6.15, and with amplitude that collapses, then revives and collapses again repetitively. The oscillation behavior suggests a sub-scale of time where dynamical events with large amplitude of oscillation and a second with collapsing amplitude are taking place. At the time instants given by $t = \tau_{2\ell} + t_k$, where $t_k \leq \tau_{2l+1} - \tau_{2l}$, the amplitude of oscillation is a maximum. On the other hand it oscillates with collapsed amplitude at the time instants given by $t = \tau_{2\ell+1} + t_{k'}$, where $t_{k'} \leq \tau_{2l+2} - \tau_{2l+1}$.

The intervals with amplified and collapsed oscillations in atomic excitations respectively correspond to the "no" and "yes" events of the photon absorption. For radiation impressed to result excitations to the spin degenerate single quantized level, the amplified oscillation or no photon absorption is when the dynamical coupling between the lower orbitals contributing for the excitation is maximum and the orbitals are entangled. The collapse in the Rabi oscillation is when the orbitals are disentangled. For the situation under discussion we can describe the response of the system by representing it on the basis of the coupled atomic states. With no mentioning of the specific nature, let for a while consider the system be described by the states

$$\left|\psi(\tau_{2\ell} + t_k)\right\rangle = \left[U(\tau_1)U(\tau_2)....U(t_{2\ell})\right]\left|\psi(t_k, \alpha_e)\right\rangle \qquad (6.34a)$$

$$\left|\psi(\tau_{2l+1}+t_{k'})\right\rangle = [U(\tau_1)U(\tau_2)....U(\tau_{2l+1})]\left|\psi(t_{k'},\alpha_{de})\right\rangle \qquad (6.34b)$$

We now assume that at all the sub time intervals where there is an amplified Rabi oscillation the system could be represented on the same basis, $\left|\psi_e\right\rangle$, and for temporal segments where there is collapse in the oscillation on the same basis $\left|\psi_{de}\right\rangle$, eq.6.34, be rewritten as

$$\left|\psi(\tau_{2\ell}+t_k)\right\rangle = [U(\tau_1)U(\tau_2)....U(\tau_{2\ell})]C(\tau_{2\ell}+t_k)\left|\psi_e\right\rangle \qquad (6.35a)$$

$$\left|\psi(\tau_{2\ell+1}+t_{k'})\right\rangle = [U(\tau_1)U(\tau_2)....U(\tau_{2\ell+1})]C(\tau_{2\ell+1}+t_{k'})\left|\psi_{de}\right\rangle \quad (6.35b)$$

Clearly, each behaviors of the probability oscillation refer a dynamic history in a continuous time between two characteristic time boundaries. The time graph in each of the intervals $(\tau_{2\ell},\tau_{2\ell+1})$ and $(\tau_{2\ell+1},\tau_{2\ell+2})$ represent a continuous dynamical history. Such a record in the continuous dynamical history is when there is a continuous measurement. A procedure for continuous measurement demands to subdivide the time interval for each sub unit of the amplified oscillation or the oscillation with collapsed amplitude in to large number of small time scales Δt.

At the time instants $t = \tau_{2\ell} + k\Delta t$, where $k_{\max} \le \frac{\tau_{2l+1}-\tau_{2l}}{\Delta t}$, the occupation probability oscillates with amplified amplitude and the system is taken to be represented by the state vector $\left|\psi(\tau_{2\ell}+t_k)\right\rangle \equiv \left|\psi(\tau_{2\ell}+k\Delta t_L)\right\rangle$. The oscillation at the time instants $t' = \tau_{2\ell+1} + k'\Delta t'$, where $k'_{\max} \le \frac{\tau_{2\ell+2}-\tau_{2\ell+1}}{\Delta t}$, is characterized by the collapse in its amplitude with $\left|\psi(\tau_{2l+1}+t'_k)\right\rangle \equiv \left|\psi(\tau_{2l+1}+k'\Delta t_L)\right\rangle$ now being the state vector. Ideally one would like to let $\Delta t \to 0$ to simulate continuous measurements. But this is

impossible in the framework of standard quantum mechanics with ideal measurements due to the quantum Zeno effect [147,148]. If $\Delta t \to 0$, according to the quantum zeno effect the system being detected as an entangled states at $t_{2\ell}$ has to remain as entangled at $t_{2\ell+1}$ and consequently at $t_{2\ell+2}$ and at later times. This means, the dynamics is frozen to the same subspace for $\Delta t \to 0$.

Intuitively, Δt should be large enough for discrimination of the observation in the monitoring process and on the other hand it should be short compared to the effective life times. The small time scale satisfying these requirements is $\Delta t \equiv \Delta t_L$;

$$\tau_{\text{int}} < \Delta t_L < \tau_{LT} \tag{6.36}$$

Again Δt_L has to be less than the period of the observed Rabi oscillation, $T_R = \frac{\omega_R^{\ell}}{2\pi}$. This then lead us to write

$$\Delta t_L = \frac{T_R}{N_c} = \frac{\omega_R^{\ell}}{2\pi N_c} \tag{6.37}$$

Using eq.6.37 and the expression for the photon number dependent Rabi frequency, eq.6.30 we can see that the requirement under the inequality in eq.6.36 to be represented as

$$\frac{4\pi \in V\delta_{\varepsilon}}{\omega d_e^2 N_c \tau_{LT}} < n_{ph} < \frac{4\pi \in V\delta_{\varepsilon}}{\omega d_e^2 N_c \tau_{\text{int}}} \tag{6.38}$$

This relation shows the limitations in the mean photon number in the radiation flux for the analytical prediction of a photon number Rabi oscillation could describe the realities in the system. If we now arbitrarily

assign some value $n_{ph,\min}$, such that $n_{ph,\min} < n_{ph}$, for the term in the extreme left in eq. 6.38 and rearrange it, we get

$$n_{ph,\min} < n_{ph} < n_{ph,\min} \frac{\tau_{LT}}{\tau_{\text{int}}} \qquad (6.39)$$

The result can be used to approximate the maximum limit of the mean photon number from a priori knowledge of the two time scales or vice versa. However, the quantitative expression is only approximate mainly because it does not include the explicit photon number dependence of the effective life time.

The result in eq6.39 points out the condition for monitoring a continuous measurement of the atomic excitation temporal fluctuation and interprets the results using the analytical expressions developed. It doesn't tell us whether or not the measurement made at each unit time scale, the interaction with the probing photons, has a back action. In general, when a continuous measurement is made with each measurement being determined by the result of an initial precise measurement, the procedure falls under a class of measurement referred as a Quantum Non-Demolition (QND) measurement. The property measured under this condition is also referred as a quantum non-demolition observable [148,149].

For the atomic orbital occupation we are dealing about so far to be a QND observable, there should be no back action generated by the action of the probing photons. In other words, the state in the subsequent temporal division need not have to be due to cumulative effects of the back actions. This logically dictates us to make close inspection of the coefficient terms multiplying the basis in eqs.6.35. The expression for the state of the system does not contain the dynamic memory of all the past as it seemingly appeared in the forms of the equations. The cancellation of each term by the term next to it in the time order was described in section 6.4. That is, in absence of dissipating effects, or when this is negligibly small,

$$f_{2\ell+j} = [U(\tau_1)U(\tau_2)....U(\tau_{2\ell+j})] \qquad ((6.40)$$

That is, the term is determined by the process it passes through as it evolves from its state just before $\tau_{2\ell+j}$ to the state where it is just after this time mark. This makes the dynamical evolution Markovian.

The state of the system at each of the sub divided small time scale could be represented as

$$\left|\psi(\tau_{2\ell} + k\Delta t_L)\right\rangle = f_{2\ell} C(\tau_{2\ell} + k\Delta t_L)\left|\psi_e\right\rangle \qquad (6.41a)$$

$$\left|\psi(\tau_{2\ell+1} + k'\Delta t_L)\right\rangle = f_{2\ell+1} C(\tau_{2\ell+1} + k'\Delta t_L)\left|\psi_{de}\right\rangle \qquad (6.41b)$$

The system resets to a different state. This resetting event is what commonly referred as quantum jump. It is interesting to notice that, our model enabled to describe such a phenomenon involving resetting events without requiring to adopt the techniques proposed explain the processes; The quantum jump approach [150], the Monte Carlo wave functions [151]. In eqs.6.41, $\left|\psi_e\right\rangle$ the state vector in the entangled sub-space while $\left|\psi_{de}\right\rangle \equiv \left|\psi_f\right\rangle$ stands to represent the state in the Fock sub-space to which the system switches as the entangled state is disentangled. The term $f_{2\ell+j}$ is the measured value of the non Hermitian quantum jump operator that switches the entangle state to a Fock state and vice versa. Lastly, $C(t)$ is a term which depending on the temporal segment referred to be identified as the projector on to either the Fock or the entangled orbital subspace. The fact that each quantum jump switches the system from one state to the other characteristically different state but not to the same state is a consolidation to the QND nature of the observable.

6.7 Conclusions

An atom initially close to resonance to the exciting radiation will obviously have high probability to undergo transition; either absorption or stimulated emission depending the system at which it is prepared in the previous interaction/ condition. The transition of this atom results modification of the atomic environment in the neighboring region, leading to a time dependent level shift. Consequently the second atom copy the change in the atomic environment and get entangled with the former atom by undergoing a transition the leaves it to a spin polarized state opposite to the former atom. The result at this step is that both atoms will come to be off-resonance and therefore sanction their energy exchange with the radiation. The entanglement will then be accompanied with the detuning (atomic level) dependent relaxation through modifying the stimulated emission and inter-atomic level fluctuation.

Under the short time perturbation, a dynamical state is evolved where the lower initially filled levels with small relative detuning are correlated via the conduction state coupling and this forms a composite state with the photon and the excited state. The photon-atom entanglement is followed by dynamical correlation between the low energy orbital electrons at neighboring regions that result orbital entanglement. The coupled HOMO levels then entangled and disentangled leading to the collapse and revival phenomenon. In absence of entanglement between the lower orbital states which is so when either the level shift in neighboring atoms is larger than the energy the dynamical correlation could compensate or when the atomic levels are spatially degenerate, the phenomenon becomes likely to be describable on the basis of the interference between the occupation probability oscillations from different atomic sites. The orbital entanglement comes in to issue in the presence of non degenerate levels with small relative detuning. As the atoms contribute as the source and sinks to the photons, the field statistics need to be related to the atomic

statistics in a systematic manner [109]. Particularly in a manner it could describe how the entangling and disentangling of the coupled orbital states leaves its signature in the photon statistics. This appears as a process leading to the quantum mechanical stabilization of the photon number.

The result not only suggest the possible existence of entanglement of electronic states in a solid structure but as well demonstrates the physical origin and its interrelations with the parameters of the perturbing field and the structural features of the material. The possibility for generating entangled orbital states and controlling through the photon number dependence together with the capability to generate preset number of photons, which is possible at the present level, shows the promise for future application as basic quantum logic gates.

7

Voltage Triggered Dynamical Correlations of the Tunneling Regime

7.1 Background

Structural inhomogneity and confinement effects have significant position in creating the atomic environment that led to the various exotic phenomena in a semiconductor nanostructure. This is among the subjects we demonstrated in our theoretical investigation of the coherent regime absorption in the preceding chapter. The energy distribution of the atomic orbitals in the envisioned material structures is spatially correlated: the higher the separation between the sites, the higher is the relative detuning between their levels. What if this energy and spatial position correlation is violated? This is the case where correlation operating in the scale larger than the scale of the nearest neighbor separation will come in to issue. How close the materials have to be or how they have to be dynamically coupled in order to give rise to the correlation of the states in the two systems are the issues very important in the steps toward studying the related phenomena and device application of the assembly.

As the case in any measurement step, device application of materials is a technical procedure where the states in the component materials are made to couple in some desirable way. The states in two systems could be dynamically coupled via mechanisms that involve the exchange of bosons, fermions or both. The proximity coupling involving the transfer of electron and spin polarization waves between the interacting systems is when the scale of the separation distance between the systems is in regime for tunneling. The interaction between the electronic states in two

materials that form contacts or close enough to ensure electronic tunneling is an obvious representative of this type. For spacing exceeding this range, the feasibility for dynamically coupling the two systems is via photon exchanging mechanisms. The phenomena observed from photon exchanges between nanostructures in a cavity are the most common natural evidence for the later [112-114]. There should be, however, no feeling of sharp boundaries in the scale.

The emergence of the dynamically correlated states in general depends on the energy distribution of the states, the length scale of the spatial separation between the states in the two systems and temporal distribution of the occupation of electronic states in each material in a complicated way. The dynamical coupling via photon exchanging process between the states in the two regions is a process which requires the presence of photon exchanging dynamically coupled states in each of the interacting material system. The dynamical coupling involving the transfer of electrons or holes between the states in the coupled materials on the other hand could take place with or without involving photon exchanging interactions between the states in each material. The transport of photo generated electrons from one region to the other is an obvious physical example of the former. This will be considered in the next chapter. The emphasis in the present chapter is on the dynamical correlation when the scale of the spatial separation is in the tunneling regime. This is made with a particular concentration on a tunnel coupled system operating without processes that involve the temporal fluctuation of the occupation of the completely filled valence states in the semiconductor nanostructures. The dynamical coupling in this particular case is practically invoked via the application of a pulsating voltage.

Tunneling of electrons between coupled structures is the mechanism that underlies the operation of practically all devices in the present day microelectronics. On the other hand the discrete nature of electrons is a fact well known to everyone with some introduction to physics. However,

for several decades physicists and electrical engineers dealing on the transport phenomena were measuring voltage-current characteristics. The experimental observation of phenomena which are straightforward reconfirmation of the interdependence between discrete electronic states has become possible only since the late 1980s when the manufacturing technology reaches the level where mesoscopic materials become feasible [115, 116]. The interdependence is a possible outcome the interplay between the time scales of the states or equivalently the transition rates or interaction energies in the two regions.

7.2 Development of the Model

Our theoretical investigation of the voltage triggered dynamical coupling between two states in two nanostructures is made using the NEGF technique as the case demonstrated in chapter 6. Since it is our aim for the theoretical model to provide quantitative description of the effects of the dynamical correlation between discrete electronic states, the states of the particles need to be represented in the basis of the Hilbert space. This naturally dictates our formulation to include spin.

The equations of motion for the correlation function for electrons at the interfacial region is rewritten, therefore, as

$$i\hbar \frac{\partial}{\partial t} G^{<}_{n\sigma,\alpha\sigma'}(t,t') = \delta(t'-t) + \varepsilon_{n\sigma}(t) G^{<}_{n\sigma,\alpha\sigma'}(t,t') + \sum_{\ell\sigma_i} \Sigma^{S}_{n\sigma,\ell\sigma_i}(t) G^{<}_{\ell\sigma_i,\alpha\sigma'}(t,t') \qquad (7.1a)$$

$$-i\hbar \frac{\partial}{\partial t'} G^{<}_{n\sigma,\alpha\sigma'}(t,t') = \delta(t'-t) + \varepsilon_{\alpha\sigma'}(t') G^{<}_{n\sigma,\alpha\sigma'}(t,t') + \sum_{\ell\sigma_i} G^{<}_{n\sigma,\ell\sigma_i}(t,t') \Sigma^{S}_{\ell\sigma_i,\alpha\sigma'}(t') \qquad (7.1b)$$

When the equal time limit of the difference of these equations is taken in the same way as it was done in the step that led to eq.6.2, one gets for the diagonal, in level index, component of the lesser Green function

$$i\hbar\frac{\partial}{\partial t}G^{<}_{\alpha\sigma,\alpha\sigma'}(t,t') = \sum_{l\sigma_i}[\Sigma^{s}_{\alpha\sigma,l\sigma_i}(t)G^{<}_{l\sigma_i,\alpha\sigma'}(t,t') - G^{<}_{\alpha\sigma,l\sigma_i}(t,t')\Sigma^{s}_{l\sigma_i,\alpha\sigma'}(t)] \qquad (7.2)$$

The corresponding expression for the diagonal, in spin orbital basis, equal time correlation functions is obtained by summing over the opposite spin polarizations σ and $\bar{\sigma} = -\sigma$ at the corresponding spin degenerate level. For the spin orbital state $|\alpha,\sigma\rangle$ and $|\alpha,\bar{\sigma}\rangle$ the corresponding equations are written, therefore, as

$$\begin{aligned} i\hbar\frac{\partial}{\partial t}G^{<}_{\alpha\sigma,\alpha\sigma}(t,t) = &\sum_{\ell}[\Sigma^{s}_{\alpha\sigma,\ell\sigma}(t)G^{<}_{\ell\sigma,\alpha\sigma}(t,t) - G^{<}_{\alpha\sigma,\ell\sigma}(t,t)\Sigma^{s}_{\ell\sigma,\alpha\sigma}(t)] \\ &+ [\Sigma^{s}_{\alpha\sigma,\ell\bar{\sigma}}(t)G^{<}_{\ell\bar{\sigma},\alpha\sigma}(t,t) - G^{<}_{\alpha\sigma,\ell\bar{\sigma}}(t,t)\Sigma^{s}_{\ell\bar{\sigma},\alpha\sigma}(t)] \end{aligned} \qquad (7.3a)$$

$$\begin{aligned} i\hbar\frac{\partial}{\partial t}G^{<}_{\alpha\bar{\sigma},\alpha\bar{\sigma}}(t,t) = &\sum_{\ell}[\Sigma^{s}_{\alpha\bar{\sigma},\ell\sigma}(t)G^{<}_{\ell\sigma,\alpha\bar{\sigma}}(t,t) - G^{<}_{\alpha\bar{\sigma},\ell\sigma}(t,t)\Sigma^{s}_{\ell\sigma,\alpha\bar{\sigma}}(t)] \\ &+ [\Sigma^{s}_{\alpha\bar{\sigma},\ell\bar{\sigma}}(t)G^{<}_{\ell\bar{\sigma},\alpha\bar{\sigma}}(t,t) - G^{<}_{\alpha\bar{\sigma},\ell\bar{\sigma}}(t,t)\Sigma^{s}_{\ell\bar{\sigma},\alpha\bar{\sigma}}(t)] \end{aligned} \qquad (7.3b)$$

Both equations contain complex conjugate pairs under summation;

$$(G^{<}_{n\sigma_i,\alpha\sigma_j}(t,t))^{\dagger} = -G^{<}_{\alpha\sigma_j,n\sigma_i}(t,t) \qquad (7.4a)$$

$$(\Sigma^{s}_{n\sigma_i,\alpha\sigma_j}(t))^{\dagger} = \Sigma^{s}_{\alpha\sigma_j,n\sigma_i}(t) \qquad (7.4b)$$

Accordingly, only the real parts of the conjugate pairs survive from the summation leading to

$$i\hbar \frac{\partial}{\partial t} G^{<}_{\alpha\sigma,\alpha\sigma}(t,t) = 2\,\mathrm{Re}\sum_{\ell}[\Sigma^{s}_{\alpha\sigma,\ell\sigma}(t)G^{<}_{\ell\sigma,\alpha\sigma}(t,t) + \Sigma^{s}_{\alpha\sigma,\ell\bar{\sigma}}(t)G^{<}_{\ell\bar{\sigma},\alpha\sigma}(t,t)] \tag{7.5a}$$

$$i\hbar \frac{\partial}{\partial t} G^{<}_{\alpha\bar{\sigma},\alpha\bar{\sigma}}(t,t) = 2\,\mathrm{Re}\sum_{\ell}\ [\Sigma^{s}_{\alpha\bar{\sigma},\ell\sigma}(t)G^{<}_{\ell\sigma,\alpha\bar{\sigma}}(t,t) + \Sigma^{s}_{\alpha\bar{\sigma},\ell\bar{\sigma}}(t)G^{<}_{\ell\bar{\sigma},\alpha\bar{\sigma}}(t,t)] \tag{7.5b}$$

Each of these equations represents the rate of change of the population of one spin polarization at the spin degenerate level α. The quantity we found from summing these two equations is

$$\begin{aligned} & i\hbar \frac{\partial}{\partial t}[G^{<}_{\alpha\sigma,\alpha\sigma}(t,t) + G^{<}_{\alpha\bar{\sigma},\alpha\bar{\sigma}}(t,t)] \\ & = 2\,\mathrm{Re}\sum_{\ell}\{[\Sigma^{s}_{\alpha\sigma,\ell\sigma}(t)G^{<}_{\ell\sigma,\alpha\sigma}(t,t) + \Sigma^{s}_{\alpha\sigma,\ell\bar{\sigma}}(t)G^{<}_{\ell\bar{\sigma},\alpha\sigma}(t,t')] \\ & + [\Sigma^{s}_{\alpha\bar{\sigma},\ell\sigma}(t)G^{<}_{\ell\sigma,\alpha\bar{\sigma}}(t,t) + \Sigma^{s}_{\alpha\bar{\sigma},\ell\bar{\sigma}}(t)G^{<}_{\ell\bar{\sigma},\alpha\bar{\sigma}}(t,t')]\} \end{aligned} \tag{7.6}$$

This is an equation representing the rate of change of the total population at the spin degenerate level α. Clearly, the equation represents a quantity which could be linked directly with the current density. The contribution to the total current density of the electrons at the spin degenerate level α, J_α, is

$$J_\alpha(t) = -\frac{\partial}{\partial t}(eN_\alpha(t)) = i\hbar e \frac{\partial}{\partial t}[G^{<}_{\alpha\sigma,\alpha\sigma}(t,t) + G^{<}_{\alpha\bar{\sigma},\alpha\bar{\sigma}}(t,t)] \tag{7.7}$$

Hence,

$$\begin{aligned} J_\alpha(t) = e2\,\mathrm{Re}\sum_{n\neq\alpha}\{&[\Sigma^{s}_{\alpha\sigma,n\sigma}(t,t)G^{<}_{n\sigma,\alpha\sigma}(t,t) + \Sigma^{s}_{\alpha\bar{\sigma},n\bar{\sigma}}(t,t)G^{<}_{n\bar{\sigma},\alpha\bar{\sigma}}(t,t)] \\ &+ [\Sigma^{s}_{\alpha\sigma,n\bar{\sigma}}(t,t)G^{<}_{n\bar{\sigma},\alpha\sigma}(t,t) + \Sigma^{s}_{\alpha\bar{\sigma},n\sigma}(t,t)G^{<}_{n\sigma,\alpha\bar{\sigma}}(t,t)]\} \end{aligned} \tag{7.8}$$

To proceed in the calculation we need first to determine the non-diagonal components of the equal time limit correlation functions that appear in the right hand side of the expression for the current density, eq.7.8. This we made after computing the generalized solution to the equations of motion to the correlation functions. The equations of motion for non diagonal matrix components of the equal time lesser Green functions could be calculated from eqs.7.1. The expression found for the diagonal, in the energy index α of the second material, from integrating the equation of motion, and of course with scattering effects neglected, is

$$
\begin{aligned}
G^{<}_{n\sigma_i,\alpha\sigma_j}(t,t) = \frac{i}{\hbar}\sum_{\sigma'} \int_{o}^{t} dt_1 e^{-\frac{i}{\hbar}\int_{t_1}^{t} d\bar{t}\,[\varepsilon_{n\sigma_i}(\bar{t})-\varepsilon_{\alpha\sigma_j}(\bar{t})]} \\
\{[G^{<}_{n\sigma_i,\alpha\sigma'}(t_1,t_1)\Sigma^{\sigma'\sigma_j}_{\alpha,\alpha}(t_1)(1-\delta_{\sigma'\sigma_j}) - \Sigma^{\sigma_i\sigma'}_{n,\alpha}(t_1)G^{<}_{\alpha\sigma',\alpha\sigma_j}(t_1,t_1)] \\
+\sum_{m}\,[G^{<}_{n\sigma_i,m\sigma'}(t_1,t_1)\Sigma^{\sigma'\sigma_j}_{m,\alpha}(t_1) - \Sigma^{\sigma_i\sigma'}_{n,m}(t_1)G^{<}_{m\sigma',\alpha\sigma_j}(t_1,t_1)(1-\delta_{mn}\delta_{\sigma'\sigma_j})]\}
\end{aligned}
\tag{7.9}
$$

Where, in the last step we switched our representation of the components of the coupling matrix as

$$
\Sigma^{\sigma\sigma_j}_{m\alpha}(t_1) = \Sigma^{s}_{m\sigma,\alpha\sigma_j}(t_1) \quad \text{and} \quad \Sigma^{\bar{\sigma}\sigma_j}_{m\alpha} = \Sigma^{s}_{m\bar{\sigma},\alpha\sigma_j} \tag{7.10}
$$

We are now to develop an expression, for the current density, which we can use for wider experimental range. We are dealing of course on the tunnel coupling between a semiconductor nanostructure and a second mesoscopic material which could be a spin degenerate metallic contact, a ferromagnetic contact or a second semiconductor with a transparent or reflecting layer in between. To proceed in our calculation, we considered both the coupled materials be approximated in general by an Anderson type model where we represent the one particle energies of the coupled electronic states by

$$\varepsilon_{n\sigma_i}(t) = \varepsilon_n^o + \Sigma_{nn}(t) + \tfrac{1}{2} U n_{n\bar{\sigma}_i}(t) \qquad (7.11a)$$

$$\varepsilon_{\alpha\sigma_i}(t) = \varepsilon_\alpha^o + \Sigma_{\alpha\alpha}(t) + [\tfrac{1}{2} U n_{\alpha\bar{\sigma}_i}(t) + \tfrac{1}{2} eV(t)] \qquad (7.11b)$$

Where, $\bar{\sigma}_i = -\sigma_i$; ε_ℓ^o is the unperturbed condition, or the ground state condition, energy of an electron at the level ℓ before the perturbation is switched on; U is the charging energy; $n_{\ell\bar{\sigma}_i}$ n is the occupation probability at the spin orbital state $|\ell, \bar{\sigma}_i\rangle$; $\Sigma^s_{\ell\ell}$ is the interaction energy developed following the temporal variation in the local density.

The calculation for the current density then proceeds from substituting the expression for the non diagonal equal time correlation function, eq.7.9, in to eq.7.8. The expression we finally obtained for the tunnel current density contribution of the spin degenerate level α of the material, or the current density in a nanostructure that is typical to be modeled by a single degenerate level is

$$J_\alpha = \frac{12e}{\hbar}\sum_{n\neq\alpha m}\sum_{\sigma^1}\int_o^t dt_1\Big\{$$

$$e^{-\frac{i}{\hbar}\int_{t_1}^{t}d\bar{t}[\varepsilon_{n\sigma}(\bar{t})-\varepsilon_{\alpha\sigma}(\bar{t})]}\;[G^{<}_{n\sigma,\alpha\sigma^1}(t_1,t_1)\Sigma^{\sigma\sigma}_{\alpha,n}(t)\Sigma^{\sigma^1\sigma}_{\alpha,\alpha}(t_1)(1-\delta_{\sigma^1\sigma})-\Sigma^{\sigma\sigma}_{\alpha,n}(t)\Sigma^{\sigma\sigma^1}_{n,\alpha}(t_1)G^{<}_{\alpha\sigma^1,\alpha\sigma}(t_1,t_1)]$$

$$+e^{-\frac{i}{\hbar}\int_{t_1}^{t}d\bar{t}[\varepsilon_{n\sigma}(\bar{t})-\varepsilon_{\alpha\sigma}(\bar{t})]}\;[G^{<}_{n\sigma,m\sigma^1}(t_1,t_1)\Sigma^{\sigma\sigma}_{\alpha,n}(t)\Sigma^{\sigma^1\sigma}_{m,\alpha}(t_1)-\Sigma^{\sigma\sigma}_{\alpha,n}(t)\Sigma^{\sigma\sigma^1}_{n,m}(t_1)G^{<}_{m\sigma^1,\alpha\sigma}(t_1,t_1)(1-\delta_{mn}\delta_{\sigma^1\sigma})]$$

$$+e^{-\frac{i}{\hbar}\int_{t_1}^{t}d\bar{t}[\varepsilon_{n\bar{\sigma}}(\bar{t})-\varepsilon_{\alpha\sigma}(\bar{t})]}\;[G^{<}_{n\bar{\sigma},\alpha\sigma^1}(t_1,t_1)\Sigma^{\sigma\bar{\sigma}}_{\alpha,n}(t)\Sigma^{\sigma^1\sigma}_{\alpha,\alpha}(t_1)(1-\delta_{\sigma^1\sigma})-\Sigma^{\sigma\bar{\sigma}}_{\alpha,n}(t)\Sigma^{\bar{\sigma}\sigma^1}_{n,\alpha}(t_1)G^{<}_{\alpha\sigma^1,\alpha\sigma}(t_1,t_1)]$$

$$+\int_o^t dt_1 e^{-\frac{i}{\hbar}\int_{t_1}^{t}d\bar{t}[\varepsilon_{n\bar{\sigma}}(\bar{t})-\varepsilon_{\alpha\sigma}(\bar{t})]}\;[G^{<}_{n\bar{\sigma},m\sigma^1}(t_1,t_1)\Sigma^{\sigma\bar{\sigma}}_{\alpha,n}(t)\Sigma^{\sigma^1\sigma}_{m,\alpha}(t_1)-\Sigma^{\sigma\bar{\sigma}}_{\alpha,n}(t)\Sigma^{\bar{\sigma}\sigma^1}_{n,m}(t_1)G^{<}_{m\sigma^1,\alpha\sigma}(t_1,t_1)(1-\delta_{mn}\delta_{\sigma^1\bar{\sigma}})]$$

$$+\int_o^t dt_1 e^{-\frac{i}{\hbar}\int_{t_1}^{t}d\bar{t}[\varepsilon_{n\sigma}(\bar{t})-\varepsilon_{\alpha\bar{\sigma}}(\bar{t})]}\;[G^{<}_{n\sigma,\alpha\sigma^1}(t_1,t_1)\Sigma^{\bar{\sigma}\sigma}_{\alpha,n}(t)\Sigma^{\sigma^1\bar{\sigma}}_{\alpha,\alpha}(t_1)(1-\delta_{\sigma^1\bar{\sigma}})-\Sigma^{\bar{\sigma}\sigma}_{\alpha,n}(t)\Sigma^{\sigma\sigma^1}_{n,\alpha}(t_1)G^{<}_{\alpha\sigma^1,\alpha\bar{\sigma}}(t_1,t_1)]$$

$$+\int_o^t dt_1 e^{-\frac{i}{\hbar}\int_{t_1}^{t}d\bar{t}[\varepsilon_{n\sigma}(\bar{t})-\varepsilon_{\alpha\bar{\sigma}}(\bar{t})]}\;[G^{<}_{n\sigma,m\sigma^1}(t_1,t_1)\Sigma^{\bar{\sigma}\sigma}_{\alpha,n}(t)\Sigma^{\sigma^1\bar{\sigma}}_{m,\alpha}(t_1)-\Sigma^{\bar{\sigma}\sigma}_{\alpha,n}(t)\Sigma^{\sigma\sigma^1}_{n,m}(t_1)G^{<}_{m\sigma^1,\alpha\bar{\sigma}}(t_1,t_1)(1-\delta_{mn}\delta_{\sigma^1\sigma})]$$

$$+\int_o^t dt_1 e^{-\frac{i}{\hbar}\int_{t_1}^{t}d\bar{t}[\varepsilon_{n\bar{\sigma}}(\bar{t})-\varepsilon_{\alpha\bar{\sigma}}(\bar{t})]}\;[G^{<}_{n\bar{\sigma},\alpha\sigma^1}(t_1,t_1)\Sigma^{\bar{\sigma}\bar{\sigma}}_{\alpha,n}(t)\Sigma^{\sigma^1\bar{\sigma}}_{\alpha,\alpha}(t_1)(1-\delta_{\sigma^1\bar{\sigma}})-\Sigma^{\bar{\sigma}\bar{\sigma}}_{\alpha,n}(t)\Sigma^{\bar{\sigma}\sigma^1}_{n,\alpha}(t_1)G^{<}_{\alpha\sigma^1,\alpha\bar{\sigma}}(t_1,t_1)]$$

$$+\int_o^t dt_1 e^{-\frac{i}{\hbar}\int_{t_1}^{t}d\bar{t}[\varepsilon_{n\bar{\sigma}}(\bar{t})-\varepsilon_{\alpha\bar{\sigma}}(\bar{t})]}\;[G^{<}_{n\bar{\sigma},m\sigma^1}(t_1,t_1)\Sigma^{\bar{\sigma}\bar{\sigma}}_{\alpha,n}(t)\Sigma^{\sigma^1\bar{\sigma}}_{m,\alpha}(t_1)-\Sigma^{\bar{\sigma}\bar{\sigma}}_{\alpha,n}(t)\Sigma^{\bar{\sigma}\sigma^1}_{n,m}(t_1)G^{<}_{m\sigma^1,\alpha\bar{\sigma}}(t_1,t_1)(1-\delta_{mn}\delta_{\sigma^1\bar{\sigma}})]$$

$$+\Gamma^{\bar{\sigma}\bar{\sigma}}_{n\alpha}+\Gamma^{\sigma\bar{\sigma}}_{n\alpha}+\Gamma^{\bar{\sigma}\sigma}_{n\alpha}+\Gamma^{\sigma\sigma}_{n\alpha} \qquad (7.12)$$

Clearly, the resulted equation is too complicated to handle and it will be logical to revert to some approximations. However, we need to take precautions for not to employ approximation techniques that make relevant information washed out in the process.

7.3 Discussion

From the energy relation in eq.7.11, it will be easy to notice that the level of the proximity coupled spin orbital states vary with variation in the applied potentials and with the fluctuation in the total occupation of the level and the occupation by electrons of the opposite spin polarization of the spin degenerate level. Of course electrons avoid one another when they have similar spin polarization and attract when the spin polarizations are opposite.

The intricate spin structure in the equation, eq.7.12, is indicative of the complicated dynamical correlation effects generated as a result of the fluctuations in the electron and spin polarization wave exchanging couplings. An insight in to the prediction of the expressions may require a close inspection of the terms, and hence the role and characteristics of the interaction terms involved. According to the prediction of the results obtained, the total electron and spin polarization wave exchange is a superposition of the contributions from the correlation of the interactions represented by the components of the corresponding singular self energy matrices. Other scattering effects such as the scattering by phonon are not part of the correlation structure since these interactions are characteristically non singular. Here it will be worth to notice the advantage the structure of the equation renders in allowing to include low temperature phonon interaction effects when inclusion of the information on the thermal interactions becomes significant in explaining the observables. This we can do by assuming the occupation probability at the contact to be approximated by the same form as the equilibrium Green function.

$$G^{<}_{\alpha\alpha}(t,t') \neq g^{<}_{\alpha\alpha}(t,t') = f_D(\varepsilon,T)e^{-\frac{i}{\hbar}\int_{t}^{t'}\varepsilon(\bar{t})d\bar{t}} \qquad (7.13a)$$

Where, the term $f_D(\varepsilon,T)$ is the Fermi-Dirac distribution function;

$$f_D(\varepsilon,T)=[1+\exp(\frac{\varepsilon+\mu}{K_BT})]^{-1} \qquad (7.13b)$$

Interestingly, the interaction between the spin degenerate states of each unit has a diagonal, in spin-orbital basis, singular self energy terms $\Sigma_{\alpha\alpha}^{\sigma\sigma}(\Sigma_{\alpha\alpha}^{\bar{\sigma}\bar{\sigma}})$ and $\Sigma_{nn}^{\sigma\sigma}(\Sigma_{nn}^{\bar{\sigma}\bar{\sigma}})$ that goes in renormalizing the electron energy (eq.7.11). In absence of these singular self energy contributions, the energies of the spin degenerate states given by eq.7.11 will be reduced to a form similar to the energy given in the Hartree-Fock model. Then comes the understanding that these terms represent the correction to the Hartree-Fock energy which there by recovering the information on the correlation contribution.

Each correlation integral in eq7.12 is consisting components of the product matrix of the interactions that form the kernel to the corresponding convolution integral. A close inspection of these terms appears suggesting the classification of the coupling interactions, on the basis of their length scales, under two major classes: The local or onsite interactions, terms diagonal in respect to level indices such as $\Sigma_{\alpha\alpha}^{\bar{\sigma}\sigma}(\Sigma_{\alpha\alpha}^{\sigma\bar{\sigma}})$ and $\Sigma_{nn}^{\bar{\sigma}\sigma}(\Sigma_{nn}^{\sigma\bar{\sigma}})$, and the proximity coupling in the tunneling regime, terms off diagonal in respect to their level indices only such as $\Sigma_{\alpha n}^{\sigma\sigma}(\Sigma_{\alpha n}^{\bar{\sigma}\bar{\sigma}})$ and $\Sigma_{\alpha n}^{\bar{\sigma}\sigma}(\Sigma_{\alpha n}^{\sigma\bar{\sigma}})$. The former of these which we now identified as the local couplings are to be associated with the local charge and spin polarization effects while the later type to be accounted to the electron-spin polarization wave tunneling in between the coupled material regions. The on site couplings are non diagonal in respect to their spin indices and there by revealing that they are representing interactions with spin switching effects.

The set representing the tunnel couplings, in eq.7.12, are also noticed to include off-diagonal terms such as $\Sigma_{\alpha n}^{\sigma\bar{\sigma}}(\Sigma_{\alpha n}^{\bar{\sigma}\sigma})$ and $\Sigma_{\alpha n}^{\sigma\sigma}(\Sigma_{\alpha n}^{\bar{\sigma}\bar{\sigma}})$. Obviously, these terms are representing the couplings between the electronic states in the two regions. The difference between the terms in this set lies in the spin contribution. The first pair, $\Sigma_{\alpha n}^{\sigma\bar{\sigma}}(\Sigma_{\alpha n}^{\bar{\sigma}\sigma})$, in this set accounts to the tunnel coupling between electronic states of opposite spin polarizations. The second pair, $\Sigma_{\alpha n}^{\sigma\sigma}(\Sigma_{\alpha n}^{\bar{\sigma}\bar{\sigma}})$, on the other hand is the tunnel coupling between electrons of like spins. Without making further investigations it will not be legitimate step, therefore, to jump over toward suppressing the later. This does not have to imply, however, that all these couplings to be significant enough to determine the system property at all experimental conditions. In many situations the tunnel couplings between opposite spin polarization states are considered to be insignificant in influencing the responses of the configuration to external perturbations. Taking this as a universal feature on the other hand may have the penalty to be paid for the washing away of information very useful in explaining observations where imprints of the electron and spin polarization wave exchange between states of opposite polarizations are noticed. In principle the effects of the off-diagonal, in spin indices, tunnel couplings could alternatively explained in light of the spin polarization environment of the interfaced structures.

The information we have so far from the forgoing explanations is still insufficient to draw conclusions. However, the equation by itself is rich in providing understandings vital for the purpose. One of these and the point we next investigate is the time structure of the interaction which the equation itself embodies. Each integral in eq.7.12 is typically a convolution integral which is in a form

$$I = \int_{o}^{t} dt_1 e^{-\frac{i}{\hbar}\int_{t_1}^{t} d\bar{t}\,[\varepsilon_{n\sigma}(\bar{t}) - \varepsilon_{\alpha\sigma}(\bar{t})]} G^{<}_{n\sigma_i, s\sigma_\ell}(t_1, t_1)\Sigma^{\sigma_i\sigma_\ell}_{\alpha,n}(t)\Sigma^{\sigma_k\sigma_j}_{s,\alpha}(t_1) \qquad (7.14)$$

The weight of the contribution of each of such terms depends on the correlation of the` interactions referred by the self energy matrix components of the integrand. It is a fact that the correlation between spin orbital states in the material configurations requires the presence of states slightly differing in energy and as well time dependent couplings. The contribution of each integral term in eq.7.12 is of a significant order, when the coupled states are correlated. When the contribution of the integral over the particular time domain of interest is at a vanishing order it will be the case where neglecting the effects of the couplings will become a reasonable approximation. This we cannot do however without further insight in the dependence of the coupling interactions on the various parameters of the system such as the energy and occupation.

The tunnel couplings are known to depend on the energy difference between the levels and the latter on the occupation of the states. In the other way round the electron and spin polarization wave transfer under the tunnel couplings result changes in the occupations and energies of the levels. More over, the change in the occupation of the spin degenerate states would lead to changes in the energy splitting between the spin degenerate states in accordance to eq.7.11. The interdependence between the cascades of process therefore eventually leads to the appearance the phenomena which are signatures of the occurrence of dynamically correlated states. One can neither expect dynamical correlations between tunnel coupled states unless they are close in energy and have a relative detuning that fluctuate with time. . Similarly, it is unlikely for opposite spin polarization states of a spin degenerate system to evolve in time dynamically correlated unless the splitting is very small and there is interdependence in the fluctuation of the occupancy of the states. To draw

meaningful conclusions on the correlation of the coupling interactions it will be compulsory to compare the time structure of the process.

As already elaborated in the preceding paragraphs, it is of course true that the closer the spin orbital levels in two coupled material regions, the more is the probability for electron and spin polarization wave exchange between the regions. This is however only as far as the state in the material unit from which the electron has to leave is occupied and the corresponding state in the second material is empty. At any moment when the state in the second material region is fully occupied, the transfer of electron to a state in this region will be blocked and remain blocked until the occupation of the level in this material region falls to the minimum following some relaxation processes. The relaxation could be as a result of the transfer of the electron to another material region or due to relaxation to other states at the same site. For operation with injection level at the near resonance condition to the lower unoccupied level of a unit modeled by confinement quantization the probability for relaxation to the lower levels vanishes since these levels are completely filled and the transition to the next higher energy levels will be unlikely in the absence of energy which the transition will cost. The relaxation with finite probability is to the spin degenerate level provided it is empty. Such a relaxation between spin degenerate states of similar levels is a quantum mechanical process involving the switching of the electron spin from one polarization to the opposite. This is quite noticeable when the tunneling in to the spin degenerate system is from a coupled non spin degenerate system such as the case in ferromagnetic materials. The length of time the electron and spin polarization wave transfer has to remain blocked is determined by the competition between the possible relaxation mechanisms and hence obviously by the relaxation time under the processes taking place. For a central region, semiconductor nanostructure of size (L_C) in the quantum confined range, the length of time (T_{tr}) necessary for the electron to sweep out from the unit at small temperature could be approximated by

$$T_{tr} = \frac{L_C}{v_F} \tag{7.15}$$

Where, the parameter v_F is the Fermi velocity for the electron. The electrons entered the spin degenerate central region are also known to preserve their spin for a characteristic time which is in the range of $10^{-9} - 10^{-6} s$. This characteristic time, the spin flipping time T_{SFL} in the local relaxation, is the time which an electron takes to relax toward an opposite spin polarization state where it will be relatively stable, It follows therefore that the transfer rate of electron and spin polarization wave in the configuration is controlled by the transit time distribution when $T_{tr} < T_{SFL}$ and by the spin flip at the local scale when $T_{SFL} < T_{tr}$. Since the transfer of electron of one spin polarization results in a level shift for the electron with the opposite spin polarization state, the process brings about fluctuations in the couplings. Relaxations taking place at shorter time scale mark the smallest time scale of the fluctuation in the tunnel couplings. The understanding on the time scale of the fluctuation in the couplings is vital for our approximation of the integrals in eq.7.12.

The singular self energy matrix product terms appearing under each convolution integral are perhaps the strategic point for our line of attack. Integrals containing singular self energy term that is diagonal in the degenerate level basis but off diagonal with respect to the spin indices are that which will be primary to be considered. These interaction matrix components, which are in the form $\Sigma_{\alpha\alpha}^{\bar{\sigma}\sigma}(\Sigma_{\alpha\alpha}^{\sigma\bar{\sigma}})$ and $\Sigma_{nn}^{\bar{\sigma}\sigma}(\Sigma_{nn}^{\sigma\bar{\sigma}})$, will be interactions to be accounted to the local spin flip if they do exist. It is however the understandings of most to associate the onsite spin relaxations with scatterings that involve boson assisted processes. On the other hand, the interactions of scattering processes do not belong to the singular self energy. Under the situation when the system is at a temperature that is very low to enhance the local spin flip and in the time

regime well before the buildup of coulomb scatterings the non singular self energy contributions could also be considered to have a vanishing contribution. In the situation where the transit time through the semiconductor nanostructure is shorter than the time scale for the spin flipping, the contribution of the convolution integrals involving the matrix products $\Sigma_{\alpha\alpha}^{\sigma\bar{\sigma}}(t_i)\Sigma_{\alpha n}^{\sigma\sigma}(t_j)$ will become negligibly small:

$$\int_o^t e^{\frac{i}{\hbar}\int_{t'}^{t}\Delta\varepsilon(\bar{t})d\bar{t}}\,\Sigma_{\alpha\alpha}^{\sigma\bar{\sigma}}(t_i)\Sigma_{\alpha n}^{\sigma\sigma}(t_j)dt_j \to 0 \qquad (7.16)$$

When this is the case, it will be a reasonable approximation if the contribution from the terms that contain integral of this form is suppressed. Indeed, this greatly simplifies the current density expression in eq.7.12 to be in the form

$$J_\alpha(t) = \mathrm{Re}\frac{2e}{\hbar^2}\sum_{n\neq\alpha}$$

$$\Big\{\int_o^t dt_1 e^{\frac{i}{\hbar}\int_{t_1}^{t}d\bar{t}\,\Delta_{\alpha\sigma,n\sigma}(\bar{t})}\,V_{\alpha,n}^{\sigma\sigma}(t)V_{\alpha,n}^{*\sigma\sigma}(t_1)[n_{\alpha\sigma}(t_1)-n_{n\sigma}(t_1)]$$

$$+\int_o^t dt_1 e^{\frac{i}{\hbar}\int_{t_1}^{t}d\bar{t}\,\Delta_{\alpha\sigma,n\bar{\sigma}}(\bar{t})}\,V_{\alpha,n}^{\sigma\bar{\sigma}}(t)V_{\alpha,n}^{*\sigma\bar{\sigma}}(t_1)[n_{\alpha\sigma}(t_1)-n_{n\bar{\sigma}}(t_1)]$$

$$+\int_o^t dt_1 e^{\frac{i}{\hbar}\int_{t_1}^{t}d\bar{t}\,\Delta_{\alpha\bar{\sigma},n\sigma}(\bar{t})}\,V_{\alpha,n}^{\bar{\sigma}\sigma}(t)V_{\alpha,n}^{*\bar{\sigma}\sigma}(t_1)[n_{\alpha\bar{\sigma}}(t_1)-n_{n\sigma}(t_1)]$$

$$+\int_o^t dt_1 e^{\frac{i}{\hbar}\int_{t_1}^{t}d\bar{t}\,\Delta_{\alpha\bar{\sigma},n\bar{\sigma}}(\bar{t})}\,V_{\alpha,n}^{\bar{\sigma}\bar{\sigma}}(t)V_{\alpha,n}^{*\bar{\sigma}\bar{\sigma}}(t)(t_1)[n_{\alpha\bar{\sigma}}(t_1)-n_{n\bar{\sigma}}(t_1)]\Big\} \qquad (7.17)$$

Where, we used the definition for the lesser Green function to replace the diagonal , in both time and state indices, lesser Green functions by the occupation probabilities of the corresponding states. All the integral terms in eq.7.17 have a similar structure of the form

$$I = \int_{o}^{t} dt_1 e^{\frac{i}{\hbar}\int_{t_1}^{t} d\bar{t}\,[\varepsilon_{\alpha\sigma_i}(\bar{t}) - \varepsilon_{n\sigma_j}(\bar{t})]} V_{\alpha,n}^{\sigma_i\sigma_j}(t) V_{\alpha,n}^{*\sigma_i\sigma_j}(t_1)[n_{\alpha\sigma_i}(t_1) - n_{n\sigma_j}(t_1)] \qquad (7.18)$$

According to the prediction of the results, the weight of the contribution from each term depends on the occupation probability difference between the coupled states. It is quite apparent that the contribution to the current density of each term in eq.7.17 vanishes whenever the occupation probabilities of tunnel coupled states become the same. This furnishes a means for explaining the well known phenomenon in quantum transport, the Coulomb blockade in low dimensional structures and for describing the operation of single electron transistors (SET).

It can be noted, of course, that the expressions in eq.7.17 still require some more work so that the analytical result be in a form that will be rather convenient for applications. On the other hand its structure is rich in reflecting the complicated correlation phenomena generated in the electron and spin polarization wave tunneling transfer. Thus it will be a logical step to revert to approximation techniques which we could employ without endangering the relevant information from being washed out in the steps. After the perturbation is switched on, the energy difference between the electronic states in the two regions fluctuates following the action of the applied field and due to the inter- and intra-element spin orbital interactions. This complicates the integrand at the exponents. To proceed in the computation it will be worth to split this energy term into a part that is easy to solve and a second part which we need to approximate. Instead of splitting into a time dependent and non time dependent components it will be worth if it is decomposed in to a term easier to handle in the computation and the difficult part which contains

the fluctuating interaction contributions. This offers an advantage to pursue the approximation and to investigate the signatures of the quantum mechanical interactions under the time dependent field. Accordingly we put eq.7.18 and the time dependent energy difference between the coupled states, of course under no external action of a magnetic field, as

$$I = \int_{o}^{t} dt_1 e^{\frac{i}{\hbar}\int_{t_1}^{t} d\bar{t}[\Delta_{\alpha n}^{\sigma\sigma}(\bar{t})+\beta_{\alpha n}^{\sigma\sigma}(\bar{t})]} V_{\alpha,n}^{\sigma\sigma}(t) V_{\alpha,n}^{*\sigma\sigma}(t_1)[n_{\alpha\sigma}(t_1) - n_{n\sigma}(t_1)] \quad (7.19a)$$

$$\varepsilon_{\alpha\sigma_i}(t) - \varepsilon_{n\sigma_j}(t) = \Delta_{\alpha n}(t) + \beta_{\alpha n}^{\sigma_i\sigma_j}(t) \quad (7.19b)$$

$$\Delta_{\alpha n}(t) = [\varepsilon_{\alpha}^{o} - \varepsilon_{n}^{o}] + \frac{eV(t)}{2} \quad (7.19c)$$

$$\beta_{\alpha n}^{\sigma_i\sigma_j}(t) = [\Sigma_{\alpha\alpha}(t) - \Sigma_{nn}(t)] + \frac{1}{2}[U_{\alpha} n_{\alpha\bar{\sigma}_i}(t) - U_n n_{n\bar{\sigma}_i}(t)] \quad (7.19d)$$

Here, it will be important to recall the circuit element in which the biasing voltage, in eq.7.19c, modifies the energies of the transport electronic states. Just as it is widely adopted in many practical calculations, we also considered the impressed small biasing voltage to be completely absorbed at the leads where it is assumed to modify the chemical potential of the contact material. Therefore the inclusion of the biasing potential term in eq.7.19c is for use when the component unit under discussion is the contact. It is of course true that in a more general case the applied voltage can be time dependent. However, this is what we could control most. We can shape and limit the amplitude of the voltage pulse and we could make in such a way we could conveniently represent in mathematical terms. On the basis of this understanding eq.7.19a is evaluated with the result

$$I = \mathsf{h}\frac{n_{\alpha\sigma_i}(o)}{\Delta_{\alpha n}(o)}\Im^{-1}\{\Gamma(\omega)\}Sin(\int_o^t d\bar{t}\,\frac{1}{\mathsf{h}}[\Delta_{\alpha n}(t)+\beta_{\alpha n}^{\sigma_i\sigma_j}(t)]) + \tilde{\mathrm{O}}\{I\} \qquad (7.20)$$

Where, the last term refers the contributions from the second and higher order contributions. The first term in the right hand side of this equation shows a direct dependence on the weight of the injecting state at the initial time, the level separation of the states prior to the application of the perturbing field and as well in the fluctuation spectrum of the tunnel coupling, $\Gamma(\omega)$. Here, the term $\Im^{-1}\{\Gamma(\omega)\}$ is the inverse Fourier transform of the fluctuation spectrum of the tunnel coupling which is given by

$$\Gamma(\omega) = \int_{-\infty}^{\infty} dt e^{i\omega t} V_{n\alpha}^{*\sigma_j\sigma_i}(t) V_{n\alpha}^{\sigma_j\sigma_i}(t_o) \qquad (7.21)$$

The driving field applied to the system reduces the level difference so that the probability for charge and polarization wave transfer through tunneling rises to the maximum. For operation at about the resonance tunneling, it happens therefore that $\Delta_{\alpha n}(t) \to 0$ (but $\Delta_{\alpha n}(o) \neq 0$). Under this condition the quantity given by eq.7.20 oscillates at the rate determined by $\beta_{\alpha n}^{\sigma_i\sigma_j}$. For values of $\beta_{\alpha n}^{\sigma_i\sigma_j}$ in the order of only a few fraction of a meV, the contribution from each term given by eq.7.17oscillates at a rate close to optical frequencies. It is known that the high oscillation in this term could eventually make the correlation between the levels in the coupled structures to vanish. Our interest is on the other hand on the short time scale where the correlation effects significantly influence the properties. This in practice refers to the phenomena observed just following the buildup of correlation but well earlier than the dephasing time:

$$\tau_c < t < \tau_{dph} \tag{7.22}$$

It will be appropriate therefore if the exponential term containing the complicated part of the energy is approximated by averaging it over the level fluctuation at short times. We do this by expanding the term using the Dyson's series expansion and through term by term averaging of each term (Appx. B). The approximation then leads us to

$$I(t) = \int_{-\infty}^{\infty} \frac{d\omega_1}{2\pi i} \frac{[n_{\alpha\sigma}(\omega_1) - n_{n\sigma}(\omega_1)]}{\omega_1 - \frac{1}{\hbar}[\Delta_{\alpha n} + \langle \beta_{\alpha n}^{\sigma\sigma} \rangle]} V_{\alpha n}^{\sigma\sigma}(t) V_{\alpha n}^{*\sigma\sigma}(\omega_1) e^{i\omega_1 t} \tag{7.23}$$

From Fourier transforming of this equation we, on the other hand, obtained

$$f(I) = I(\omega) = \frac{[n_{\alpha\sigma_i} - n_{n\sigma_j}]}{\omega - \frac{1}{\hbar}[\Delta_{\alpha n} + \langle \beta_{\alpha n}^{\sigma_i\sigma_j} \rangle]} V_{\alpha,n}^{\sigma_i\sigma_j}(\omega) V_{\alpha n}^{*\sigma_i\sigma_j}(\omega) \tag{7.24}$$

This represents the Fourier transform of the integral terms in eq.7.17. Upon using this result it leads the tunneling current spectrum to be written as

$$J_{\alpha}(\omega) = \frac{2e}{\mathrm{h}^2} \sum_{n \neq \alpha} \Big\{ \frac{[n_{\alpha\sigma} - n_{n\sigma}]}{\omega - \frac{1}{\mathrm{h}}[\Delta_{\alpha n} + \beta_{\alpha n}^{\sigma\sigma}]} V_{\alpha,n}^{\sigma\sigma}(\omega) V_{\alpha n}^{*\sigma\sigma}(\omega)$$

$$+ \frac{[n_{\alpha\bar{\sigma}} - n_{n\bar{\sigma}}]}{\omega - \frac{1}{\hbar}[\Delta_{\alpha n} + \beta_{\alpha n}^{\bar{\sigma}\bar{\sigma}}]} V_{\alpha,n}^{\bar{\sigma}\bar{\sigma}}(\omega) V_{\alpha n}^{*\bar{\sigma}\bar{\sigma}}(\omega)$$

$$+ \frac{[n_{\alpha\sigma} - n_{n\bar{\sigma}}]}{\omega - \frac{1}{\mathrm{h}}[\Delta_{\alpha n} + \beta_{\alpha n}^{\sigma\bar{\sigma}}]} V_{\alpha,n}^{\sigma\bar{\sigma}}(\omega) V_{\alpha n}^{*\sigma\bar{\sigma}}(\omega)$$

$$+ \frac{[n_{\alpha\bar{\sigma}} - n_{n\sigma}]}{\omega - \frac{1}{\mathrm{h}}[\Delta_{\alpha n} + \beta_{\alpha n}^{\bar{\sigma}\sigma}]} V_{\alpha,n}^{\bar{\sigma}\sigma}(\omega) V_{\alpha n}^{*\bar{\sigma}\sigma}(\omega) \Big\} \qquad (7.25)$$

Where, the terms $n_{\ell\sigma_i}$'s here refer the short time average of the occupation at the observation period. The expression for the density of current tunneling into the semiconductor nano structure is a combination of contributions associated to the couplings between the spin orbital states in the nanostructure and the material which is tunnel coupled with the former. The contribution from each is determined by the strength of the coupling, the difference in the occupation probabilities of the tunnel coupled states of the two regions and the detuning between the states.

The tunneling of current in to a semiconductor nano structure from a spin degenerate metallic contact, from a non spin degenerate contact such as a contact made up of a ferromagnetic material and from another semiconductor nanostructure could be described by the same equation. This will be among the points of emphasis in the following sections.

7.3.1 Semiconductor nanostructure with a spin degenerate Point Contact

The metallic point contact is a material with high concentration of electrons, of both spin polarizations, at energies near the Fermi level of the material. The contact material could be prepared either from a spin degenerate metallic material or from a semiconductor material which is doped beyond the Mott transition. The electronic concentration at the contact material is very high such that both the occupation probabilities and the levels at the contact will practically remain unchanged even though electrons are tunneling out from it in the process. That is, the contact is which we could conveniently model as a reservoir of electrons of both spin polarizations, up spin and down spin polarizations.

In absence of external magnetic field and prior to the application of the perturbation, there is no splitting in the spin degenerate levels of the constituent materials. The electronic level in the semiconductor material that is to be tunnel coupled during the process is initially empty. For a semiconductor nanostructure of size in the length scale of quantum confinement regime, it may happen that only one level of the semiconductor material be accessible for tunnel coupling at lower biasing voltage. Depending on the spin polarization of an electron that is tunneled from the contact region the spin degenerate single level in the semiconductor nanostructure splits as predicted by the energy relation in eq.7.11. The electron and spin polarization transfer in the tunnel coupled system could be described by setting $\varepsilon_{\alpha\sigma}(t) = \varepsilon_{\alpha\bar{\sigma}}(t)$ and $n_{\alpha\sigma} = n_{\alpha\bar{\sigma}}$. Accordingly the expression for the tunneling, from the states $|\alpha\rangle$ in the contact region to the states $|n\rangle$ of the semiconductor nanostructure (Fig.7.1), current density will become

$$J_\alpha(\omega)=\frac{2e}{\hbar^2}\sum_{n\neq\alpha}\left\{\frac{[n_{\alpha\sigma}-n_{n\sigma}]}{[\omega-\frac{1}{\hbar}(\Delta_{\alpha n}-\frac{1}{2}U_n n_{n\bar{\sigma}})]}[V_{\alpha n}^{\sigma\sigma}(\omega)V_{\alpha n}^{*\sigma\sigma}(\omega)+V_{\alpha n}^{\bar{\sigma}\sigma}(\omega)V_{\alpha n}^{*\bar{\sigma}\sigma}(\omega)]\right.$$

$$\left.+\frac{[n_{\alpha\sigma}-n_{n\bar{\sigma}}]}{[\omega-\frac{1}{\hbar}(\Delta_{\alpha n}-\frac{1}{2}U_n n_{n\sigma})]}[V_{\alpha n}^{\bar{\sigma}\bar{\sigma}}(\omega)V_{\alpha n}^{*\bar{\sigma}\bar{\sigma}}(\omega)+V_{\alpha n}^{\sigma\bar{\sigma}}(\omega)V_{\alpha n}^{*\sigma\bar{\sigma}}(\omega)]\right\} \qquad (7.26)$$

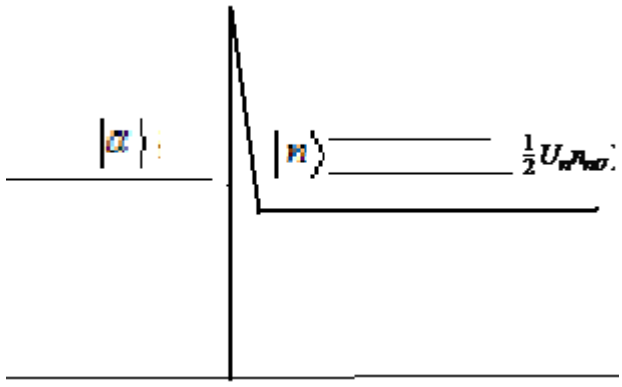

Fig.7.1*: Contact metal-Semiconductor dot energy diagram*

The right hand side of this last expression is a sum of the contributions due to the transfer to the spin up state, the first term, and due to the transfer to the spin down state, the second term, in the semiconductor nanostructure. For fixed values of the tunnel coupling potentials, the contribution due to the transfer to either spin polarization state in the semiconductor nanostructure vanishes if the state is occupied and maximum when empty. The current will be blocked if both spin degenerate states of the semiconductor dot are occupied and remained so until the electrons relax to states in the adjacent material next in the transfer chain.

Here it will be worth to notice that the profile of the current spectrum is also to depend on whether or not the tunneling is spin selective. The spectrum of the current predicted by eq.7.26 under the tunneling process that is characterized by the presence of spin fluctuation is found to exhibit two characteristic maxima, Fig.7.2 centered at the spectral points ω_o and ω given by

$$\omega_o = \frac{1}{\hbar}\Delta_{\alpha n} \qquad (7.27a)$$

$$\omega = \frac{1}{\hbar}(\Delta_{\alpha n} - \frac{1}{2}U_n) \qquad (7.27b)$$

The spectral peaks are centered at spectral points spaced by an order that corresponds to one half of the charging energy and contain the information in the strength of the coupling potentials. The height of the spectral peak at ω_o corresponds to the sum of the squares of the four coupling potentials $\left|I(\omega_o)\right|^2$ where as the height at ω is nearly one half of the former, $\left|I(\omega)\right|^2 \approx \frac{1}{2}\left|I(\omega_o)\right|^2$.

Each of the two terms in eq.7.26 on the other hand is due to the combined contributions of a spin preserving and a spin switching tunneling transfers. It describes therefore the situation where there is inter material coupling that could result spin flipping, which could be considered as fast spin flipping, within the time scale for the electron relaxation between the states in the coupled materials. In absence of fast spin flipping interactions, or when these are negligible to influence the overall transfer, the expression in eq.7.26 reduces to

$$J_\alpha(\omega) = \frac{2e}{\hbar^2}\sum_{n\neq\alpha}\left\{\frac{[n_{\alpha\sigma} - n_{n\sigma}]}{[\omega - \frac{1}{\hbar}[\Delta_{\alpha\sigma} - \frac{1}{2}U_n n_{n\bar{\sigma}}]}[V_{\alpha n}^{\sigma\sigma}(\omega)V_{\alpha n}^{*\sigma\sigma}(\omega)]\right.$$

$$\left. + \frac{[n_{\alpha\sigma} - n_{n\bar{\sigma}}]}{[\omega - \frac{1}{\hbar}[\Delta_{\alpha\sigma} - \frac{1}{2}U_n n_{n\sigma}]}[V_{\alpha n}^{\bar{\sigma}\bar{\sigma}}(\omega)V_{\alpha n}^{*\bar{\sigma}\bar{\sigma}}(\omega)]\right\} \qquad (7.28)$$

We notice from comparing the expressions in the last two equations that the absence or presence of the fast spin flipping results in no change on

the spectral peak position but mainly modifies the height of the spectral peak.

The analysis we made thus far is by assuming finite probabilities for the electrons to undergo relaxations both energetically and in their spin polarizations. If the later is to be suppressed, the coupling terms that are non diagonal in respect to their spin indices need to be at vanishing order. As we already mentioned in the arguments that lead to eq.7.25, the electrons could remain with their spin preserved for a period longer than the time scale for relaxing energetically to a state in the second material region. This has the implication that $V_{\alpha n}^{\bar{\sigma}\sigma}$ and $V_{\alpha n}^{\sigma\bar{\sigma}}$ are negligibly small in the initial part of the coherent transport but builds up at later stage which immediately followed by temporal region for observing marked loss of coherence in the system. Under the situation as $V_{\alpha n}^{\bar{\sigma}\sigma}(V_{\alpha n}^{\sigma\bar{\sigma}}) \to 0$ when compared to the diagonal couplings, the last two terms in eq.7.25 and the second term in eq.7.28 could be suppressed to zero and the transfer will be non spin polarization switching. When both spin polarizations only relax energetically with their spin polarization preserved, it follows therefore that the current spectrum will only peak at one spectral point; It peaks only at ω_o with the same height as in the former (Fig.7.2). We can say that the appearance of a doublet in the current spectrum is a characteristic feature of the charge and spin polarization transfer under the situation where non equilibrium spin fluctuation persists. It appears on the other hand as a singlet when the transfer is without disturbing the initial zero spin condition of the material.

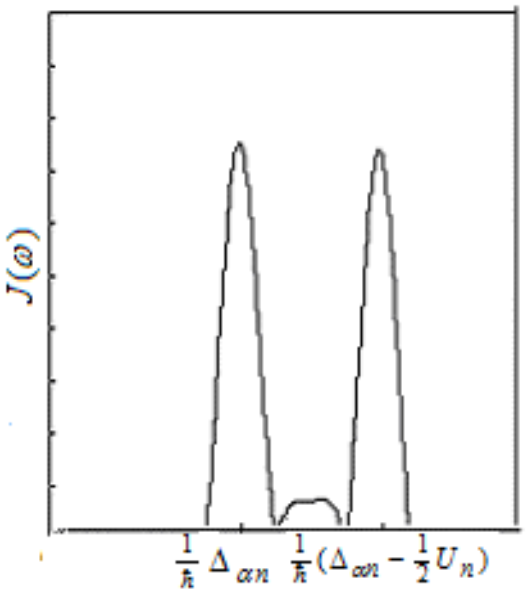

Fig.7.2: *Tunneling current spectrum under a non-spin flipping condition*

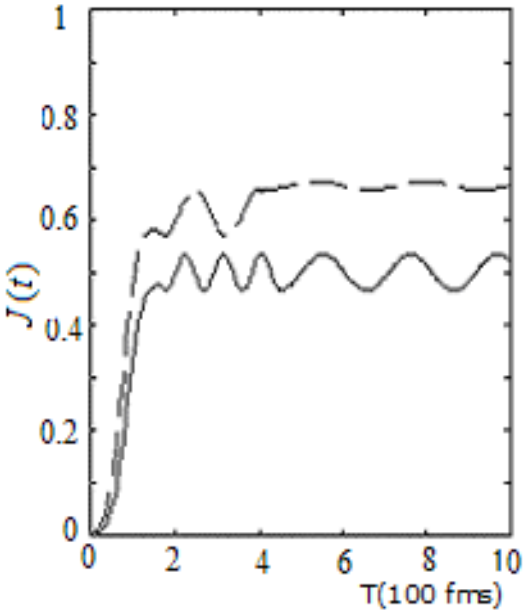

Fig.7.3: *Ringing current under a short* pulse biasing *voltage.*

Just following the tunneling in to the region of the electron with one spin polarization, the state for the opposite spin polarization is set at the energy that is displaced from the ground state value of the level by one half times the charging energy U_n. For a given value of the weight of the spin degenerate level the splitting is proportional with the charging energy. As the weight of the opposite spin rises, the splitting between the degenerate levels decreases as a result of the shift in the energy of the former due to the interaction. Provided the injection time is smaller than the relaxation time for the spin orbital state, the buildup of the occupation of the later to the maximum value, would result in a degenerate level at the shifted energy.

The resulting current predicted by the formulation, for the condition of resonant tunneling is also shown in Fig.7.3. The current versus time diagram here is drawn for a metal contact-semiconductor dot configuration under a small rectangular voltage pulse of width in the order of nanosecond scale.

The current is computed assuming a spin conserving tunneling. In contrast to the non spin conserving processes there noticed no splitting of the spin degenerate levels. The tunneling current in this second case is found to oscillate at a frequency of

$$\omega_s = \tfrac{1}{4} U_n \qquad (7.29)$$

7.3.2 Semiconductor nanostructure with non spin *degenerate Contact*

A non spin degenerate contact refers to contacts prepared from materials with a net spin of one polarization type. These materials are magnetic in their nature. The use of ferromagnetic leads in circuits is well known to its effect for transporting one spin polarization electron and in probing the spin polarizations of current in circuits. In using eq.7.25 for a configuration where the contact is ferromagnetic, we need to constrain the couplings and the occupation probabilities to only one spin polarization type. Without going to the energy relation, this will reduce the number of contributing terms in the current density expression into two. For a ferromagnetic contact characterized by a spin up electronic state,

$$V_{\alpha n}^{\bar{\sigma}\bar{\sigma}} = V_{\alpha n}^{\bar{\sigma}\sigma} = 0 \qquad (7.30a)$$

$$n_{\alpha\bar{\sigma}} = 0 \qquad (7.30b)$$

The spectrum of current density resulting from the tunneling process that involve fluctuation in the spin polarization according to eq.7.25 is

$$J_{\alpha}(\omega) = \frac{2e}{\mathrm{h}^2} \sum_{n \neq \alpha} \Big[\frac{[n_{\alpha\sigma} - n_{n\sigma}]}{[\omega - \frac{1}{\mathrm{h}}(\Delta_{\alpha n} - \frac{1}{2} U_n n_{n\bar{\sigma}})]} V_{\alpha n}^{\sigma\sigma}(\omega) V_{\alpha n}^{*\sigma\sigma}(\omega)$$

$$+ \frac{[n_{\alpha\sigma} - n_{n\bar{\sigma}}]}{[\omega - \frac{1}{\hbar}(\Delta_{\alpha n} - \frac{1}{2} U_n n_{n\sigma})]} V_{\alpha n}^{\sigma\bar{\sigma}}(\omega) V_{\alpha n}^{*\sigma\bar{\sigma}}(\omega) \Big] \qquad (7.31)$$

Clearly, in the absence of interactions leading to fast spin flipping of the electrons the second term in this equation vanishes. As a result, there will be no tunneling of electron into the semiconductor nanostructure if the state for the spin up electron is occupied and this remains so until the electron in the semiconductor relaxes energetically to another material region next in the transmission chain. When the system is operating in this condition, the net spin in the semiconductor nanostructures fluctuate between zero and unity.

When there are no other sources to generate or inject electrons with spin opposite to the spin polarization of the electron in the injecting contact, tunneling is blocked while the nanostructure has a net spin. This will not be the case if instead fast flipping persists. In the presence of fast spin flip, the spin polarization neutrality can take place either when the tunneling is blocked or it builds up to its maximum. The former is when the spin degenerate level is totally filled and the second is when it is empty. From inspection of eq.7.31, we can easily find that in the absence of fast spin flip and other sources to generate electron at the spin down electronic state of the semiconductor nanostructure, the current density spectrum is described by

$$J_{\alpha}(\omega)\Big|_{sc} = \frac{2e}{\hbar^2} \sum_{n \neq \alpha} \Big\{ \Big[\frac{[n_{\alpha\sigma} - n_{n\sigma}]}{[\omega - \frac{1}{\hbar}[\Delta_{\alpha n}]]} [V_{\alpha n}^{\sigma\sigma}(\omega) V_{\alpha n}^{*\sigma\sigma}(\omega)] \qquad (7.32)$$

The current spectrum appears as a singlet centered at $\omega = \frac{1}{\hbar}\Delta_{\alpha n}^{\sigma\sigma}$ and with height of the spectral peak giving the measure of the tunnel coupling between the states of electrons of like spin in the coupled materials. In the presence of fast spin flip, the probability for the tunneling of the spin polarized electron at the contact to both spin polarization states of the degenerate level in the nanostructure will become finite. When there is strong correlation between the spin degenerate single level states of the nanostructure, the corresponding current spectrum could be determined using eq.7.25 and setting the requirement for strong correlation

$$n_{n\bar{\sigma}} + n_{n\sigma} = 1 \tag{7.33}$$

Then the step will finally leads to

$$J_{\alpha}(\omega)\Big|_{Cor} = \frac{2e}{\hbar^2}\sum_{n\neq\alpha}\left\{\left[\frac{[n_{\alpha\sigma} - n_{n\sigma}]}{[\omega - \frac{1}{\hbar}[\Delta_{\alpha n} - \frac{1}{2}U_n + \frac{1}{2}U_n n_{n\sigma}]}V_{\alpha n}^{\sigma\sigma}(\omega)V_{\alpha n}^{*\sigma\sigma}(\omega)\right.\right.$$

$$\left.\left. + \frac{[n_{n\sigma}]}{[\omega - \frac{1}{\hbar}[\Delta_{\alpha n} - \frac{1}{2}U_n n_{n\sigma}]}V_{\alpha n}^{\sigma\bar{\sigma}}(\omega)V_{\alpha n}^{*\sigma\bar{\sigma}}(\omega)\right]\right\} \tag{7.34}$$

The second term in the right hand side of this equation vanishes when the spin up state in the semiconductor nanostructure is unoccupied $(n_{n\sigma} = 0)$. Also, the contribution from the first term in the equation vanishes when the spin up state in the nanostructure is occupied. The contribution to the current spectrum peaks at $\omega = \frac{1}{\hbar}[\Delta_{\alpha n} - \frac{1}{2}U_n]$ with the height of the peak is determined by both the coupling between states with like spins and the coupling between electronic states of unlike spins. In general, the correlation between the states varies with time and as a result the current spectrum appears in the form of a doublet with peaks, Fig.7.2, at $\omega_o = \frac{1}{\hbar}[\Delta_{\alpha n}]$ and $\omega = \frac{1}{\hbar}[\Delta_{\alpha n} - \frac{1}{2}U_n]$.

7.3.3 Tunnel coupled Semiconductor Nanostructures

A double well like configuration, Fig.7.4, is the model structure we will now consider for investigating the effects of dynamical correlation when the cell is under short voltage pulse. The structure consists two contacting semiconductor nanostructures each with dimension in the length scale for strong quantum confinement. The dimension of the constituent semiconductor nanostructures is such that each could be modeled as a unit characterized by widely separated unoccupied spin degenerate levels. This stems from the requirement that transitions from the lower unoccupied orbital to the next higher level become nearly unlikely under the experimental conditions of interest. For such a splitting of levels be realized, it will be of great importance for the constituents be prepared from high purity material and with high geometrical perfection. Moreover, the surface states also need to be controlled sufficiently by passivating under appropriate chemical environment as mentioned in chapter2.

For the structure to ensure strong correlation between the spin degenerate states when operated at small perturbing field, the lower unoccupied spin degenerate levels in the coupled semiconductors need to be very close and the thickness of the interspersing layer between the two nanostructures must be very small, not exceeding few atomic dimensions. This together with the perfection in contact makings will be important to make the contacting layer transparent for tunneling and ensure strong coupling of the states in the two semiconductor regions: The first region represented by spin degenerate level α, and the second which is represented by the level n, as shown in Fig.7.4. For low applied voltage, the maximum probability for the tunneling of electrons into and out of the each dot region in such an assembly is due to the charge and spin polarization transferring proximity coupling between the lower unoccupied levels in the coupled structure.

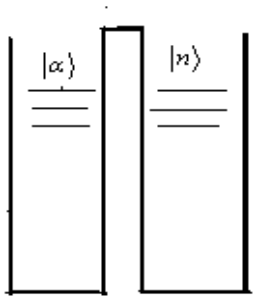

Fig.7.4: *Schematic diagram for coupled dot structure*

The coupled semiconductor nanostructures could be operated under a spin polarized electron injection or via injection of both spin polarizations from the contact at one side, from left end in Fig7.4, of the coupled structure. The charge and spin polarization transfer through the coupled structures is described using the same package of eq.7.25 but with a modification of the single electron energy according to

$$\varepsilon_{\alpha\sigma_i}(t) = \varepsilon^{o}_{\alpha\sigma_i} + \Sigma_{\alpha\alpha}(t) + \tfrac{1}{2}U_{\alpha}n_{\alpha\bar{\sigma}_i}(t) \qquad (7.35a)$$

$$\varepsilon_{n\sigma_i}(t) = \varepsilon^{o}_{n\sigma_i} + \Sigma_{nn}(t) + \tfrac{1}{2}U_{n}n_{n\bar{\sigma}_i}(t) \qquad (7.35b)$$

As a general feature of the tunnel transfer it will be worth to recall that the resulting current to depend on the injection or the generation of the transport electrons, the influence of fast spin flipping processes, the charging energies of the component semiconductor nanostructures, the biasing potential and of course on the level difference of the electrons in the coupled materials and the occupation of these levels. This last mentioned feature is an important element as far as the distinction of the configuration from those presented in the preceding sections is considered. The Fermi gas approximation made for the contact material in the preceding sections has no validity for application to the semiconductor

from which the tunneling out of the electrons is taking place. The occupation of the level α in the left semiconductor is determined by the rate of injection or rate of generation in the case when the operation is under radiation, and the spin polarization of the injected electrons at the far left end of the coupled structure, Fig.7.4. In the following, we will continue in dealing on the correlation effects when the device structure is under different operating conditions.

When the device is operating through the injection of a spin polarized electron to the level α of the semiconductor at the left and under no fast flipping effect at the interface with the injecting lead, the spectrum of the current density tunneling to the second semiconductor, by virtue of eq.7.25, is

$$J_\alpha(\omega) = \frac{2e}{\hbar^2} \sum_{n\neq\alpha} \{ \frac{[n_{\alpha\sigma} - n_{n\sigma}]}{\omega - \frac{1}{\hbar}[\Delta_{\alpha n} - \frac{1}{2}U_n n_{n\bar{\sigma}})]} V_{\alpha,n}^{\sigma\sigma}(\omega) V_{\alpha n}^{*\sigma\sigma}(\omega)$$

$$+ \frac{[n_{\alpha\sigma} - n_{n\bar{\sigma}}]}{\omega - \frac{1}{\hbar}[\Delta_{\alpha n} - \frac{1}{2}U_n n_{n\sigma})]} V_{\alpha,n}^{\sigma\bar{\sigma}}(\omega) V_{\alpha n}^{*\sigma\bar{\sigma}}(\omega) \} \qquad (7.36)$$

This is the tunneling current spectrum in the absence of the local spin flip effects. Clearly there is no current tunneling into the second region when the state $|\alpha\sigma\rangle$ in the first is empty which is so prior to the injection at the left contact or during the time interval between the tunneling out of injected electron to the second region and the next injection at the left contact. There will be no tunneling transfer even when there is an electron at the state $|\alpha\sigma\rangle$ as far as the spin degenerate level in the second is occupied. The time distribution for this blockade phenomenon depends on the relaxation of the electron in each unit, the injection rate at the left contact and as well on the spin flip effects if that is present. The spectrum of the current tunneling in to the second nanostructure will appear in the form of a doublet with peaks at $\omega = \frac{1}{\hbar}[\Delta_{\alpha n} - \frac{1}{2}U_n]$ and $\omega = \frac{1}{\hbar}[\Delta_{\alpha n}]$. The peak

at $\omega = \frac{1}{\hbar}[\Delta_{\alpha n}]$ refers the tunneling when the spin degenerate levels in the second material is empty. The measure of the spectral height of this second peak corresponds to the effective coupling, $\left|V_{\alpha n}^{\sigma\sigma}(\omega)\right|^2 + \left|V_{\alpha n}^{\sigma\bar{\sigma}}(\omega)\right|^2$. The peak at the lower spectral point on the other hand corresponds to a situation where fast spin flipping interaction at the interface between the two semiconductors and processes that could lead to the generation of electron of either spin polarization in the second material are present. We recall however that the local spin flipping effects are already considered negligible, or absent. In absence of interaction with external radiation field or other circuits of the second material, the only option for generation of electron of opposite spin polarization is when there is a fast spin flipping interaction at the interface between the semiconductors. In a special case when the interaction at the interface has no a fast spin flipping effect, the current contribution corresponding to the lower spectral peak diminishes. This leads to a spin polarized current described by

$$J_\alpha(\omega) = \frac{2e}{\mathrm{h}^2} \sum_{n \neq \alpha} \frac{[n_{\alpha\sigma} - n_{n\sigma}]}{\omega - \frac{1}{\mathrm{h}}\Delta_{\alpha n}} \left|V_{\alpha n}^{\sigma\sigma}(\omega)\right|^2 \qquad (7.37)$$

The situation is more complex when the configuration is operating via filling the single spin degenerate level by electrons which are opposite in their spin polarizations. This readily occur when the injection at the left contact, Fig.7.4 is from a spin degenerate contact or when the generation of the transport carriers is by radiation or when both radiation and injection from contacts are the methods involved.

Under the condition where the occupation in both the coupled units are time dependent, the system could follow complex pathways: The tunneling could be while both the degenerate states in the first are occupied while the states in the second are empty or only partly filled or when the degenerate levels in both are only partially filled. In the case of the

second, the system can follow two pathways; while the spin degenerate level in the first dot is completely occupied, the level in the second may be occupied only by a spin up electron or by a spin down electron. Similarly the situation in the third case offers the possibility for more pathways. The partial filling of the levels could be with the single electron in the levels in the two regions are either similar or opposite in their spin polarization. According to the laws of quantum mechanics, the total state of the system at any moment thus becomes a superposition of these configurations. The tunneling current accordingly is the outcome of the electron and spin polarization wave tunneling transfer from one region to the other of the system which itself is characterized to be a superposition state of the various configurations.

One could find therefore when analyzed on the basis of this understanding the expression in eq.7.25 suggests the spectrum of the current tunneling into the second region under this general situation to exhibit the features reflected by the spectral curves in Fig.7.5. We notice that the tunneling current in a general case to appear with four characteristic maxima located at $\omega_1 = \frac{1}{\hbar}[\Delta_{\alpha n} - \frac{1}{2}U_n]$, $\omega_2 = \frac{1}{\hbar}[\Delta_{\alpha n}]$, $\omega_3 = \frac{1}{\hbar}[\Delta_{\alpha n} + \frac{1}{2}(U_\alpha - U_n)]$ and $\omega_4 = \frac{1}{\hbar}[\Delta_{\alpha n} + \frac{1}{2}U_\alpha]$. The positions and height measures of the spectral peaks are of course valuable resources rendering important information on the interactions underlying the transport. As predicted by the characteristic relationships in eq.7.25, the height measure of the spectral peaks corresponds to the strength of the coupling responsible for the tunneling transfer. However, to interpret the result we primarily require filtering out the nature of the electron-spin polarization transfer implied by the characteristic relations. From inspection of the characteristic equations we can easily notice that the spectral peak at ω_4 is to be associated to the transfer of two electrons of

opposite spins from the shifted energy at $\varepsilon_\alpha = \varepsilon_\alpha^o + \frac{1}{2}U_\alpha$ in the nanostructure at the left (Fig.7.4) to the spin degenerate level at energy ε_n^o in the second material. Since the presence of the two electrons of opposite spins modifies the energy structure in the material regions it is unlikely both to make the transition to the ground state energy of the unoccupied single spin degenerate level. It is only one electron that could make the transition to the level at ε_n^o. This leads us to think of a process involving two types of transitions; the transfer of one electron to the unoccupied state degenerate level in the second material region and the tunneling to a virtual state of the second electron. Such a tunneling to a virtual state, which also referred as co-tunneling, is known to have negligible contribution to the measurable current [117,118]. As a result the height of the spectral peak at ω_4 due to the tunneling that results in the occupation of the single level ε_n^o in the second region by an electron of spin σ or $\bar{\sigma}$ respectively would be either

$$I(\omega_4) = \left|V_{\alpha n}^{\sigma\sigma}(\omega)\right|^2 + \left|V_{\alpha n}^{\bar{\sigma}\sigma}(\omega)\right|^2 \qquad (7.38a)$$

or,

$$I(\omega_4) = \left|V_{\alpha n}^{\bar{\sigma}\bar{\sigma}}(\omega)\right|^2 + \left|V_{\alpha n}^{\sigma\bar{\sigma}}(\omega)\right|^2 \qquad (7.38b)$$

In absence of fast spin flipping or when the influence of this is of a negligible order, the contributions of the last term is suppressed giving

$$I(\omega_4) = \left|V_{\alpha n}^{\sigma\sigma}(\omega)\right|^2 \text{ or } \left(\left|V_{\alpha n}^{\bar{\sigma}\bar{\sigma}}(\omega)\right|^2\right) \qquad (7.38c)$$

The strength of the coupling represented by the height measures at the remaining three spectral peak positions; ω_1, ω_2 and ω_3, under the

condition of no fast flipping effects are similarly approximated by equations of the form

$$I(\omega) = \left| V_{\alpha n}^{\sigma\sigma}(\omega) \right|^2 \quad \text{or} \quad I(\omega) = \left| V_{\alpha n}^{\bar{\sigma}\bar{\sigma}}(\omega) \right|^2 \tag{7.39}$$

In the situation when the fast spin flipping effects become significant, this in fact needs the corresponding contributions to be considered.

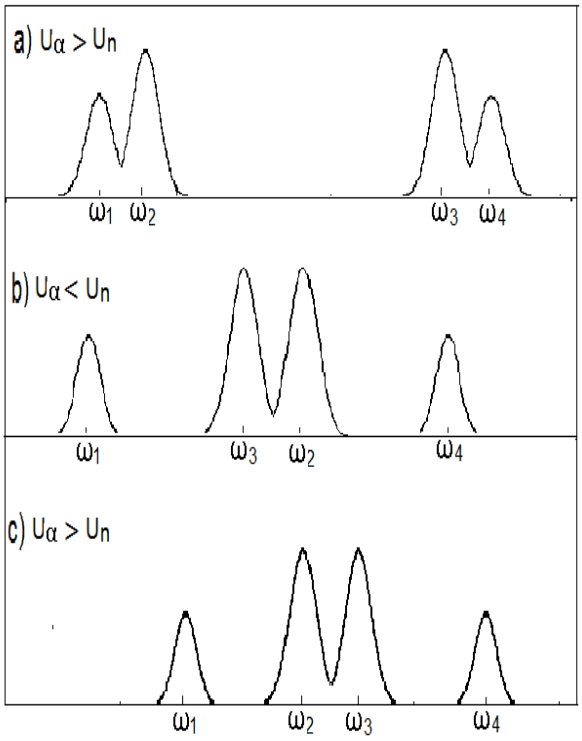

Fig.7.5: *Spectral diagram of the tunneling current density in coupled semiconductor nanostructures predicted by the model.*

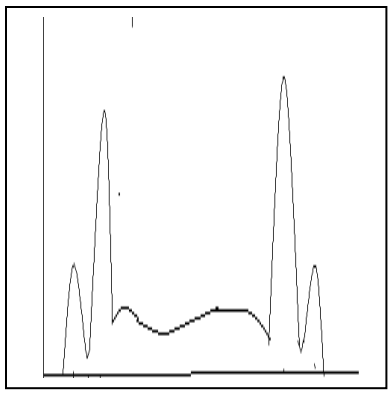

Fig.7.6: *Spectral diagram of the tunneli current density in coupled semiconduct nanostructures after [119].*

In the spectral diagrams of Fig.7.5, the relative positions between ω_2 and ω_3 may vary in sign, spacing or both depending on the charging energies. When the applied biasing potential is assumed to be completely absorbed at the contacts, the relative positions between ω_2 and ω_3, and also all spectral peak locations in general vary with changes in the charging energies. This clearly suggests the possibility of tuning the tunneling transfer by a mechanism that allows monitoring of the charging

energies in each region independently. Of course, this calls for the technical step of using a gating structure.

One special case we may come across when dealing on the effect of varying the charging energies is the situation where the charging energies in both the coupled units are set at equal values. From taking the expressions in eq.7.25 for the limiting case when $U_\alpha \to U_n$ we can easily find that the spectral peaks at ω_2 and ω_3 coincide with the other two side peaks centered at equal distance but from opposite sides of the central maxima. The resulting current spectrum is a triplet (Fig.7.7) with peaks at $\omega_1 = \frac{1}{\hbar}[\Delta_{\alpha n} - \frac{1}{2}U_\alpha]$, $\omega_2 = \omega_3 = \frac{1}{\hbar}\Delta_{\alpha n}$, and $\omega_4 = \frac{1}{\hbar}[\Delta_{\alpha n} + \frac{1}{2}U_\alpha]$. The spectral position $\omega_2 = \omega_3$ is the common peak position of the current spectrum due to two tunneling transfers that cost the same amount of energy. This becomes so since the tunneling from the state at $\varepsilon_{\alpha 1}$ in the first region to the state at ε_{n1} in the second and the tunneling transfer from $\varepsilon_{\alpha 1} + \frac{1}{2}U_\alpha$ to $\varepsilon_{n1} + \frac{1}{2}U_n$ be relaxations across the same energy difference when $U_\alpha = U_n$.

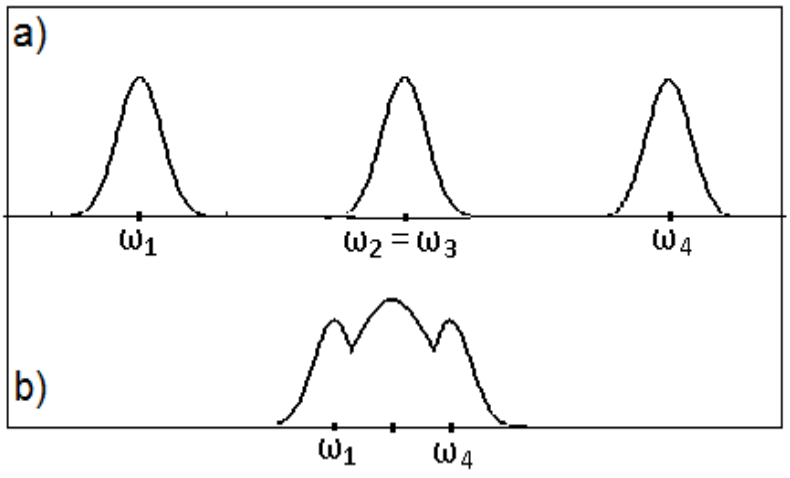

Fig. 7.7: *Current density in coupled semiconductors with the same charging energy.*

In many practical situations, there is strong interest for the two elements to correlate strongly, which may be the case for instance when applied for measurement purposes. When this is for spin preserving transfer, the condition for strong correlation between inter-dot states is (eq.7.33)

$$n_{\alpha\sigma} + n_{n\sigma} = n_{\alpha\bar{\sigma}} + n_{n\bar{\sigma}} = 1 \tag{7.40}$$

By virtue of this criterion the tunneling current spectrum (eq.7.25) will become

$$\begin{aligned} J_\alpha(\omega) = \frac{2e}{\hbar^2} \sum_{n\neq\alpha} \Bigg\{ & \frac{[2n_{\alpha\sigma} - 1]}{\omega - \frac{1}{\hbar}[\Delta_{\alpha n} + \frac{1}{2}(U_\alpha + U_n)n_{\alpha\bar{\sigma}} - \frac{1}{2}U_n]} V_{\alpha,n}^{\sigma\sigma}(\omega) V_{\alpha n}^{*\sigma\sigma}(\omega) \\ & + \frac{[2n_{\alpha\bar{\sigma}} - 1]}{\omega - \frac{1}{\hbar}[\Delta_{\alpha n} + \frac{1}{2}(U_\alpha + U_n)n_{\alpha\sigma} - \frac{1}{2}U_n]} V_{\alpha,n}^{\bar{\sigma}\bar{\sigma}}(\omega) V_{\alpha n}^{*\bar{\sigma}\bar{\sigma}}(\omega) \\ & + \frac{[n_{\alpha\sigma} + n_{\alpha\bar{\sigma}} - 1]}{\omega - \frac{1}{\hbar}[\Delta_{\alpha n} + \frac{1}{2}(U_\alpha n_{\alpha\bar{\sigma}} + U_n n_{\alpha\sigma}) - \frac{1}{2}U_n)]} V_{\alpha,n}^{\sigma\bar{\sigma}}(\omega) V_{\alpha n}^{*\sigma\bar{\sigma}}(\omega) \\ & + \frac{[n_{\alpha\bar{\sigma}} + n_{\alpha\sigma} - 1]}{\omega - \frac{1}{\hbar}[\Delta_{\alpha n} + \frac{1}{2}(U_\alpha n_{\alpha\sigma} + U_n n_{\alpha\bar{\sigma}}) - \frac{1}{2}U_n]} V_{\alpha,n}^{\bar{\sigma}\sigma}(\omega) V_{\alpha n}^{*\bar{\sigma}\sigma}(\omega) \Bigg\} \end{aligned} \tag{7.41}$$

This result indicates two special cases which are of interest both from theoretical and practical points of view. One of these is the tunneling transport when in addition to the inter-dot state correlations the intra-dot states of the spin degenerate single level are also strongly correlated. Under this condition the last two terms in eq.7.41 and either of the first two terms in the equation vanish leading to

$$J_\alpha(\omega) = \frac{2e}{\hbar^2} \sum_{n\neq\alpha} \frac{\left| V_{\alpha n}^{\sigma_i\sigma_i}(\omega) \right|^2}{\omega - \frac{1}{\hbar}[\Delta_{\alpha n} - \frac{1}{2}U_n]} \tag{7.42}$$

Where, σ_i refers to either of the two spin polarizations, σ or $\bar{\sigma}$. According to the predictions, lack of correlation between intra-dot states is leading to a situation where co-tunneling and spin flipping significantly influence the transport. This is in agreement with the understandings which the formulations in many contributions that devote in studying the transport in mesoscopic systems are based [117-119]. The current density spectrum given by the relation in eq.7.42 represent the electron and spin polarization current tunneling from one of the coupled nanostructures to the other under the condition of strong inter-dot and intra-dot states correlations. This is practically representing the current spectrum in sequential tunneling transport.

The spectral diagram in Fig.7.6 provides the summary of recent studies conducted in the tunneling of electrons in coupled semiconductor dots [119]. The reported spectral diagram has four spectral maxima emerging as pairs of closely spaced peaks similarly to that predicted by the spectral

diagram in Fig.7.5 of the present study. As will be explained by comparing to other results shortly, the difference in the distribution and spacing of the spectral peaks in Fig. 7.5 and Fig.7.7 from that reported in [119] is for the same reason that lead to similar variations among the spectral curves produced in this work for different experimental conditions. In clear statements, the tunneling current spectral graph depicted in Fig.7.7 refers only to a particular experimental condition. However, this alone cannot be sufficient to be the reason for the variations in the spectral features predicted in the present work and that of the result in Fig.7.6 reported in [119].

Primarily, the possibility for observing the tunneling current is only when the tunneling is a likely process for the particular condition of the system. For the charge and spin polarization transfer to take place when $U_\alpha < U_n$ and without assisted by other interactions, such as the

interactions with photons and phonons, it requires the time dependent level difference to satisfy the condition

$$\varepsilon_\alpha - \varepsilon_n > \frac{1}{2}(U_n - U_\alpha) \qquad \text{for} \quad U_\alpha < U_n \tag{7.43a}$$

$$(\varepsilon_\alpha^o - \varepsilon_n^o) + (\Sigma_{\alpha\alpha}^s - \Sigma_{nn}^s) > \frac{1}{2}(U_n - U_\alpha) \tag{7.43b}$$

This may require therefore structural tuning of the system so that the ground state level energy in the first to exceed the corresponding energy value in the second or to employ biasing voltage tuning. On the other hand when $U_\alpha > U_n$, the peak at ω_3 of the current spectrum will obviously lie in the higher spectral side from the spectral peak at ω_2 . However, this prediction could be valid only as far as the time dependent difference between the spin degenerate levels in the two regions is less in value from the barrier height, φ_B ;

$$\varepsilon_\alpha - \varepsilon_n + \frac{1}{2}(U_\alpha - U_n) < \varphi_B \quad \text{for} \quad U_\alpha > U_n \tag{7.44}$$

This is a condition which only demands the transport to remain in the tunneling regime. We also notice on the other hand that the charging energy determines the position in the spectral graph of the current peaks and consequently the spacing between the spectral peaks. This characteristic dependence of the current on the charging energies is of practical interest since it offers the opportunity for controlling the dynamical correlation effects. The spacing, Δ_p, between the centers of the current spectrum peaks from the lower spectral side, ω_1 and ω_2, and the spacing of the spectral peak positions in the higher spectral side, ω_3 and ω_4, measure the same:

$$\Delta_p = \omega_2 - \omega_1 = \omega_4 - \omega_3 = \frac{1}{2\hbar} U_n \qquad (7.45)$$

This is signifying that the dynamical correlation deteriorates and consequently the adjacent peaks in Fig. 7.5 practically coincide resulting in a doublet as U_n becomes vanishingly small, $U_n \to 0$.

The height difference of the spectral peaks predicted by the result in this work and the appearance of the spectral peak in the form of a triplet as depicted in Fig.7.7a is in good agreement with the reports in other contributions [120-122].This could be explained quite easily on the basis of the evolution of the occupation probabilities of the spin degenerate states as in. In Fig. 7.7b is shown a diagram that depicts the probability of finding an electron of one spin polarization with energy corresponding to the single spin degenerate level of a double dot configuration similar to that considered in our study. It demonstrates that under the condition of strong correlation between the states in the two regions the sum of the occupation probability in the coupled materials is unity and the probability for occupation in either dot varies with time: It starts where the occupation in the first semiconductor close to unity while in the other is vanishingly small. Then, the occupation in the later grows in time at the expense of reduction in the former until the probability in the second material reaches its maximum. There could be no more probability transfer until the electron in the second region relaxes energetically and the process repeats following the relaxation. The same is true also for the electron with opposite spin polarization when it is under strong correlation. For the spin degenerate coupled system where the first region is populated by electrons of both spin polarizations, the transfer of both electrons at the spin degenerate level have finite probabilities there by leading to tunneling current contribution exceeding from that resulted from the tunneling transfer of the electron of one spin polarization alone.

The triplet shown in Fig.7.7 represents the current spectrum in the double dot structure when it is under the condition of strong correlation and with the charging energies in both units is kept the same. This will be more realistic when the detuning between the spin degenerate single levels in the two semiconductor dots vanishingly small so that the level variation not to impede the tunneling transfer under small biasing voltage. The phenomenon predicted by the result is in agreement with other studies [120-122]. In absence of time varying levels and occupation of the states in the first semiconductor from where the tunneling to the other unit is taking place, the triplets are unlikely.

7.4 Conclusion

In the discussion presented thus far in this chapter dynamical correlation effects in between proximity coupled units of three typical structures that involve semiconductor nanostructures are considered. Under the experimental conditions where the effects of scatterings due to other interactions, such as the interactions with phonons, are suppressed, the dynamical correlations are noticed in living their signature on experimentally accessible quantities such as the current as in the present case. As it is demonstrated in the discussions we have made so far for three typical semiconductor based structures with dimension in the order of the length scale for strong quantum confinement, the dynamical correlation effects exhibit characteristic dependence on the time dependent level difference between the states in the coupled structures, the occupation of the states, the fluctuation in the inter element couplings, the charging energy and the perturbing field. From the results we found above we noted a characteristic difference in the spectral features of the current in the three structures considered in our study. The presence of a spin degenerate state in both the coupled materials which is offering different pathways and which there by leads the system evolve as a superposition of states is among the factor to be accounted for the

semiconductor −non spin degenerate contact characteristically differ from the other two structures considered. Under the condition of strong correlation between the states in the coupled materials, the current spectrum in the former appears as a singlet while in a general case it is a doublet for a single dot- spin degenerate structure and a more complex spectrum with four peaks for a double dot configuration. With the later two are structures formed from coupling of two material regions with spin degenerate levels, there still show property variations which to be linked again to the temporal behavior of the levels and the occupancy of the states.

In a single semiconductor dot coupled with metallic contacts the region with which the electrons in the semiconductor are correlated has no fluctuation in occupation and energies of the carriers. In contrast the coupling in between the semiconductor dots appears characteristically as a superposition of different configurations and prominently homes electron and spin entanglement. The tunneling from the first semiconductor to the second is blocked whenever the spin degenerate level in the second is completely filled or when the level in the first is empty. In absence of fast spin flipping processes, the blockade may also take place when the single spin degenerate levels in each of the two material regions are partially occupied by electrons with like spins. Fast spin flipping appears as a process furnishing an additional pathway in tunnel transfer. As it is revealed by the results spin flips are expected to have no role in influencing the dynamic behavior in a coupled semiconductor nanostructure when there is strong dynamical correlation in between inter-dot states and between the intra-dot states. Under such a strong dynamic correlations, the local spin fluctuates about its ground state condition zero value and also the value of the local spin taking place when the current is blocked.

Contrarily is the situation where the strong dynamical correlation between inter-dot states is along with preserving the ground state

condition of zero local spin polarization. This is the situation calling the coupled electron tunneling phenomenon and characterized by larger current spectra. Then follows the anticipation that the coupled nano structures exhibit a superconducting behavior in the limit of very low temperature where the couplings in between the states could be nearly free from the competition with phonon interaction effects. This understanding is in agreement with theoretical and experimental studies conducted on low temperature regime transport properties in solids at the mesoscopic scale.

One could note that spin conservation destroys the characteristics that lead the current density spectrum appears in a form of a triplet. It is neither the correlation in the local spin degenerate states that to be accounted to this feature. The dynamic correlation associated to the fluctuation in the tunnel coupling is what comes as the factor responsible for the observed spectral behavior. When it is said the fluctuation in the tunnel couplings, it is in the sense that the couplings transferring electrons between states with opposite spin polarizations are included. In absence of this tunnel coupling and a non vanishing net spin in the regions, the triplet will become unlikely to occur. There come the anticipation that this same phenomenon could be realized in absence of a spin switching tunneling if the charge and spin polarization transfers are enhanced by photon assisted processes: A condition which is sometimes regarded as a means for realizing the Schrödinger cat state.

8

Optically Triggered Dynamical Correlation in Proximity Coupled Semiconductor Nanostructures with Transparent Boundaries

8.1 Background

The resonant exchange of photons by closely spaced atoms has been studied by various groups [123-124]. It is presently well established in the field of atomic optics that atoms can become photon coupled when they are placed very close to each other, leading to dipole-dipole interactions and the Förster exchange process. Similar studies conducted on quantum dots have also shown evidences of photon coupling between closely spaced nanodots in a cavity. Nanostructures have a discrete energy structure that makes them interact through exchanging photons just as it is between atoms [112,113].Evidences of photon exchange between closely spaced quantum dots under a radiation field and the possibilities for charge and spin polarization exchange when the interacting inter-dot spacing is in the tunneling regime points out the presence of a physical situation where understanding of the interlacing between the two processes will be important. In this work we theoretically investigate the influence of a photon assisted electron and spin polarization wave exchange couplings in between neighboring QDs interspersed by interfacial regions of different transparency.

8.2 Modeling the dynamics of Interaction

The prime interest here is on the short time response of silicon nanostructure, both with and without inbuilt contacts. The sketch of a double nanostructure assembly with contacting layer of atomic dimension is shown in Fig.8.1. The two quantum point contacts are where the connection to the external elements maintaining the biasing potential difference is made. This is, perhaps, identical in configuration with the unit devices available in many complex systems. The central region or the active material, which is a silicon nano structure for the present case, is in a form of spherical dot. An active region built from a material of high chemical purity, geometrical perfection, and appropriately tailored surface structure is considered. The samples are considered to be passivated under appropriate environment such that the surface contributions to the states in between the lower empty and the higher occupied molecular levels are pushed out of this range. In devices prepared under this condition, the orbital energy of the electrons undergoes a level shift that decays with distance from the surface. This is perhaps a feature to be exploited for fixed tuning of devices. As a step toward this, we limit our discussion to nanostructures of dimension in quantum confinement regime.

The fluctuating interactions induced between the sub band states following the action of radiation, give rise to dynamical correlations of inter-band states in each region and between intra sub band states from opposite sides of the interface. Because the correlated sub band states at the interfacial region in both sides are coupled with the valence states by the photon assisted electron and polarization wave exchanging coupling, the process is likely to lead to the formation of inter sub-band correlations. The whole set of interaction has the feature typical to be represented by the V configuration as shown in Fig.8.1. The physical situation is where the interplay between the whole cascade of process; tunneling, absorption-

direct transition, absorption-indirect transition and stimulated emission is evidenced. More populated state in the first material suffers more in stimulated emission and counter resistance for tunneling if the action of the tunneling is to result transfer of spin polarization of same kind. For barrier width in the order of only few atomic spacing (~3a), the indirect transition in real space could not be undermined which is very much true especially at the mesoscopic scale where finding small scale is the challenge. Consequently the transfer of opposite spin polarization by the indirect transition in real space and the depopulation of excessive electrons of one spin polarization by stimulated transition become processes having the role of attending the spin polarization book keeping.

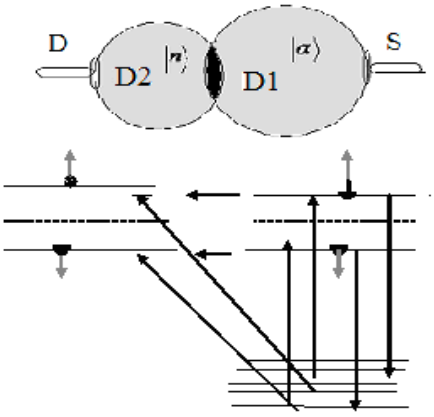

Fig. 8.1: *Interaction diagram for coupled nanostructures with transparent boundary.*

The coupling between the states at the two regions cannot be constant even when the coupled configuration is under a fixed bias. Since these electrons and spin polarization wave exchanging states have fluctuating levels and occupation probabilities, the dynamical influence has a similar effect as the fluctuating couplings. In short, the coupling between the fluctuating levels leads to the formation of states that evolve under variable correlations. Because of the contribution of these processes, the exchange between the conduction states of the interfacial region will not be delayed until the temporal limit for the spin conserving mechanism. The indirect transition in real space appears with a spin valving role against the delay

for spin conservation. This complex dynamical situation is valuable in leading to the entanglement of the spin degenerate states. When entanglement takes place, the situation could no more be possible to be described by superposing the bare spin degenerate states as we did in the preceding section.

Investigation of the population fluctuation will be a suitable gate way for analyzing the effects of dynamical correlations between the states in the coupled double nanostructure assembly. One experimentally accessible quantity which we can conveniently link with the fluctuation in the equal time correlation is the current density. This is however a step subject to our precession in accounting the states under the particular electron exchanging couplings. Of course the present discussion concentrates on coupled semiconductor nanostructures of dimension in the quantum confinement regime. Also, the system is considered to be excited by radiation of frequency at about the HOMO-LUMO transition frequency. This allows modeling each dot by a single unfilled level. In the special case when the radiation field is to bath only one of the dots, the possibility for the influx optical information to reach deeper in the region of the second will greatly depend on the relative detuning between levels in the two regions and the nature of the inter-dot boundary.

The current density resulting from the transfer of electron to the LUMO level $|\alpha\rangle$ in the second material is

$$J_{\alpha}(t) = \frac{d}{dt}\left(eN_{\alpha}(t)\right) = i\hbar e \frac{d}{dt} G^{<}_{\alpha,\alpha}(t,t) \qquad (8.1a)$$

The change through time of the occupation probability of the LUMO state in the second material, for the case under consideration, is in general to be accounted to two transfer processes; processes that link this state with the states $|C\rangle$ and $|Vj\rangle$, the LUMO and HOMO states, in the first material. Accordingly, eq.8.1a could be rewritten as

$$J_\alpha(t) = e2\,\mathrm{Re}[\Sigma^s_{\alpha,V_j}(t,t)G^<_{V_j,\alpha}(t,t) + \Sigma^s_{\alpha,c}(t,t)G^<_{c,\alpha}(t,t)] \qquad (8.1b)$$

To proceed in computing for the current density, one requires first to find out the non-diagonal, in respect to energy indices, lesser Green functions appearing in the right hand side of the equation (eq.8.1). This will dictate us to go to the Dyson's equation (eq.3.25) all over again. We are now familiar that the equation of motion of the two time correlation function $G^<(r,t;r',t')$, in the primed temporal coordinate basis is (eq.3.28b)

$$\begin{aligned}\left[\frac{\partial}{\partial t'} - \frac{i}{\hbar}\varepsilon_\alpha(r',t')\right]G^<_{n\alpha}(r,t;r',t') &= \frac{i}{\hbar}\delta(r-r')\delta(t-t') \\ &+ \frac{i}{\hbar}\sum_{m\neq\alpha}\{\int_{-\infty}^{t} d\bar{t}\,G^r_{nm}(r,t;r,\bar{t})\Sigma^<_{m\alpha}(r,\bar{t};r',t') \\ &+ \int_{-\infty}^{t'} d\bar{t}\,G^<_{nm}(r,t;r,\bar{t})\Sigma^a_{m\alpha}(r,\bar{t};r',t')\}\end{aligned} \qquad (8.2a)$$

This is the equation of motion from which the correlation functions in eq.8.1 would be calculated. The equation is solved with the state index $"n"$ in the expressions is replaced by the corresponding state indices $"V_j"$ and $"C"$ in the optically excited material. For time $t' > t$, the lesser Green functions $G^<_{n\alpha}(r,t;r',t')$ refers the transfer of electrons from the state $|n\rangle$ at the position r in the first material to a state $|\alpha\rangle$ at r' which is in the second material region. Clearly, $r \neq r'$ and the first term in the right hand side of eq.8.2a vanishes. On the other hand $r'-r$ must be small enough so that the coupling could result electron transfer in between the sites. Since the presence of the spatial coordinate in the equation is no more than

providing the information which is already included via the state indices, the equation could be rewritten using only the temporal coordinates:

$$[\frac{\partial}{\partial t'} - \frac{i}{\hbar}\varepsilon_\alpha(t')]G^<_{n\alpha}(t,t') = \frac{i}{\hbar}\sum_{m\neq\alpha}\{\int_{-\infty}^{t} d\bar{t}\,G^r_{nm}(t,\bar{t})\Sigma^<_{m\alpha}(\bar{t},t') + \int_{-\infty}^{t'} d\bar{t}\,G^<_{nm}(t,\bar{t})\Sigma^a_{m\alpha}(\bar{t},t')\} \quad (8.2b)$$

The correlation functions $G^<_{C\alpha}(t,t')$ and $G^<_{Vj\alpha}(t,t')$, which one easily identifies following the replacement of the index $"n"$ by the HOMO and LUMO states indices in the first material, are representing dynamical processes with characteristically different time scales. Therefore, it will be necessary for the equations of motion for the two time correlation functions in eqs.8.2 be computed without losing the relevant information. The solution to eq.8.2 is calculated in Appendix D. The solution determined to describe the phenomenon in the temporal regime well before the scattering contributions become significant, is in the form (D13)

$$G^<_{n\alpha}(t,t) = -\frac{1}{2}\sum_{m,s\neq\alpha}\int_{t_c}^{t} dt_1 e^{\frac{i}{\hbar}\int_{t_1}^{t} d\bar{t}\,\varepsilon_\alpha(\bar{t})} G^r_{ns}(t,t_1)G^<_{sm}(t_1,t_1)\Sigma^s_{m\alpha}(t_1) \quad (8.3)$$

Substituting this result in to eq.8.1 then yields,

$$J_\alpha(t) = -e\,\mathrm{Re}\sum_{m,s\neq\alpha}\int_{t_c}^{t} dt_1 e^{\frac{i}{\hbar}\int_{t_1}^{t} d\bar{t}\,\varepsilon_\alpha(\bar{t})}\{G^r_{ns}(t,t_1)G^<_{sm}(t_1,t_1)\Sigma^s_{m\alpha}(t_1)\Sigma^s_{\alpha C}(t) + G^r_{Vjs}(t,t_1)G^<_{sm}(t_1,t_1)\Sigma^s_{m\alpha}(t_1)\Sigma^s_{\alpha Vj}(t)\} \quad (8.4a)$$

That is,

$$J_\alpha(t) = -e\,\mathrm{Re}\int_{t_c}^{t} dt_1 e^{\frac{i}{\hbar}\int_{t_1}^{t} d\bar{t}\,\varepsilon_\alpha(\bar{t})} \Big\{$$

$$G^r_{CC}(t,t_1)[G^<_{CC}(t_1,t_1)\Sigma^s_{C\alpha}(t_1) + G^<_{CVj}(t_1,t_1)\Sigma^s_{Vj\alpha}(t_1)]\Sigma^s_{\alpha C}(t)$$

$$+G^r_{VjVj}(t,t_1)[G^<_{VjC}(t_1,t_1)\Sigma^s_{C\alpha}(t_1) + G^<_{VjVj}(t_1,t_1)\Sigma^s_{Vj\alpha}(t_1)]\Sigma^s_{\alpha Vj}(t)\Big\} \qquad (8.4b)$$

To get a physical meaning out of the mathematical expressions in the preceding steps, we need first to identify the interactions the self energy terms are representing. One should bear in mind that the diagonal singular self energy term $\Sigma^s_{\alpha\alpha}(t)$ is absorbed in renormalizing the electronic energy $\varepsilon_\alpha(t)$ at the state $|\alpha\rangle$. On the other hand, the non diagonal singular self energy, $\Sigma^s_{\alpha n}(t)$, is the term which naturally consists of the energy associated with the coupling interation:

$$\Sigma^s_{\alpha n}(t) = \left(\Sigma^s_{n\alpha}(t)\right)^\dagger = -[eV_{\alpha n}(t)\delta_{nc} + e^{-i\omega_p t}\Omega_{\alpha n}\delta_{nVj}] \qquad (8.5)$$

Here, $V_{\alpha n}(t)\delta_{nc} = V_{\alpha c}(t)$ is the effective tunneling potential and includes the modification of the barrier region by the biasing field. The term $\Omega_{\alpha n}\delta_{nVj} = \Omega_{\alpha Vj}$ in the equation accounts the coupling responsible for the indirect, in real space, transition. The quantity ω_p in eq.8.5 is the radiation frequency. The equation (eq.8.4) contains lesser and retarded Green functions. All the lesser Green functions in the expression are diagonal in time and therefore represent the number density in a state if they are diagonal in energy state basis or the induced polarization when non diagonal in energy state basis. Both $G^<_{VjVj}(t_1,t_1)$ and

$G^{<}_{CC}(t_1,t_1)$ represents the occupation probabilities of photon coupled states in the same material. We have seen in chapter 6 that the occupation probabilities of atomic states strongly coupled under the action of radiation undergo Rabi oscillation. For the period within the coherent temporal regime, these can be approximated by equation similar to eq.6.14:

$$G^{<}_{nn}(t_1,t_1) = -\frac{i}{\hbar}\rho_{nn}(t_1) = -\frac{i}{\hbar}\rho_{nn}(t_C)e^{-i\omega^{\ell}_{R}t_1} \qquad (n \in V_j, C) \qquad (8.6)$$

On the other hand the non-diagonal in energy state basis equal time correlation function could be replaced by

$$G^{<}_{CVj}(t_1,t_1) = \left(G^{<}_{CVj}(t_1,t_1)\right)^{\dagger} = -\frac{i}{\hbar}\rho_{CVj}(t_1)e^{-i\,\omega_p\,t_1} \qquad (8.7)$$

In principle, the retarded Green function has to be calculated starting from the Dyson's equation. For the retarded Green function that is non diagonal in time, the solution is in the form [64]

$$G^{r}_{\beta\beta}(t,t_1) = \frac{i}{2\hbar}e^{-i\int_{t_1}^{t}(\frac{1}{\hbar}\varepsilon_\beta(\bar{t})-i\lambda_\beta)d\bar{t}} \qquad (8.8a)$$

$$G^{r}_{\alpha\beta}(t,t_1) = \frac{i}{2\hbar}e^{-i\int_{t_1}^{t}(\frac{1}{\hbar}[\varepsilon_\alpha(\bar{t})-\varepsilon_\beta(\bar{t})]-i\lambda_\beta)d\bar{t}} \qquad (8.8b)$$

We notice that the structure of the expression for the retarded Green function (eq.8.8) is suitable to make corrections against the information lost in neglecting the scattering terms during the formulation.

Replacing the self energies and the Green functions in eq.8.4 by the respective values given in eqs.8.5-8.8 and rearranging we can find that for the temporal regime well before the buildup of scattering effects the current density to be represented by

$$J_\alpha(t) = -\frac{e}{2\hbar^2}\,\mathrm{Re}\int_{t_c}^{t} dt_1 \{$$

$$\frac{1}{2}\rho_{CC}(t_C)e^{-A_\ell}e^{-i\delta_B(t-t_1)}\left(e^{i\omega_R^\ell t_1}+e^{-i\omega_R^\ell t_1}\right)eV^\dagger_{\alpha C}(t_1)eV_{\alpha C}(t)$$

$$+\frac{1}{2}\rho_{VjVj}(t_C)e^{-A_\ell}e^{-i[\delta_B-\delta_\omega](t-t_1)}\left(e^{i\omega_R^\ell t_1}+e^{-i\omega_R^\ell t_1}\right)\Omega^\dagger_{\alpha Vj}(t_1)\Omega_{\alpha Vj}(t)$$

$$+\rho_{CVj}(t_C)e^{-i\delta_B(t-t_1)}\Omega^\dagger_{\alpha Vj}(t_1)eV_{\alpha C}(t)$$

$$-\rho_{VjC}(t_C)e^{-i[\delta_B-\delta_\omega](t-t_1)}eV^\dagger_{\alpha C}(t_1)\Omega_{\alpha Vj}(t)\}\qquad (8.9)$$

Where, the parameter $\delta_\omega(t)$ in here refers the detuning and $\delta_B(t)$ is the time dependent diference between the LUMO levels in the two dots;

$$\delta_\omega = \frac{1}{\hbar}[\varepsilon_C(t)-\varepsilon_{Vj}(t)]-\omega_p \qquad (8.10a)$$

$$\delta_B = \frac{1}{\hbar}[\varepsilon_C(t)-\varepsilon_\alpha(t)] \qquad (8.10b)$$

We shall notice that the damping parameters are omitted. This is because the temporal regime of interest is assumed to be too early for the scattering contributions to significantly influence the result. The damping parameters λ_C and λ_{Vj} can be installed back at the respective positions whenever the interest goes to a temporal regime where the role of scattering effects become significant.

The current density expression in eq.8.9 is the sum of four component contributions, each with a magnitude that reflects the correlation structure between the inter-dot couplings. The component contributions given by the first two expressions in eq.8.9 are related to the two time correlations of the same coupling: The correlations between the tunnel couplings at times

t and t_1 , $eV^{\dagger}_{\alpha C}(t_1)eV_{\alpha C}(t)$, and that between the coupling responsible for the indirect transition in real space, $\Omega^{\dagger}_{\alpha Vj}(t_1)\Omega_{\alpha Vj}(t)$. The component contributions given by the last two terms are related, on the other hand, with the inter-coupling field correlation terms, $\Omega^{\dagger}_{\alpha Vj}(t_1)eV_{\alpha C}(t)$, and $eV^{\dagger}_{\alpha C}(t_1)\Omega_{\alpha Vj}(t)$. For interactions that are switched on smoothly, the two time products of the coupling terms can be approximated to depend on the difference $t-t_1$ of the two times. However, each field correlation term incidentaly vanishes for values of t_1 in the temporal regime before the build up of the inter-dot couplings. Making advantage of this last feature, the lower limit of the integrals in eq. 8.9 can be taken to minus infinity. Accordingly, eq.8.9 can be rewritten in the form

$$
\begin{aligned}
J_{\alpha}(t) = \frac{e}{2\hbar^2}\,\mathrm{Re}\int_{-\infty}^{t} dt_1 \{ & \\
& \frac{1}{2}e^{-A_{\ell}}\big[\rho_{CC}(t_c)e^{-i\delta_B(t-t_1)}\big(e^{i\omega_R^{\ell}t_1}+e^{-i\omega_R^{\ell}t_1}\big)K_T(t-t_1) \\
& +\rho_{VjVj}(t_c)e^{-i[\delta_B-\delta_{\omega}](t-t_1)}\big(e^{i\omega_R^{\ell}t_1}+e^{-i\omega_R^{\ell}t_1}\big)K_X(t-t_1)\big] \\
& +\big[\rho_{CVj}(t_c)e^{-i\delta_B(t-t_1)}K_{XT}(t-t_1) \\
& -\rho_{VjC}(t_c)e^{-i[\delta_B-\delta_{\omega}](t-t_1)}K_{TX}(t-t_1)\big]\}
\end{aligned}
\qquad (8.11)
$$

Where, K_T and K_X refer the kernels for the two time correlations of the tunnel coupling and the photon assisted proximity coupling respectively while K_{XT} and K_{TX} are the kernels for the correlation between the two couplings:

$$K_T(t-t_1) = eV^{\dagger}_{\alpha Vj}(t_1)eV_{\alpha Vj}(t) \tag{8.12a}$$

$$K_X(t-t_1) = \Omega^{\dagger}_{\alpha Vj}(t_1)\Omega_{\alpha Vj}(t) \tag{8.12b}$$

$$K_{XT}(t-t_1) = \Omega^{\dagger}_{\alpha Vj}(t_1)eV_{\alpha C}(t) \tag{8.12c}$$

$$K_{TX}(t-t_1) = eV^{\dagger}_{\alpha C}(t_1)\Omega^{\dagger}_{\alpha Vj}(t) \tag{8.12d}$$

By introducing an exponential term, $e^{\eta(t-t_1)}$, the upper limit of the intrgral is shifted to $+\infty$ such that eq.8.11 is rewritten as

$$\begin{aligned} J_\alpha(t) = \frac{e}{2\hbar^2}\,\mathrm{Re}\int_{-\infty}^{\infty}\frac{d\omega_1}{2\pi i}\int_{-\infty}^{\infty}dt_1\{ \\ \frac{1}{2}e^{-A_\ell}[\rho_{CC}(t_c)\frac{e^{-i\omega_1(t-t_1)}}{\omega_1-(\delta_B+i\eta)}(e^{i\omega_R^\ell t_1}+e^{-i\omega_R^\ell t_1})K_T(t-t_1) \\ +\rho_{VjVj}(t_c)\frac{e^{-i\omega_1(t-t_1)}}{\omega_1-(\delta_B-\delta_\omega+i\eta)}(e^{i\omega_R^\ell t_1}+e^{-i\omega_R^\ell t_1})K_X(t-t_1)] \\ +[\rho_{CVj}(t_c)\frac{e^{-i\omega_1(t-t_1)}}{\omega_1-(\delta_B+i\eta)}K_{XT}(t-t_1) \\ -\rho_{VjC}(t_c)\frac{e^{-i\omega_1(t-t_1)}}{\omega_1-(\delta_B-\delta_\omega+i\eta)}K_{XT}(t-t_1)]\} \end{aligned} \tag{8.13}$$

Upon Fourier transforming this equation, we then find the Fourier transform of the current density, $\tilde{J}_\alpha(\omega)$, to be given as

$$\tilde{J}_\alpha(\omega) = \frac{e}{2\hbar^2}\,\mathrm{Re}\int_{-\infty}^{\infty}\frac{d\omega_1}{2\pi i}\int_{-\infty}^{\infty}dt e^{-i[\omega+\omega_1]t}\int_{-\infty}^{\infty}dt_1\{$$

$$\frac{1}{2}e^{-A_\ell}[\rho_{CC}(t_c)\frac{K_T(t-t_1)}{\omega_1-(\delta_B+i\eta)}(e^{i[\omega_1+\omega_R^\ell]t_1}+e^{i[\omega_1-\omega_R^\ell]t_1})$$

$$+\rho_{VjVj}(t_c)\frac{K_X(t-t_1)}{\omega_1-(\delta_B-\delta_\omega+i\eta)}(e^{i[\omega_1+\omega_R^\ell]t_1}+e^{i[\omega_1-\omega_R^\ell]t_1})]$$

$$+[\rho_{CVj}(t_c)\frac{K_{TX}(t-t_1)}{\omega_1-(\delta_B+i\eta)}-\rho_{VjC}(t_c)\frac{K_{TX}(t-t_1)}{\omega_1-(\delta_B-\delta_\omega+i\eta)}]\}\qquad(8.14)$$

The entire expression under the outer integral is the sum of the Fourier transforms of three convolution integrals. Upon evaluating the integrals one obtains

$$\tilde{J}_\alpha(\varpi) =$$

$$\frac{\pi e^2}{4\hbar^2}e^{-A_\ell}\rho_{CC}(t_C)[\delta(\varpi-(\delta_B-\omega_R^\ell))+\delta(\varpi-(\delta_B+\omega_R^\ell))]\tilde{K}_T(\varpi)$$

$$+\frac{\pi e^2}{4\hbar^2}e^{-A_\ell}\rho_{VjVj}(t_C)[\delta(\varpi-(\delta_B-\delta_\omega-\omega_R^\ell))+\delta(\varpi-(\delta_B-\delta_\omega+\omega_R^\ell))]\tilde{K}_X(\varpi)$$

$$+\frac{\pi e^2}{2\hbar^2}[\rho_{CVj}(t_C)\delta(\varpi-\delta_B)\tilde{K}_{XT}(\varpi)-\rho_{VjC}(t_C)\delta(\varpi-(\delta_B-\delta_\omega))\tilde{K}_{TX}(\varpi)]\qquad(8.15)$$

The $\tilde{K}_S(\omega)\quad(S=X,T,XT,TX)$ here refers the transform of the respective kernels.

8.3 Discussion of Results

Eq.8.15 is developed to describe the photo current generated in coupled nanostructures with transparent boundaries when only one of the coupled units is illuminated by a radiation at the HOMO-LUMO transition frequency. It is noticed from the result that the total current density is composed of components due to bare contributions from the two proximity couplings; the tunnel coupling and photon assisted proximity coupling or indirect transition, in real space, and the superposition of the two processes. The contributions from the former two, the terms in the first two lines in the right hand side of eq.8.15, are oscillatory in nature. These components are oscillating at the Rabi frequency ω_R^{ℓ} while this is not the case for the component represented by the last term in eq.8.15.

The Fourier transform of each component contribution to the total current density is proportional to the product of a delta term and the transform of the Kernel of the couplings responsible for the electron transfer. Clearly, the current density profile is determind by the correlation structure of the dynamic couplings $eV_{\alpha c}(t)$ and $\Omega_{\alpha Vj}(t)$. The direct relationship between each component contribution in eq.8.15 and the transforms of the Kernels is to witness this feature. The delta multipliers in the equation, eq.8.15, on the otherhand stand for locking the respective term at the the spectral position where the contribution from the corresponding component is concentrated. There are six spectral peak position for $\tilde{J}_{\alpha}(\varpi)$ when the detuning, δ_{ω}, is different from zero (Fig.8.2a). The bare tunneling contribution peaks up at two spectral points that are spaced by $2\omega_R^{\ell}$. Similarily is the contribution from the bare indirect, in real space, transition. The peak position of the contribution determind by the correlation between the two electron transfering

processes constitute the central maxima separated by δ_ω. Since the detuning is small in most practical situation, there will be an overlap between the adjacent spectral peaks of the component contributions from the bare tunnel and the bare indirect transition. The detuning broadens the current spectra.

When the double dot structure is entirely in resonance with respect to the optical transition, we set $\delta_\omega = 0$ in eq.8.15. This leads $\tilde{J}_\alpha(\omega)$ to be modified as

$$\tilde{J}_\alpha(\varpi) = \frac{\pi e^2}{4\hbar^2} e^{-A_\ell} [\rho_{CC}(t_C)\tilde{K}_T(\varpi) + \rho_{VjVj}(t_C)\tilde{K}_X(\varpi)]\delta(\varpi - (\delta_B - \omega_R^\ell))$$
$$+ \frac{\pi e^2}{4\hbar^2} e^{-A_\ell} [\rho_{CC}(t_C)\tilde{K}_T(\varpi) + \rho_{VjVj}(t_C)\tilde{K}_X(\varpi)]\delta(\varpi - (\delta_B + \omega_R^\ell))$$

$$+ \frac{\pi e^2}{2\hbar^2} [\rho_{CVj}(t_C)\tilde{K}_{XT}(\varpi) - \rho_{VjC}(t_C)\tilde{K}_{TX}(\varpi)]\delta(\varpi - \delta_B) \qquad (8.16)$$

The resonance interaction with the light field modifies the photo electron transport behaviour. The contribution from the two bare transfer mechanisms, tunneling and indirect transition, become spectrally indistinguishable as the system approaches to a resonance condition. The current spetral graph in Fig.8.2b is illustrating this fact. The current density spectral graph is sharply peaked at three spectral points: at $\omega = \delta_B \pm \omega_R^\ell$ and $\omega = \delta_B$ (Fig.8.2b). The spectral curve resembles the Rabi splitting in atomic fluorescent spectral [150,151].

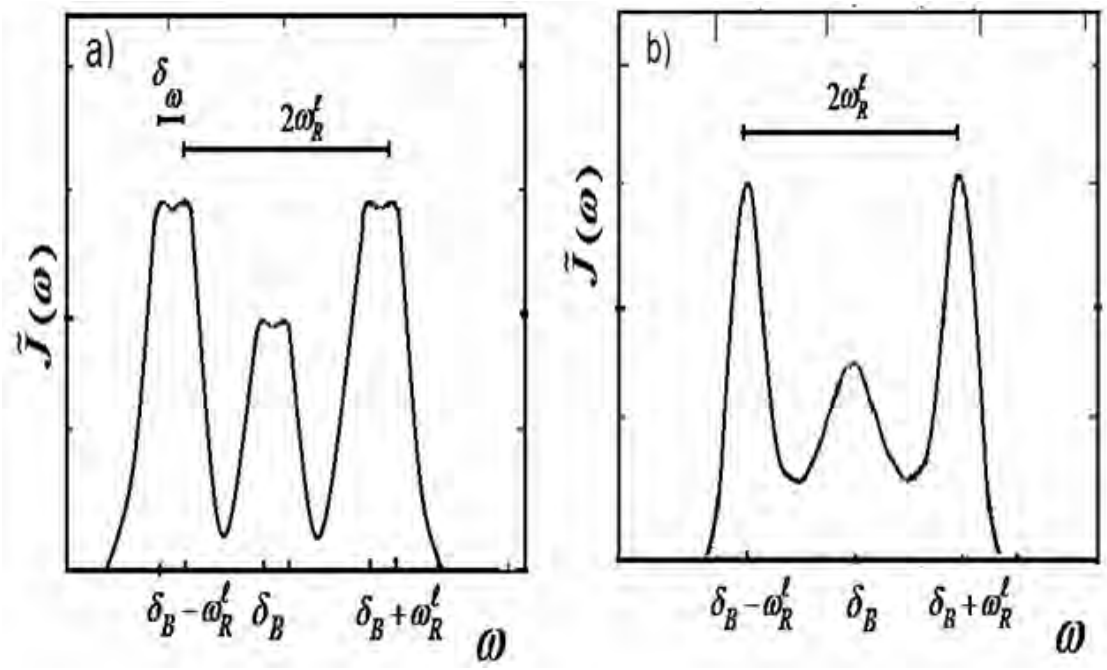

Fig.8.2*: The spectral diagram of the photo current across a transparent barrier* ***a)*** *when there is a detuning,* $\delta_\omega \neq 0$. ***b)*** *When under resonant interaction with the photon field.*

Each of the contributions peaking at $\omega = \delta_B \pm \omega_R^\ell$ is a sum of the contributions from the two bare transfer mechanisms. The height measure of the two side peaks (Fig.8.2b) is the weighted sum of the spectrum of the two coupling field intensities and is determind by the correlation structures of the corresponding couplings. For delta correlated fields, for instance, $\tilde{K}_T(\omega) = |eV_{\alpha c}|^2$ and $\tilde{K}_X(\omega) = |\Omega_{\alpha V_j}|^2$. If on the otherhand the fields have a correlation structure that follows a Gaussian profie, there will be an additional factor of the form $\sqrt{\frac{\pi}{D}}e^{-\frac{\omega^2}{4D}}$ to be introduced as a multiplying factor.

The peak measure of the central peak in Fig.8.2b is determind, on the otherhand, by the cross-correlation between the two coupling fields of

different nature: the tunnel coupling and photon assisted proximity coupling. As revealed by eq.8.15 and eq.8.16, there are two component contributions to be associated with the inter-coupling field correlations. The measure of each of these component contributions is related with the Fourier transform of the Kernel for the corresponding cross correlation: $\tilde{K}_{TX}(\omega)$ and $\tilde{K}_{XT}(\omega)$. An interesting question one may come across while inspecting the contributions from the cross correlation terms is whether there is a mutual cancellation of the two during resonance. There is no doubt that there is an overlap of the two contributions when $\delta_\omega = 0$. But, this alone will not be sufficient to draw conclusion on the quantitative measure of the central maximum.

It is clear from the result in eq.8.16 that the cross correlation term is the reason for the triplet feature in the current density spectrum. To proceed in the quantitative estimation of the spectral weight at $\omega = \delta_B$, we need to once again consider the Real part of the integrand of the third component in eq.8.14. We could represent this term as:

$$I_{(XT)}(t_1,t) = \mathrm{Re}[\rho_{CVj}(t_c)K_{TX}(t-t_1) - \rho_{VjC}(t_c)K_{XT}(t-t_1)]$$

$$= \mathrm{Re}[\rho_{CVj}(t_c)\Omega^{\dagger}_{\alpha Vj}(t_1)eV_{\alpha c}(t) - (\rho_{VjC}(t_c)\Omega^{\dagger}_{\alpha Vj}(t)eV_{\alpha c}(t_1))^{\dagger}] \quad (8.17)$$

Where, the second line in eq.8.17 follows from substituting for the respective kernels from eq.8.12. Clearly, $I_{(XT)}$ vanishes at equal times and if each of the two terms in the right hand side is vanishing. But this is determind by the cross correlation between the two couplings. It is ofcourse doubtful to adopt a delta correlation structure for the interdependence between the tunnel and the photon assisted proximity couplings. We rather think of interdependence where the increase toward a maximum of the strength of one is when the other is at a vanishing order. That is, the

electron transfer due to one blocks further transfer by the same coupling and maximizes the probability for electron transfer due to the other. The presence of the photon assisted proximity coupling destroys the condition for transport in the regime of coulomb blockade. Besides this is the treathening of the system coherence by the cross correlation term. This component fluctuats differentely from the Rabi oscillating components that contribute to the side peaks. For large induced polarization the cross correlation contributes a non vanishing component oscilating at the frequency of the input radiation. The term in general has the nature of impairing the coherence in the system. A control over the barrier transparency is a crucial step for overcoming these limitations.

When the indirect transition vanishes, only the tunneling contribution survives leading to

$$\tilde{J}_{\alpha}(\varpi) = \frac{\pi e^2}{4\hbar^2} e^{-A_{\ell}} \rho_{CC}(t_C)[\delta(\varpi - (\delta_B - \omega_R^{\ell})) + \delta(\varpi - (\delta_B + \omega_R^{\ell}))]\tilde{K}_T(\varpi) \quad (8.18)$$

This is a situation at which the current density spectrum appears in a form of a doublet (Fig.8.3). The height of the peaks at Overcoming the barrier transparency problem is an important step for the realization of the single electron or single spin polarization electron transfer. This will be the point of emphasis in the next chapter.

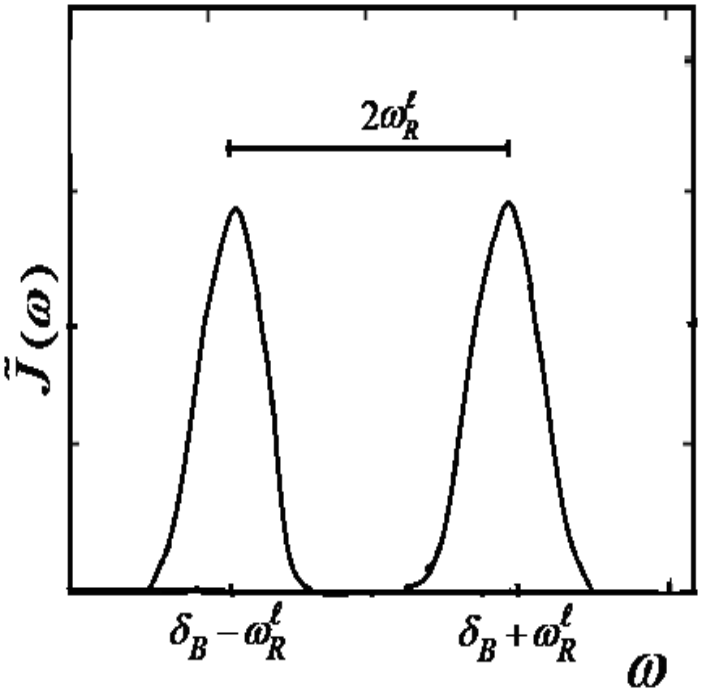

Fig.8.3: *Photo-current spectrum in the limit of a non transparent barrier*

8.4 Conclusion

When two coupled semiconductor nanostructures are interspersed by a transparent barrier region, the indirect in real space optical transition provides additional path way for communicating the two regions via particle transfer. The indirect transition is against the tendency to a Coulomb blockade and coherence. For a transport taking place between the single spin degenerate LUMO levels in the coupled materials, the effect is leading to the disappearance of a single electron sequential tunneling. This is in agreement with experimental results obtained from studying Coulomb blockade effects in semiconductor dots under strong couplings [125-127]. For a coupled structure under optical excitation, the approach toward a transport behavior in the Coulomb blockade regime requires the presence of an opaque boundary between the coupled units.

9

Optically Triggered Correlations in the Regime of Coulomb Blockade (Electron-Spin entangler Turnstile)

9.1 Background

In the preceding chapter we investigated the dynamical correlation effects in optically triggered double dot assemblies. There, the material region interspersing between the coupled dots is considered transparent for tunneling such that under the assumed strong tunnel coupling the transmission of the barrier between the coupled dots approaches unity.

In the following section we consider the situation where the interspersing region between the coupled nanostructures constitutes an opaque barrier. In this case the contribution due to the indirect transition in real space obviously vanishes. Tunneling then appears as the sole mechanism of electron and spin polarization transfer under this weak coupling condition. This is in a system where sizing effects and dynamical correlations simultaneously become relevant aspects to determine the transport properties of the structure. The strong quantum confinement effects in material systems at the nanoscale the local dynamic correlations and the dynamic correlations between the states in the coupled regions start becoming prominent in their combined role that lead to the well known transport phenomena such as the Coulomb blockade [128-132]. The coupled nanostructures, which are interspersed by non transmitting barrier, are therefore ideal for sequential tunneling in the Coulomb blockade regime. This is a candidature property for a single electron at a time tunneling transport.

Mechanisms for single charge and spin polarization transport and single photon generation have become hot research issues starting from the early period of single electron and single photon device researches [133,135]. Turnstiles are one variety of single electron transistors. In recent years spectacular examples, such as single-photon or single-electron turnstile devices, have been demonstrated [135,139]. The electron turnstile of Zrenner *et al* [138] is an optically triggered turnstile; consists of a single quantum dot embedded in a field effect structure. optical excitation creates a single electron-hole pair (exciton), which decays through tunneling into a separate electron and hole in the contacts detectable as a photocurrent. An optically triggered turnstile recently proposed by [140,141] similarly is a single electron transistor intended to support a spin polarized electron transport. The spin current is generated by leading a spin polarization independent current through a ferromagnetic material so that the spins of the out flowing electrons adopt the preferential spin direction in the domain structure of the lead. .

Our aim here is to theoretically investigate the finger prints of dynamic correlation in the spin polarized photocurrent under the coulomb blockade regime and propose model turnstile for application, in an optically triggered mode, in the near IR spectral range.

9.2 The Dynamics of carrier transfer - Modeling the Device

The transport is through a coupled nano dot, schematically shown by the inset in Fig.9.1, and incorporates a spin polarized sequential tunneling of electron under the action of radiation and biasing field. This primarily requires first to limit the transport to be limited to be through a single level. This is likely if the transport is via the Lower Unoccupied Molecular Orbital (LUMO). For this required condition to be met, the design and manufacturing of the device structure need to be in such a way both the injection from the contact and the generation of excited electron by optical

radiation not to populate the higher unoccupied levels. This could be achieved through limiting the Fermi-energy of the contact materials, the order of the biasing voltage and the spectral range of the exciting radiation. Of course the later will be much difficult unless the energy and spatial distributions of both the occupied and the unoccupied orbital states of the semiconductor nanostructures are carefully studied. Whether or not the sizes of these materials is in the order where the structure could supports bulk properties at the interior regions, the broadening of the absorption due to the level shifts for atomic sites closer to the surface is an obvious natural consequence. To overcome the complication due to this broadening of absorption and also since perfect monochromaticity is ideal, use of a radiation at about the threshold wavelength for absorption is a good alternative. This is how our choice of the exciting radiation spectrum in this discussion is guided.

To meet the requirement for a spin polarized electron tunneling, we considered the use an injecting contact that is made from a material of anti ferromagnetic nature. A contact made up of MnO fulfils both the requirement for spin polarized injection at the Fermi energy of 1.12eV. For the parameters considered in table 9.1, this value of the contact Fermi energy allows selecting a biasing voltage up to about 80meV. As a step toward ensuring the sequential tunneling of one spin polarization, the Fermi energy is limited to remain below the energy of the unoccupied state of the partially filled spin degenerate level, by an order exceeding $K_B T$. The perturbing radiation is considered to correspond to the transition from the Higher Occupied Molecular Orbital (HOMO) to this level; $\varepsilon_{\alpha\sigma} - \varepsilon_{VH} = \varepsilon_{gL} + \frac{\hbar^2\gamma^2}{2m_{ef}R_\alpha^2} + \frac{1}{2}U_\alpha$. Where, ε_{VH} is the energy of the HUMO level , ε_{gL} is the energy above the HUMO level of the conduction edge, and with the parameters in the confinement potential have their meaning as in sec. 2.3. The radii of the two silicon nanostructures, of spherical geometry,

constituting the coupled semiconductor configuration are considered as to be in accordance to the condition for sequential tunneling of the electron at $\varepsilon_{\alpha\sigma}$. This is when the confinement energies in the coupled units satisfy the inequality

$$K_B T < \frac{\hbar^2 \gamma^2}{2mR_n^2} - \frac{\hbar^2 \gamma^2}{2mR_\alpha^2} < \frac{1}{2} U_\alpha \qquad (9.1)$$

The structural parameters of the first dot set the limit for the wavelength of radiation to be used for excitation. For the dimensions considered in table.9.1, the analysis suggests use of radiation in the near IR spectral range with the operating temperature to be set below the temperature values indicated in the same table.

Table 9.1: *LUMO-LUMO splitting and maximum sample temperature of Si-double dot of different size*

Radius of Coupled Si dots (nm)		LUMO- LUMO Split (meV)	Cooling Temperature (K)
Receiver 1st dot	2nd dot		
3	5	31.73	368
4	10	23.43	272
4	12	24.79	287
5	8	10.88	125
5	10	13.39	155
5	15	15.87	184
10	15	2.48	28

The charge and spin polarization exchange between the units constituting the double dot configuration could be described well using our results in chapter six. Inverse transforming the expression in eq.6.25, we can easily

find that the current density tunneling from D_1 to D_2 under the condition of no spin flipping could be described by

$$J(t) = \frac{2e}{\hbar^2}\left|V_{\alpha,n}^{\sigma\sigma}\right|^2 [n_{\alpha\sigma} - n_{n\sigma}] \frac{Sin\left(\frac{1}{\hbar}[(\varepsilon_\alpha^o + \frac{1}{2}U_\alpha n_{\alpha\bar{\sigma}}) - (\varepsilon_n^o + \frac{1}{2}U_n n_{n\bar{\sigma}})]t\right)}{\frac{1}{\hbar}[(\varepsilon_\alpha^o + \frac{1}{2}U_\alpha n_{\alpha\bar{\sigma}}) - (\varepsilon_n^o + \frac{1}{2}U_n n_{n\bar{\sigma}})]}$$

$$+ \frac{2e}{\hbar^2}\left|V_{\alpha,n}^{\bar{\sigma}\sigma}\right|^2 [n_{\alpha\bar{\sigma}} - n_{n\bar{\sigma}}] \frac{Sin\left(\frac{1}{\hbar}[(\varepsilon_\alpha^o + \frac{1}{2}U_\alpha n_{\alpha\sigma}) - (\varepsilon_n^o + \frac{1}{2}U_n n_{n\sigma})]t\right)}{\frac{1}{\hbar}[(\varepsilon_\alpha^o + \frac{1}{2}U_\alpha n_{\alpha\sigma}) - (\varepsilon_n^o + \frac{1}{2}U_n n_{n\sigma})]} \qquad (9.2)$$

Prior to excitation and just following the injection of the spin down electron, $n_{\alpha\sigma} = n_{n\sigma} = n_{n\bar{\sigma}} = 0$ and the current density expression reduces to

$$J(t) = \frac{2e}{\hbar^2}\left|V_{\alpha,n}^{\bar{\sigma}\bar{\sigma}}\right|^2 n_{\alpha\bar{\sigma}} \frac{Sin\left(\frac{(\varepsilon_\alpha^o - \varepsilon_n^o)t}{\hbar}\right)}{\frac{1}{\hbar}[\varepsilon_\alpha^o - \varepsilon_n^o]} \qquad (9.3)$$

However, the delta function term is also insignificant since $\varepsilon_n^o > \varepsilon_\alpha^o$. Therefore, it follows that $J(t) \approx 0$ prior to the excitation.

When the spin degenerate level in the second dot is completely filled, $n_{\alpha\sigma} = n_{\alpha\bar{\sigma}} \neq 0$ and the occupation in the second dot depends on whether there is an electron that is already tunneled in to the second region. This is when the relaxation time of the second dot is large. If there is a spin up electron already tunneled in to the second dot, $n_{\alpha\sigma} - n_{n\sigma} = 0$

$$J(t) = \frac{2e}{\hbar^2}\left|V_{\alpha,n}^{\bar{\sigma}\bar{\sigma}}\right|^2 n_{\alpha\bar{\sigma}} \frac{Sin\left(\frac{1}{\hbar}[(\varepsilon_\alpha^o - \varepsilon_n^o) + \frac{1}{2}(U_\alpha - U_n)n_\sigma]t\right)}{\frac{1}{\hbar}[(\varepsilon_\alpha^o - \varepsilon_n^o) + \frac{1}{2}(U_\alpha - U_n)n_\sigma]} \qquad (9.4)$$

Again the contribution of the right hand side in this expression is suppressed by the delta function and therefore, $J(t) \approx 0$. On the other

hand when the level in D_2 is empty while the spin degenerate level in D_1 is completely filled, $n_{\alpha\sigma} = n_{\alpha\bar{\sigma}} \neq 0$ and $n_{n\sigma} = n_{n\bar{\sigma}} = 0$. Consequently eq.9.2 reduces for this case to

$$J(t) = \frac{2e}{\hbar^2}\left|V_{\alpha,n}^{\sigma\sigma}\right|^2 n_{\alpha\sigma}\,\frac{Sin\left(\frac{1}{\hbar}[(\varepsilon_\alpha^o + \frac{1}{2}U_\alpha n_{\alpha\bar{\sigma}}) - \varepsilon_n^o]t\right)}{\frac{1}{\hbar}[(\varepsilon_\alpha^o + \frac{1}{2}U_\alpha n_{\alpha\bar{\sigma}}) - \varepsilon_n^o]}$$

$$+ \frac{2e}{\hbar^2}\left|V_{\alpha,n}^{\bar{\sigma}\bar{\sigma}}\right|^2 [n_{\alpha\bar{\sigma}}]\,\frac{Sin\left(\frac{1}{\hbar}[(\varepsilon_\alpha^o + \frac{1}{2}U_\alpha n_{\alpha\sigma}) - \varepsilon_n^o]t\right)}{\frac{1}{\hbar}[(\varepsilon_\alpha^o + \frac{1}{2}U_\alpha n_{\alpha\sigma}) - \varepsilon_n^o]} \qquad (9.5)$$

Here, we come to the point where the difference in the tunneling probabilities of the two spin polarizations decides the type of the spin polarization that contributes to the transport. Both can be of significant order but with the probability to tunnel of one exceeding from the other. The non vanishing probability will not however make both contributions to be considered. The event is a competition in a time frame. The tunneling of one ahead of the other alters the situation such that the contribution of the other to be no more relevant. This information is contained in the tunneling potential term. The spin polarization with maximum tunneling probability and hence maximum tunnel coupling tunnels out from the photo excited region. It is the spin up electron, σ in the present case, which contributes to the tunneling current. The tunneling of the spin up electron alters the distribution of the occupation leading the current expression in eq.9.5 to be

$$J(t) = \frac{2e}{\hbar^2}\left|V_{\alpha,n}^{\bar{\sigma}\bar{\sigma}}\right|^2 n_{\alpha\bar{\sigma}}\,\frac{Sin\left(\frac{1}{\hbar}[\varepsilon_n^o + \frac{1}{2}U_n n_{n\sigma} - \varepsilon_\alpha^o]t\right)}{\frac{1}{\hbar}[\varepsilon_n^o + \frac{1}{2}U_n n_{n\sigma} - \varepsilon_\alpha^o]} \qquad (9.6a)$$

Hence,

$$J(t) \approx 0 \qquad (9.6b)$$

The last step follows because the delta function vanishes when the energies of the coupled states are well separated.

9.3 Basic Performance Features of the Model Device

The cascade of processes involving the injection at the contact, excitation to the unoccupied state of the spin degenerate level and the tunneling to the remaining regions then result the spin polarized tunneling phenomenon in the regime of coulomb blockade. The analysis we made using the mathematical formulation in this work is potentially powerful.

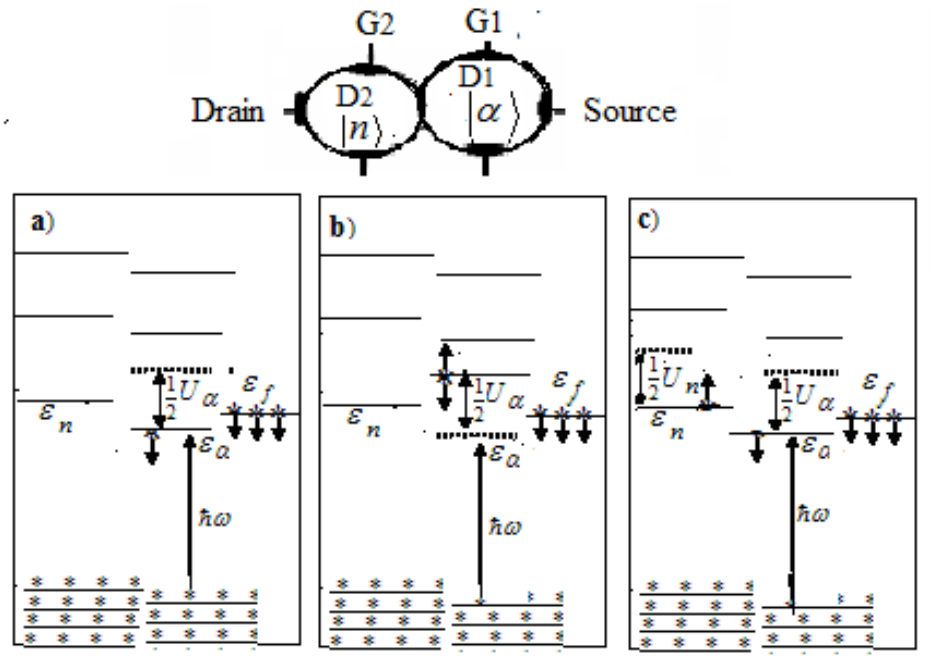

Fig.9.1: *Evolution of optically triggered charge and spin polarization in a turnstile under fixed bias.* ***a)*** *Spin down electron is injected from the contact (at* ε_f *) in to* D_1 *(at* ε_α *) and this shifts the energy of the unfilled state to* $\varepsilon_\alpha + \frac{1}{2}eU_\alpha$ ***b)*** *Transition, by absorption of photon energy* $\hbar\omega$*, in* D_1 *resulting a degenerate filled level at* $\varepsilon_\alpha + \frac{1}{2}eU_\alpha$*.* ***c)*** *Tunneling of the spin up electron in to* D_2 *(at* ε_n*) shifts the energy of the unfilled state, blocking the tunneling.*

The diagrams in Fig.9.1 and Fig.9.2 illustrate the charge and spin polarizations of the regions of the double dot configurations that predicted by our analysis in the preceding few paragraphs. In Fig.9.1 is depicted the charge and spin polarization temporal distributions in the coupled region when the system is under exciting radiation and with a fixed biasing voltage. Fig.9.2 on the other hand illustrates the situation when the turnstile is operated under optical radiation and with a pulsed biasing voltage.

Electron with minus spin polarization is tunneled from the left contact to the semiconductor nanostructure that has a spin degenerate level ε_α at the ground state condition. The presence of the injected electron will result an energy split such that the energy to the unfilled state of the degenerate level shifts up to the value $\varepsilon_\alpha + \frac{1}{2}U_\alpha$ (Fig.9.1). When the new transition frequency is close to the frequency of the perturbing radiation, it effectively result an absorption transition to the state at energy $\varepsilon_\alpha + \frac{1}{2}U_\alpha$ in the first dot. Now the filled spin degenerate level at energy $\varepsilon_\alpha + \frac{1}{2}U_\alpha$ two electrons of opposite spin polarizations, eventually to relax through quantum mechanically allowed transitions. These include the spontaneous emission, with characteristic relaxation time τ_{es} and the energy relaxation to the second dot, with characteristic time τ_{T1}. The electrons occupying the shifted energy could only relax to the energy level ε_n in the second dot. If the level ε_n in the second dot is occupied by a single electron, the available unfilled state in the second will be at the shifted energy $\varepsilon_n + \frac{1}{2}U_n$ and the injected and optically excited electrons in the first dot could neither relax in to this region unless assisted by another energy supplying mechanism. In absence of such an additional mechanism the tunneling to the second dot and hence the current will remain blocked until the electron

in the second region relaxed to the state in the adjacent region. This is so when $\varepsilon_\alpha + \frac{1}{2}U_\alpha + K_B T < \varepsilon_n + \frac{1}{2}U_n$ so that phonon.

When the level ε_n in the second dot is empty, the electron excited to the level $\varepsilon_\alpha + \frac{1}{2}U_\alpha$ in the first dot relaxes to the energy level ε_n while the associated hole diffuses in the opposite direction. Since this is accompanied by energy relaxation of the remaining electron, this makes the first dot to be ready for the next cycle. Along with providing an illustration on the line up of the process, the preceding discussion also messages how the temporal distribution of the charge and spin polarization transfer is determined by the time scale τ_{T_2} an electron in the second dot require to relax energetically to a state in the adjacent region.

During the operation of the device, the occupation of the levels in each dot and hence the electronic and spin polarizations in each region and the temporal distribution of the transport are determined by the time scale of the relaxation processes, the injection rate at the contact and the temporal characteristics, pulse width and cycle, of the radiation field. When operating under short radiation pulse and fixed biasing field, the first and the last time scales will be the prominent to determine the temporal characteristics of the observed. Primarily, the condition $\tau_{T_1} < \tau_{es}$ needs to be met if the information from the exciting pulse to be effectively communicated to the other units of the circuit. Then, the larger time scale from τ_{T_1} and τ_{T_2} will be the predominant in deciding the charge and spin polarization tunneling out from the optically excited region. Electrons of one spin polarization tunnels out from the excited region in sequence at a rate determined by τ_{T_1} if $\tau_{T_2} < \tau_{T_1}$ and at a rate determined by τ_{T_2} when $\tau_{T_2} > \tau_{T_1}$.

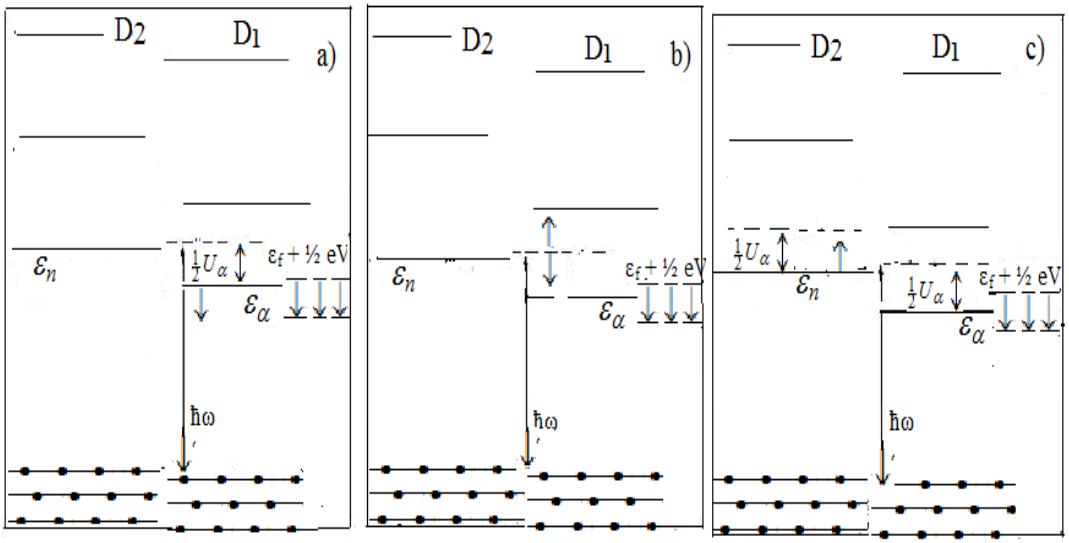

Fig.9.2: *Evolution of charge and spin polarization in the turnstile under a pulsed biasing field.* ***a)*** *Spin down electron is injected from level* $\varepsilon_f + \frac{1}{2}eV$ *in the contact to a level* ε_α *in* D_1 *and the unfilled state in* D_1 *shifts to* $\varepsilon_\alpha + \frac{1}{2}eU_\alpha$. ***b)*** *Transition, by absorption of photon energy* $\hbar\omega$, *to the* $\varepsilon_\alpha + \frac{1}{2}eU_\alpha$ *in* D_1 *leading to a degenerate filled level at this energy.* ***c)*** *Tunneling of the spin up electron to* ε_n *in D2 shifts the unfilled state of the level to* $\varepsilon_n + \frac{1}{2}eU_n$ *and leads to the relaxation of the spin down electron in* D_1.

From what has been mentioned in the preceding paragraph it could be quite apparent that the coupled structure is operating in the regime of quantum blockade, transfers single electron in sequence. The occupations of the levels in both regions fluctuate in time. Also, the charge and spin polarizations fluctuate accordingly. As the spin polarization in D_2 changes from zero to plus as electron tunnels in to it and then to zero following the electron relaxation, the spin polarization in D_1 swings from zero to minus due to the tunneling out of electron and then back again to zero following absorption transition (Figs.9.1). The charge and spin evolution in the coupled structure in the case when the operation is under a pulsed biasing field (Fig.9.2) could also be explained in the same way. The difference in the evolution indicated in Fig. 9.1 and Fig. 9.2 is that the occupation of the

spin down electron in D_1 and hence the polarization of the region oscillates due to sequence of scattering and interaction with the contact, for the first case, until the next absorption. On the other hand for a system under pulsed biasing field there is a possibility for a spin polarization distribution different from the former to be observed. When the width of the biasing field in the case illustrated by Fig.9.2 is less than the total time the electron require to undergo relaxations by tunneling from the regions of D_1 and D_2, there come a finite time in which the spin polarization of D_1 is zero while the spin polarization of D_2 is positive.

The double dot structure could support the charge and spin polarization tunneling transport in the quantum blockade regime with a promise as a realizable turnstile device. The sequential tunneling of an electron and spin polarization tunneling transfer is the out come of the intra- and inter-dot correlations. Robust condition in the first dot enhanced the spin entanglement in the coupled structure.

10

Summary

Semiconductor nanostructures are characteristically inhomogeneous. The structural inhomogeneity together with the confinement effects, make these classes of materials have energy structure leading to the formation of correlated states when under time dependent perturbations. The structure could be tailored to suit the requirement for various applications by structural tuning or monitoring the parameters of the external perturbation. The ground state property characterization of the silicon nanostructure we have made based on the OF-LDA in the DFT technique has rendered parametric association of the sample dimension, geometry and surface structure to the range of pointer state features.

The structure now supports spin degenerate states. Under the action of ultra short pulse and in the early stage of the coherent regime just following the action, the occupation probability of the dynamically coupled states oscillates at the modified Rabi frequency that carries the information on the many body aspect of the interaction. While the system is in the coherent regime absorption, the valence electronic states evolve dynamically correlated. The states evolve in such a way that the spatial degeneracy within a characteristic size of the sample becomes indistinguishable. This entanglement of the spatially degenerate states manifests in the oscillation of the coherent regime absorption. Our theoretical investigation has shown that the occupation probabilities in an optically excited nanostructure oscillate at a modified Rabi frequency $\Omega^1 = \Omega f$. Where, f is the ratio between the photon flux and the width, in energy the correlated states are distributed or the rate the correlation builds up. This quantitative result differs from the probability

oscillation in a two level system by the presence of the parameter f which carries information both in the photon number and the many body aspect of the material medium. The photon number dependent Rabi oscillation is in general complex and predicted to undergo a sequence of collapse and revival. The collapse follows as the entangled pairs are disentangled and the revival is when the states are entangled again. The sequence is found to be explained as a physical manifestation of the change of the system from a state in Fock space to an entangled state and vice versa. We found this sequence of variation in the oscillating amplitude to be described as a quantum jump effect with the number density in each state qualifies the requirement for QND observables. Although there is no quantitative description of the phenomenon so far and up to our knowledge, the application of the result for the short time scale tunneling photocurrent between proximity coupled nanostructures is found witnessing the value of the result for use as a tool in explaining the physical ground for an electron entangler turnstile which at present is under intensive research by various groups [138].

With the NEGF as the theoretical frame work, the role of electron and spin polarization exchange couplings in between proximity coupled nanostructures is also demonstrated. For nanostructures separated by an interspersing gap or material of dimension at the length scale of the tunneling regime, dynamically correlated states could be made to occur by external perturbation that could induce fluctuations in the levels. The voltage controlled fluctuation in the electron and spin polarization exchanging proximity couplings is a long time scale phenomenon. The dynamical correlation triggered by short voltage pulses lead to a spin polarization dependent phenomena. The spectrum of the tunneling current generated under short voltage pulse has two characteristic peaks separated by an order that correspond to the energy difference in the spin degenerate levels. This is however only in the situation where the materials are under the resonant tunnel coupled condition. The tunneling current under this situation has a ringing behavior. This prediction of the

result is in agreement with results in other reports and is accounted to represent the entanglement of the spin degenerate levels in the coupled materials. In a situation when the coupling is away from resonance, the resulting current spectrum may appear with two more additional spectral peaks and even diffuse more. The observed current under this situation fluctuates variably. The close agreement of the result with observations shows a promise for applications in the characterization and design of spin conserving turnstiles.

Photon assisted dynamical correlation of states under electron and spin polarization exchanging couplings is predicted to be the shortest time scale phenomenon in non photon coupled configurations. The realization of the supporting structure demands two nanostructures with small relative detuning in their confinement quantized levels to be proximity coupled with an interspersing layer in the order of atomic dimensions. The construction enables the stimulated emission and the indirect absorption transition in real space to be the fastest mechanisms attending the balance in the spin polarization wave transfer. When the coupled double structure is biased under very small potential and optically triggered, it results an electron and spin polarization current with spectral distribution characterized by a triplet similar to the Mollow's triplet in resonance electro fluorescence. The two side peaks of the tunneling photo-current appearing in opposite sides of the central maxima are distant from the later by the photon number dependent Rabi frequency. The two side peaks are noted to be proportional to the measures of two different dynamical couplings of the states in the two regions: One is proportional to the strength of the ordinary tunnel coupling while the other to the photon assisted electron exchanging coupling. The central peak incorporates polarization contributions that will not vanish even under the condition of strong correlation.

We found, in general, that the Rabi splitting in the tunneling photo-current is because of the dynamical couplings of entangled states in the

photo excited material with the LUMO state in the second. Since this higher order correlation is impaired by the non vanishing polarization contribution, the entanglement is, however, only short lived. The results are noted, therefore, pointing out the need for structural tailoring of the interfacing region whenever observing electron and spin entanglement becomes the objective. Coupled silicon nanostructures manufactured with small relative detuning between their LUMO levels and a non transparent interspersing boundary can suit for the purpose. Even though the indirect band gap in bulk silicon has degraded the importance of the material for optical applications, the same is not true for silicon nanostructures. Our results have shown that silicon nanostructures are potential candidates for the realization of a silicon based electron and spin entangler single electron photo transistors.

.

Bibliography

1. L.P.Kouwenhoven, A. T. Johnson, N. C. van der Vaart, C. J. P. M. Harmans and C. T. Foxon, Phys. Rev. Lett. **67** 1626(1991).

2. N. Gisin, G. Ribordy, W. Tittel, and H. Zbinden, Rev. Mod. Phys. **74**, 145(2002).

3. C. W. J. Beenakker, Phys. Rev. B **44**, 1646 (1991).

4. P. Delsing, K. K. Likharev, L. S. Kuzmin and T. Claeson, Phys. Rev.Lett. **63**, 1861, (1989).; X. Hu and S. Das Sarma, Phys. Status Solidi B **238**, 360 (2003)

5. C. H. Patterson, R. P. Messmer. Phys. Rev. B **42** 7530 (1990).

6. C. J. Wang, L. Y. Lin, B. A. Parviz, IEEE Journal of Selected Topics in Quantum Electronics, **11** 2 (2005)

7. L. Pavesi, R. Guardini, Brazilian Journal of Physics, **26** (1), (1996).

8. L. Jacak, P. Hawrylak and A. W´ojs , Quantum Dots (Berlin: Springer), 1998

9. T. V. Buuren, L. N. Dinh, L. L. Chase, W. J. Siekhaus, and L. J. Terminello Phys. Rev. Let. **27** April 1998

10. S. P. Singhal, Phys. Rev. B **4**, 2497 (1971).

11. C. Huang, E. A. Carter, Phys. Rev. B **81**, 045206 (2010)

12. D. M. Lyons, K. M. Ryan , M. A. Morris and J. D. Holmes, Nano Lett., **2**, 811 (2002).

13. O. Bisi, S. Ossicini, and L. Pavesi, Surf. Sci. Reports 38, 1(2000).

14. M. V. Wodkin, J. Jocne, P. M. Francher ; Phys. Rev. Lett. **82** 1(1999)

15. E. Luppi, F. Iori, R. Magri, O. Pulci, S. Ossicini, E. Degoli, V. Olevano, Phys. Rev. B **75**, 033303 (2007).

16. T. Tanaka, J. Singh, Y. Arakawa, and P. Bhattacharya, Appl. Phys. Lett. **62**, 756 (1993).

17. P. C. Sercel and K. J. Vahala, Phys. Rev. **44**, 5681 (1991).

18. K. Leo, T.C. Damen, J. Shah, K. Kohler, Phys. Rev. B **42**, 11359(1990).

19. L. Banyai, D, B. Tran Thoai, R. Remling, H. Haug, Phys. Status Solidi (b) **173**, 149 (1992).

20. I. Ionescu, H. Fan, C. Annesley, J. Xin, and S. A. Reid, J. Chem. Phys.**120**, 1164 (2004).

21. D. A. B. Miller, J. S. Weiner, D. S. Chemla, IEEE J. Quantum electronics, **32**,1816 (1986)

22. B. J. vanWees, H. van Houten, C. W. J. Beenakker, J. G. Williamson, L. P. Kouwenhoven, D. van der Marel, C. T. Foxon, Phys. Rev. Lett. **60**, 848 (1988).

23. D. A. Wharam, T. J. Thornton, R. Newbury, M. Pepper, H. Ahmed, J. E. F. Frost, D. G. Hasko, D. C. Peacock, D. A. Ritchie, G. A. C. Jones, J. Phys. C **21**, L209 (1988);. M. Büttiker, Phys. Rev. B **33**, 3020 (1986).

24. E. Yablonovich, J. Phys. Condens. Matter **5** , 2443 (1993).

25. W. Nakawaski, R.P. Sarzala, M. Wasiak, T. Czyszanowski, P. Maćkowiak Opto-Electronics Review **11** (2), 127 (2003).

26. L.Visscher, T. Saue, W. C. Nieuwpoort, K. Faegri, O. Gropen, J. Chem. Phys, **99** (9), 6704 (1993)

27. D. R. B. Brittain, C. Y. Lin, A. T. B. Gilbert, E. I. Izgorodina, P. M. W. Gill and M. L. Coote, Chem. Phys. **11**, 1138 (2009).

28. E. Hagley and S. Haroche et al., Phys. Rev. Lett. **79**, 1 (1997).

29. S. Hughes, Phys. Rev. Lett 94, 227402 (2005).

30. L. A. Wu, D. A. Lidar and M. Friesen, Phys. Rev. Lett. **93**, 030501 (2004).

31. R. Pollet, A. Savin, T. Leininger, and H. Stoll. J. Chem. Phys. **116**, 1250, (2002).

32. W. Pötz, J. Appl. Phys. **66**, 2458 (1989).

33. W. R. Frensley, Rev. Mod. Phys. **62**, 745(1990).

34. P. Miller and J. K. Freericks, J. Phys.: Condens. Matter **13**, 3187, (2001).

35. L. Catto, C. Le Bris and P.-L. Lions, Mathematical Models and Methods for Ab Initio Quantum Chemistry, Springer, 95-119 (2000).

36. V. Bach, E. H. Lieb, M. Loss, and J. P. Solovej, Phys. Rev. Lett. **72** (19), 2981 (1994).

37. P. Hohenberg , W. Kohn . Inhomogeneous electron gas Phys. Rev. B **136**, 864 (1964).

38. W. Kohn, L. J. Sham, Phys. Rev. A **140**, 1133 (1965).

39. H. Chen and A. Zhou, Numer. Math. Theor. Meth. Appl. **1** (1), 1-28 (2008).

40. J. M. Pèrez-Jordà, E. San-Fabiàn, and F. Moscardò. Phys. Rev. A **45**,

4407, (1992).

41. L. Goodwin , R. J. Needs and V. Heine , J. Phys.: Condens. Matter **2** , 351 (1990).

42. A. T. Karathanos, I. E. Perakis, N.A. Fromer and D. S. Chemla, Phys. Rev.B **67**, 035316 (2003).

43. R. Gebauer and R. Car, Phys. Rev. Lett. **93**, 160404(2004).

44. M. Elhassan, J. P. Bird, R. Akis, D. K. Ferry, T. Ida, and K.Ishibashi, J. Phys. Condens. Matter **17**, L351 (2005).

45. A.T. Karathanos, I.E. Perakis, N.A.Fromer and D.S.Chemla, Phys. Rev. B **67**,035316(2003).

46. J. Shah, Ultrafast spectroscopy of semiconductors and semiconductor nanostructures (Springer, Heidelberg, Germany (1996).

47. V. M. Axt and T. Kuhn,"Femtosecond spectroscopy in semiconductors: a key to coherences, correlations and quantum kinetics," Reports on Progress in Physics **67**, 433-512 (2004).

48. D.-S. Kim, J. Shah, T. C. Damen, W. Schäfer, F. Jahnke, S. Schmitt-Rink, and K. Köhler, Phys. Rev. Lett. **69**, 2725-2728 (1992).

49. Y.-X. Yan, J. Edward B. Gamble, and K. A. Nelson, J. Chem. Phys. **83**, 5391-5399 (1985).

50. I. Knezevic, Phys. Rev. B **77**, 125301 (2008).

51 I. Knezevic and D. K. Ferry, Phys. Rev. A **69**, 012104 (2004).

52. K. K. Thornbur, Solid State Electron. **21**, 259 (1978).

53. R. Brunetti, C. Jacoboni, and F. Rossi, Phys. Rev. B **39**, 10781 (1989).

54. E. Ciancio, R. C. Iotti, and F. Rossi, Phys. Rev. B **69**, 165319(2004).

55. F. Evers, F. Weigend, M. Koentopp, Phys. Rev. B **69**, 235411 (2004).

56. J. Seminario, A. Zacarias and P. Derosa, J. Chem. Phys. **116** (9), 1671 (2002).

57. G. D. Mahan, Phys. Rep. **145**, 251 (1987).

58. S. Datta and M. P. Anantram, Phys. Rev. B **45**, 13761 (1992).

59. D. Mamaluy, D. Vasileska, M. Sabathil, T. Zibold, and P. Vogl, Phys. Rev. B **71**, 245321 (2005).

60. H. Raza, Phys. Rev. B **76**, 045308 (2007).

61. X. Blanc, A mathematical insight into ab initio simulations of solid phase; Lecture notes in chemistry **74** p.p134-158 Springer (2000).

62. S. J. C. Slater, G. F. Koster. 1954 Phys. Rev. **94** 1498-1524 (1954).

63. K. C. Pandey, J. C. Phillips, Solid St. Commun. **14** , 439441 (1974).

64. H. Haug, A. P. Jauho, Quamtum Kinetics in Transport and Optics of Semiconductors. (p157) Springer, Berlin, Germany (1996).

65. J. Rammer, H. Smith, Rev.Mod.Phys **58**,323 (1986).

66. D. C. Langreth, P. Norrlander , Phys. Rev. B **43**, 2541 (1991).

67. V. L. Ligneres and E. A. Carter, Hand Book of Material Modelling, 137-148 (2005) Springer, Netherlands.

68. DA Vanden Bout, J. Kerimo, DA . Higgins, PF. Barbara, J. Phys. Chem. **100**, 11843 (1996).

69. M. V. Wodkin, J. Jocne, P. M. Francher,Phys. Rev. Lett. **82**, 1 (1999).

70. C. J. Garcia-Cervera, An efficient real space method for orbital-free density-functional theory, Commun. Comput. Phys. **2**, 334 (2007).

71. J. P. Perdew, A. Zunger, Phys. Rev. B **45**, 13244 (1992).

72. C. Lee, R. G. Parr, W. Y. Yang, Phys. Rev. B **37**, 785 (1988).

73. E.W. Draeger, J.C. Grossman, A.J. Williamson, and G.Galli, J. Chem. Phys. **22**, 120 (2004).

74. C. Cohen-Tannoudji, B. Diu, and F. Lalo¨e, Quantum Mechanics, vol. **2**, Hermann,Paris, France (1977).

75. A. Einstein, B. Podolsky, and N. Rosen, Phys. Rev. **47**, 777(1935).

76. J. S. Bell, Physics **1**, 195 (1964).

77. S. L. Braunstein, A. Mann, and M. Revzen, Phys. Rev. Lett. **68**, 3259 (1992).

78. X. Hu, arXiv, cond-matt. **1**, 0411012 (2004).

79. D Loss and D P DiVincenzo. Quantum computation with quantum dots. Phy. Rev A, **57**, 120, (1998).

80. G. Burkard, D. Loss and D. P. DiVincenzo, Phy. Rev. B, **59**, 2070, (1999).

81. J. Schliemann, J.I. Cirac, M. Kus, M. Lewenstein, and D. Loss, Phys. Rev. A **64**,022303 (2001).

82. X. Hu and S. Das Sarma, Phys. Rev. A **61**, 062301 (2000).

83. G. Burkard, D. Loss, and E.V. Sukhorukov, Phys. Rev. B **61**, R16303 (2000).

84. C. K. Hong, Z. Y. Ou, and L. Mandel, Phys. Rev. Lett. **59** (18), 2044 (1987).

85. W. Tittel, J. Brendel, H. Zbinden, and N. Gisin, Phys. Rev. Lett. **81**, 3563 (1998).

86. J. Schliemann, D. Loss, and A. H. MacDonald, Phys. Rev. B **63**, 085311 (2001).

87. C. H. Bennett, G. Brassard, C. Cr´epeau, R. Jozsa, A. Peres, and W. K. Wootters, Phys.Rev. Lett. **70**, 1895 (1993).

88. I. Devetak, A. W. Harrow, and A. Winter, Phys. Rev. Lett. **93**, 230504, (2004).

89. D. Mozyrsky, V. Privman, and M.L. Glasser,Phys. Rev. Lett. **86**, 5112 (2001).

90. A.J. Skinner, M.E. Davenport, and B.E. Kane, Phys. Rev. Lett. **90**, 087901 (2003).

91. D. B. Tran Thoai, H. Haug, Phys. Rev. B **47**, 3574 (1993).

92. M. Brune, F. Schmidt-Kaler, A. Maali , J. Dreyer, E. Hagley, J.M. Raimond and S. Haroche, Phys. Rev. Lett.**76**, 1800 (1996).

93. S. Hughes, Phys. Rev. Lett. **81**, 3363 (1998).

94. O.D. Mucke, T. Tritschler, M. Wegener, U. Morgner, and F. X. Kartner," Phys. Rev. Lett. **87**, 057401 (2001).

95. N. C. Kluksdaki, A. M. Kriman, D. K. Ferry, C. Ringhofer, Phys. Rev. B **39**, 7720 (1989).

96. W. R. Frensley, Phys. Rev. B **36**, 1570 (1987).

97. H. Haug a.¬P. Jauho, Quantum Kinetics in Transport and Optics of Semiconductors, Springer, P.P 261-275, (1996).

98. E.T. Jaynes and F.W. Cummings Proc. IEEE 51, 89−109 (1963)

99. G. Lindblad, Commun. Math. Phys. **48**, 199 (1976)

100. B.W. Shore, P.L. Knight, J. Mod. Optics **40**, 1195 (1993).

101. M. Brune, F. Schmidt-Kaler, A. Maali, J. Dreyer, E. Hagley, J.M. Raimond and S. Haroche, Phys. Rev. Lett.**76**, 1800(1996).

102. W. A. Al-Saidi and D. Stroud, Phys. Rev. B **65**, 014512 (2001)

103. T. H. Stievater, X. Q. Li, D. G. Steel, D. Gammon, D. S. Katzer, D. Park, C. Piermarocchi, and L. J. Sham,Phys. Rev. Lett. **87**, 133603 (2001).

104. H. Kamada, H. Gotoh, J. Temmyo, T. Takagahara, and H. Ando, Phys. Rev. Lett. **87**, 246401 (2001).

105. H. Htoon, T. Takagahara, D. Kulik, O. Baklenov, A. L. Holmes, and C. K. Shih, Phys. Rev. Lett. **88**, 087401 (2002).

106. T. Unold, K. Mueller, C. Lienau, T. Elsaesser, and A. D. Wieck, Phys. Rev. Lett. **94**, 137404 (2005).

107. G. Rempe , F. Schmidt-Kaler and H. Walther, Phys. Rev. Lett. **64** 2783 (1990).

108. P. Elmfors , B. Lautrup and B-S Skagerstam, Phys. Rev. A **54**, 5171 (1996).

109. H-J. Briegel, B-G. Englert, N. Sterpi and H. Walther, Phys. Rev. A **49**, 2962 (1994).

110. G. Rempe and H. Walther, Phys. Rev. A **42**, 1650 (1990).

111. M. Orszag, Quantum optics, Springer-verlag, pp 269-290 (2000).

112. M. Sherwin , A. Imamoglu and T. Montrag Phys. Rev. A **60** 3508−14 (1999).

113. E Peter, P Senellart, D Martrou, A Lemaître, J Hours, J M Gérard and J Bloch, Phys Rev Lett **95**, 67401 (2005).

114. N L Thomas, U. Woggon, O. Schöps, M.V. Artemyev, M. Kazes and U. Banin, Nano Lett. **6**, 557 (2006).

115. A. M. Chang, H. U. Baranger, L. N. Pfeiffer, K. W. West, and T. Y. Chang, Phys. Rev. Lett. **76**, 1695 (1996).

116. H. Wang, M. Hofheinz, M. Ansmann, R. C. Bialczak, E. Lucero, M. Neeley, A. D. O'Connell, D. Sank, J. Wenner, A. N. Cleland, and J. M. Martinis, Phys. Rev. Lett. **101**, 240401 (2008).

117. J. Aghassi, A. Thielmann, M. H. Hettler, and G. Schon, Phys. Rev. B **73**, 195323 (2006).

118. T. B. Traran, I. S. Beloborodov, X. M. Lin, T. P. Bigioni, V. M. Vinokur, And H. M. Jaeger, Phys. Rev. Lett. **95**, 076806 (2005).

119. W. Rudzi¶nski, Acta Physica Polonica, **115** (2009)

120. C. Niu, L. Liu, Phys. Rev. B 51, 5130 (1995).

121. W. Rudzi¶nski, J. Barna¶s, R. ¶Swirkowicz, M. Wilczy¶nski, Phys. Rev. B **71**, 205307 (2005).

122. Yan Chen, Z. D. Wang, Y. Q. Li and F. C. Zhang, Phys. Rev. B **75**, 195113 (2007).

123. T. Unold, K. Mueller, C. Lienau, T. Elsaesser, and A. D. Wieck, Phys. Rev. Lett. **94**, 137404 (2005).

124. J. Danckwerts and K. J. Ahn, J. Fˆrstner, and A. Knorr, Phys. Rev. B **73**, 165318 (2006).

125. C.A. Stafford and N.S. Wingreen, Phys. Rev. Lett. **76**, 1916 (1996).

126. T. H. Stoof and Yu. V. Nazarov, Phys. Rev. B **53**, 1050 (1996).

127. M. Holthaus and D. Hone, Phys. Rev. B **47**, 6499 (1993).

128. Y. Zhang, J. P. Hu, B. A. Bernevig, X. R. Wang, X. C. Xie, and W. M. Liu,Phys. R ev. B **78**, 155413(2008).

129. E. Leobandung, L. Guo, Y. Wang and S. Y. Chou, Appl. Phys. Lett. **67** 938 (1995).

130. S. Möller, H. Buhmann, S. F. Godijn, and L.W. Molenkamp, Phys. Rev. Lett. **81**, 5197 (1998).

131. C. H. Cho, B. H. Kim, and S. J. Park, Appl. Phys. Lett. **89**, 013116 (2006).

132. J. Park, A. N. Pasupathy, J. I. Goldsmith, C. Chang, Y. Yaish, J. R. Petta, M. Rinkoski, J. P. Sethna, H. D. Abruña, P. L. McEuen & D. C. Ralph Nature **417**, 722 (2002).

133. P. Delsing, K. K. Likharev, L. S. Kuzmin and T. Claeson: Phys. Rev.Lett. **63**, 1861(1989).

134. L. J. Geerligs, V. F. Anderegg, P. A. M. Holweg, J. E. Mooij, H.Pothier, D. Esteve, C. Urbina and M. H. Devoret: Phys. Rev. Lett. **64**, 2691 (1990).

135. C. Santori, M. Pelton, G. Solomon, Y. Dale, and Y. Yamamoto, Phys. Rev.Lett. **86**, 1502 (2001).

136. E. Moreau, I. Robert, L. Manin, V. Thierry-Mieg, J. M. Ge´rard, and L. Abram, Phys. Rev. Lett. **87**, 183601 (2001).

137. Z. Yuan, B. E. Kardynal, R. M. Stevenson, A. J. Shields, C. J. Lobo, K. Cooper, N. S. Beattie, D. A. Ritchie, and M. Pepper, Science **295**, 102 (2002).

138. A. Zrenner, E. Beham, S. Stufler, F. Findeis, M. Bichler, and B. Abstreiter, Nature **418**, 612 (2002).

139. E. Beham, A. Zrenner, F. Findeis, M. Bichler, and G. Abstreiter, Appl. phys. Lett. **79**, 2808 (2001).

140. Claudia Sifel and Ulrich Hohenester , Appl. Phys. Lett. **83**, 153 (2003).

141. X. Hu and S. Das Sarma, arXiv:cond-mat **2**, 0307024 (2004).

142. Y. Tomishima and K.Yonei, J. Phys. Soc. Jpn. **21**, 142 (1996).

143. H. Chen and A. Zhou Numer, Orbital-Free Density Functional Theory for Molecular Structure calculations, Math. Theor. Meth. Appl. **1**, 1 (2008).

144. K Seino, F Bechstedt and P Kroll, Nanotechnology **20** , 135702, (2009).

145. P.Carrier, Phys. Rev. B **80**, 075319 (2009).

146. J.Williamson, J. C. Grossman, R. Q. Hood, A. Puzder and G. Galli, Phys. Rev.Lett. **89**, 196803 (2002).

147. W.M. Itano, D.J. Heizen, J.J. Bollinger, D.J. Wineland, Phys. Rev.A **41**, 2295 (1990).

148. L. Tian, H. J. Carmichael, Phys.Rev.A **46**,6801(1992).

149. M.Ueda, N.Imoto, H.Nagaoka, T.Ogawa, Phys. Rev. A **46**, 2859 (1992).

150. G.C. Hegerfeldt, Phys. Rev. A **47**, 449 (1993).

151. J. Dalibard, Y. Castin, and K. Mølmer, Phys. Lett. **68**, 580 (1992).

A

Appendix

A. The equal Time Limit Correlation Function

The equations of motion for the equal time limit correlation function $G^{<}_{\alpha\beta}(t,t)$ given by eq.5.5 to describe the coherent regime absorption in a nano structure is

$$[\frac{\partial}{\partial t}+\frac{i}{\hbar}\{\varepsilon_{\alpha}-\varepsilon_{\beta}\}]G^{<}_{\alpha\beta}(t,t)=-\frac{i}{\hbar}\sum_{m}\ [\Sigma^{S}_{\alpha m}(t)G^{<}_{m\beta}(t,t)-G^{<}_{\alpha m}(t,t)\Sigma^{S}_{m\beta}(t)] \quad \text{A1}$$

When the singular self energy terms are substituted by the corresponding expressions in eq.6.2 and eq.6.3, the equation of motion for the non diagonal, in energy basis, lesser Green functions will be in the form

$$\frac{\partial}{\partial t}G^{<}_{VjC}(t,t)=\frac{i}{\hbar}[\varepsilon_{C}(t)-\varepsilon_{V_j}(t)]G^{<}_{VjC}(t,t)$$
$$+\frac{i}{\hbar}[G^{<}_{VjVj}(t,t)\Sigma^{S}_{VjC}(t)-\Sigma^{S}_{VjC}(t)G^{<}_{CC}(t,t)]-\frac{\partial}{\partial t}\Gamma^{<}_{VjC}(t,t) \quad \text{A2}$$

$$\frac{\partial}{\partial t}G^{<}_{CVj}(t,t)=-\frac{i}{\hbar}[\varepsilon_{C}(t)-\varepsilon_{V_j}(t)]G^{<}_{CVj}(t,t)$$
$$-\frac{i}{\hbar}[\Sigma^{S}_{CVj}(t)G^{<}_{VjVj}(t,t)-G^{<}_{CC}(t,t)\Sigma^{S}_{CVj}(t)]-\frac{\partial}{\partial t}\Gamma^{<}_{CVj}(t,t) \quad \text{A3}$$

Similarly the diagonal lesser Green functions could be obtained as

$$\frac{\partial}{\partial t} G^{<}_{VjVj}(t,t) = -\frac{i}{\hbar}[\Sigma^{S}_{VjC}(t,t)G^{<}_{CVj}(t,t) - G^{<}_{VjC}(t,t)\Sigma^{<}_{CVj}(t,t)] - \frac{\partial}{\partial t}\Gamma^{<}_{VjVj} \quad \text{A4}$$

$$\frac{\partial}{\partial t} G^{<}_{CC}(t,t) = -\frac{i}{\hbar}[\Sigma^{<}_{CVj}(t,t)G^{<}_{VjC}(t,t) - G^{<}_{CVj}(t,t)\Sigma^{<}_{VjC}(t,t)] - \frac{\partial}{\partial t}\Gamma^{<}_{CC} \quad \text{A5}$$

$$\varepsilon_{C}(r,t) = \varepsilon^{o}_{C}(r) + \Sigma^{S}_{CC}(r.t) \quad \text{A6.1}$$

$$\varepsilon_{Vj}(r,t) = \varepsilon^{o}_{Vj}(r) + \Sigma^{S}_{VjVJ}(r.t) \quad \text{A6.2}$$

Where the diagonal self energy components are given as

$$\Sigma^{S}_{ClCl}(r,t) = V_{eff}(r,t)\rho_{Cl}(r,t) \quad \text{A7.1}$$

$$\Sigma^{S}_{VjVJ}(r,t) = V_{eff}(r,t)\rho_{Vj}(r,t) \quad \text{A7.2}$$

If we use the Jaynes-Cummings model to represent the radiation field, we find on the other hand the off-diagonal self energy terms taking the form

$$\Sigma^{S}_{\alpha n}(t) = -[\frac{1}{2} dE_{0}(t)(\hat{b}e^{-i(\omega t+\phi)} + \hat{b}^{\dagger}e^{i(\omega t+\phi)}) + V_{eff}\hat{a}^{\dagger}_{\alpha}(t)\hat{a}_{n}(t)](1-\delta_{\alpha n}) \quad \text{A8.1}$$

If we make the rotating wave approximation, this turns out to be reduced to the form

$$\Sigma^{S}_{\alpha n}(t) = -e^{i(\omega t+\varphi)}[\frac{1}{2} dE_{0}(t)\hat{b}^{\dagger} + V_{eff}\hat{a}^{\dagger}_{\alpha}(t)\hat{a}_{n}(t)e^{-i(\omega t+\varphi)}](1-\delta_{\alpha n}) \quad \text{A8.2}$$

$$\Sigma^{S}_{\alpha n}(t) = -e^{i(\omega t+\phi)}\Omega^{\dagger}_{\alpha n}(1-\delta_{\alpha n}) \quad \text{A8.3}$$

Where

$$\Omega_R^{\dagger}(t) = [\frac{1}{2} dE_0(t)\hat{b}^{\dagger} + V_{eff}\rho_{\alpha n}(t)] \qquad \text{A8.4}$$

Similarly, one could easily show that

$$\Sigma_{n\alpha}^{S}(t) = -\Omega_R(t)e^{-i(\omega t+\varphi)}(1-\delta_{n\alpha}) \qquad \text{A8.5}$$

With,

$$\Omega_R(t) = [\frac{1}{2} dE_0(t)\hat{b} + V_{eff}\rho_{n\alpha}(t)] \qquad \text{A8.6}$$

The diagonal and off-diagonal self energy matrix components go in renormalizing the levels and the field respectively. Considering the equations for the non-diagonal components,

$$G_{VjC}^{<}(t,t) = \frac{i}{\hbar}\int_o^t dt' e^{\frac{i}{\hbar}\int_{t'}^{t} dt[\varepsilon_C(t)-\varepsilon_{Vj}(t)]}[G_{VjVj}^{<}(t',t')\Sigma_{VjC}^{s}(t') - \Sigma_{VjC}^{s}(t')G_{CC}^{<}(t',t')] \quad \text{A9}$$

$$G_{CVj}^{<}(t,t) = -\frac{i}{\hbar}\int_o^t dt' e^{-\frac{i}{\hbar}\int_{t'}^{t} dt[\varepsilon_C(t)-\varepsilon_{Vj}(t)]}[\Sigma_{CVj}^{s}(t')G_{VjVj}^{<}(t',t') - G_{CC}^{<}(t',t')\Sigma_{CVj}^{s}(t')] \quad \text{A10}$$

$$\Sigma_{VjC}^{s}(t)G_{CVj}^{<}(t,t) = -\frac{i}{\hbar}\int_o^t dt' e^{-\frac{i}{\hbar}\int_{t'}^{t} dt[\varepsilon_C(t)-\varepsilon_{Vj}(t)]}[\Sigma_{VjC}^{s}(t)\Sigma_{CVj}^{s}(t')G_{VjVj}^{<}(t',t') - \Sigma_{VjC}^{s}(t)G_{CC}^{<}(t',t')\Sigma_{CVj}^{s}(t')] \qquad \text{A11.1}$$

$$G_{VjC}^{<}(t,t)\Sigma_{CVj}^{s}(t) = \frac{i}{\hbar}\int_o^t dt' e^{\frac{i}{\hbar}\int_{t'}^{t} dt[\varepsilon_C(t)-\varepsilon_{Vj}(t)]}[G_{VjVj}^{<}(t',t')\Sigma_{VjC}^{s}(t')\Sigma_{CVj}^{s}(t) - \Sigma_{VjC}^{s}(t')G_{CC}^{<}(t',t')\Sigma_{CVj}^{s}(t)] \qquad \text{A11.2}$$

Upon substituting the expressions in equations A8 and A11 in to eqs.A4 and A5 we respectively find

$$\frac{\partial}{\partial t}G^{<}_{VjVj}(t,t) = -\frac{1}{\hbar^2}\int_o^t dt'\Big[e^{-\frac{i}{\hbar}\int_{t'}^{t} d\bar{t}\Delta_{\varepsilon}(\bar{t})}\Omega^{\dagger}_R(t)\Omega_R(t')G^{<}_{VjVj}(t',t')$$
$$+ e^{\frac{i}{\hbar}\int_{t'}^{t} d\bar{t}\Delta_{\varepsilon}(\bar{t})}G^{<}_{VjV\bar{j}}(t',t')\Omega^{\dagger}_R(t')\Omega_R(t)$$
$$- e^{-\frac{i}{\hbar}\int_{t'}^{t} d\bar{t}\Delta_{\varepsilon}(\bar{t})}\Omega^{\dagger}_R(t)G^{<}_{CC}(t',t')\Omega_R(t') \qquad \text{A12}$$
$$- e^{\frac{i}{\hbar}\int_{t'}^{t} d\bar{t}\Delta_{\varepsilon}(\bar{t})}\Omega^{\dagger}_R(t')G^{<}_{CC}(t',t')\Omega_R(t)\Big]$$

Where,

$$\Delta_{\varepsilon}(t) = \varepsilon_C(t) - \varepsilon_{Vj}(t) - \hbar\omega \qquad \text{A13}$$

$$\frac{\partial}{\partial t}G^{<}_{VjVj}(t,t) = \frac{i}{\hbar\Delta(t)}\{[\Omega^{\dagger}_R(t)\Omega_R(t)G^{<}_{VjVj}(t,t) - G^{<}_{VjVj}(t,t)\Omega^{\dagger}_R(t)\Omega_R(t)]$$

$$+[\Omega^{\dagger}_R(t)G^{<}_{C\ell C\ell}(t,t)\Omega_R(t) - \Omega^{\dagger}_R(t)G^{<}_{C\ell C\ell}(t,t)\Omega_R(t)]\}$$

$$-\frac{i}{\hbar\Delta(t_o)}\{[G^{<}_{VjVj}(t_o,t_o)\Omega^{\dagger}_R(t_o) + \Omega^{\dagger}_R(t_o)G^{<}_{C\ell C\ell}(t_o,t_o)]\Omega_R(t)e^{\frac{i}{\hbar}\int_{t_o}^{t} d\bar{t}\Delta(\bar{t})}$$

$$-\Omega^{\dagger}_R(t)[\Omega_R(t_o)G^{<}_{VjVj}(t_o,t_o) + G^{<}_{C\ell C\ell}(t_o,t_o)\Omega_R(t_o)]e^{-\frac{i}{\hbar}\int_{t_o}^{t} d\bar{t}\Delta(\bar{t})}\} \qquad \text{A14}$$

The first term in this equation could be noticed having a structure of a commutation relation. The second term on the other hand vanishes. The remaining two terms are still requiring some care. In developing the equation we considered the radiation-atom system to be modeled as correlated system. In reality the system requires finite time to be dynamically correlated. To make the problem more simplified without endangering this information from being washed out in the approximation, we shift the lower limit of the integral to this characteristic time τ_c and evaluate the integral with the lower limit at $\tau_c - \varsigma$ where ς is close to zero

such that $\Omega_R(\tau_c - \varsigma) = \Omega_R(\tau_c)$ and $G^<_{VjVj}(\tau_c - \varsigma, \tau_c - \varsigma) = G^<_{VjVj}(\tau_c, \tau_c)$ in the limit of small values of the parameter ς. This leads equation A14 to be in the form

$$\frac{\partial}{\partial t} G^<_{VjVj}(t,t) = \frac{i}{\hbar\Delta(t)} \{[\Omega^\dagger_R(t)\Omega_R(t) G^<_{VjVj}(t,t) - G^<_{VjVj}(t,t)\Omega^\dagger_R(t)\Omega_R(t)] \qquad \text{A15}$$

$$\frac{d}{dt} G^<_{VjVj}(t,t) = \frac{i}{\hbar}[\frac{\Omega^\dagger_R(t)\Omega_R(t)}{\Delta(t)}, G^<_{VjVj}(t,t)] \qquad \text{A16}$$

Using the defining relation for the lesser Green function this could also be written as the equation of motion for the occupation probability at state Vj. The resulting equation is in the Lindblad form;

$$\frac{d}{dt}\rho_{Vj}(t) = \hat{L}\rho_{Vj}(t) \qquad \text{A17}$$

This equation has a formal solution in the form

$$\rho_{Vj}(t) = \rho_{Vj}(t_c) exp\{\int_{t_c}^{t} \hat{L}(\bar{t})d\bar{t}\} \qquad \text{A18}$$

$$\rho_{Vj}(t) = \rho_{Vj}(\tau_c) exp\{\frac{i}{\hbar}\int_{\tau_c}^{t} d\bar{t}\ \frac{\Omega^\dagger_R(t)\Omega_R(t)}{\Delta(t)}\} \qquad \text{A19}$$

Because of the fluctuations in the atomic levels of the specimen under a short exciting radiation pulse, the range of integration of the integral at the exponent of the term in the right hand side of this equation may include points of singularities. This may call the use of pole approximation technique. As the observation time become larger but still within the coherent temporal regime, the number of poles within the integration range may increase. The diagram in Fig.A1 illustrates the contour for integration at over the time domain that incorporates three singularities. The poles are located on the real axis and all to the right of the origin. When evaluated

for each case, the radius of the corresponding unit circle, in the upper half plane could be considered to extend to infinity. The residue determined at each pole, which is surrounded by the small circle gives the Lorenzian term.

Each characteristic time τ_ℓ is the time at which the detuning comes to vanish;

$$\Delta_\varepsilon(\tau_\ell) = 0 \qquad \text{A20}$$

This is when

$$\varepsilon_C^o - \varepsilon_V^o - \omega + \Sigma_{CC}^S(\tau_\ell) - \Sigma_{VV}^S(\tau_\ell) = 0 \qquad \text{A21}$$

$$\varepsilon_C^o - \varepsilon_V^o - \omega = \rho_V(\tau_\ell)V_{eff}(\tau_\ell) - \rho_C(\tau_\ell)V_{eff}(\tau_\ell) \qquad \text{A22}$$

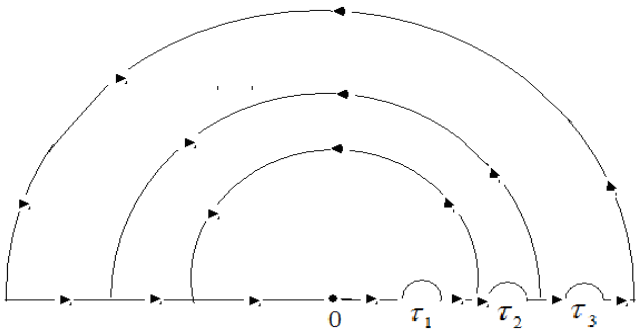

Fig. A1: *Contour for pole approximation at multiple discrete poles*

In making the calculation we assumed the detuning in the neighborhood of the singularity be expanded in Taylor's series as

$$\Delta_\varepsilon(t) = \Delta_\varepsilon(\tau_\ell) + (t-\tau_\ell)\dot{\Delta}_\varepsilon(\tau_\ell) + \tfrac{1}{2}(t-\tau_\ell)^2\ddot{\Delta}_\varepsilon(\tau_\ell) + \ldots \qquad \text{A23}$$

Where, the dot over the term representing the detuning shows the order of the differentiation. Recalling that $\Delta_{\varepsilon}(\tau_{\ell}) = 0$, the series could be approximated, to the first order, by

$$\Delta_{\varepsilon}(t) \cong (t - \tau_{\ell})\dot{\Delta}_{\varepsilon}(\tau_{\ell}) \qquad \text{A24}$$

Since the observation time may cover the range that goes over a number of singularity points, the integral will in general contain the sum of the values determined at each pole and the principal integral;

$$\begin{aligned}\rho_{Vj}(t) &= e^{\frac{i}{\hbar}\int_{\tau_c}^{t} d\bar{t}\frac{\Omega_R^{\dagger}(t)\Omega_R(t)}{\Delta_{\varepsilon}(t)}}\rho_{Vj}(\tau_C) \\ &= e^{\frac{i}{\hbar}P\int_{\tau_c}^{t} d\bar{t}\frac{\Omega_R^{\dagger}(t)\Omega_R(t)}{\Delta_{\varepsilon}(t)}} e^{-\frac{\pi}{\hbar}\sum_{\ell}\frac{\Omega_R^{\dagger}(t)\Omega_R(t)}{\dot{\Delta}_{\varepsilon}(t)}\delta(t-\tau_{\ell})}\rho_{Vj}(\tau_C)\end{aligned} \qquad \text{A25}$$

Clearly the Lorenzian has contribution that goes to the amplitude term. Each time the system approach to the near resonance condition, the Lorenzian term makes a contribution that goes to renormalize the amplitude. The Principal integral, on the other hand, has the contribution that to be associated with the frequency shift. For the temporal regime close to the resonance that corresponds to the divergence of the expression at the first singularity, we therefore have

$$\rho_{Vj}(t = \tau_1 + t') = \rho_{Vj}(\tau_C)[e^{\frac{i}{\hbar}\{\int_{\tau_c}^{\tau_1 - x} d\bar{t}\frac{\Omega_R^{\dagger}(t)\Omega_R(t)}{\Delta_{\varepsilon}(t)} + \int_{\tau_1 + x}^{t} d\bar{t}\frac{\Omega_R^{\dagger}(t)\Omega_R(t)}{\Delta_{\varepsilon}(t)}\}}]e^{-\frac{\pi}{\hbar}\frac{\Omega_R^{\dagger}(\tau_1)\Omega_R(\tau_1)}{\Delta_{\varepsilon}(\tau_1)}} \qquad \text{A26}$$

Where the integral at the exponents are evaluated in the limit of small x; $x \to 0$. Evaluating the term under the square bracketin eq.A26 using the method that led to eq.B10 leadsto

$$\rho_{Vj}(t=\tau_1+t')=\mathrm{Re}\{\rho_{Vj}(\tau_c)e^{i[\omega_R^1(t-\tau_1)]-\frac{\pi}{\hbar}\frac{\Omega_R^{\dagger}(\tau_1)\Omega_R(\tau_1)}{\dot{\Delta}_{\varepsilon}(\tau_1)}}\} \quad \text{A27}$$

Where, $\boldsymbol{\omega_R^1}$ is the oscillation frequency which is determind from the integral in eq.A26 using the result in eq.B9.

$$\boldsymbol{\omega_R^1}=\left\langle\frac{\boldsymbol{\Omega_R^{\dagger}(\tau^1)\Omega_R(\tau^1)}}{\boldsymbol{2\hbar\Delta_{\varepsilon}(\tau^1)}}\right\rangle \quad \text{A28}$$

Where, $2\tau^1<\tau_2-\tau_1$ is the period over which the frequency is averaged and $\phi_1=\omega_R^c(\tau_1-\tau_c)$. Similarly, for an observation that includes the second and third singularities respectively we get

$$\rho_{Vj}(t=\tau_2+t')=\mathrm{Re}\{\rho_{Vj}(\tau_c)e^{i[\omega_R^2(t-\tau_2)+\phi_2]-\frac{\pi}{\hbar}\{\frac{\Omega_R^{\dagger}(\tau_1)\Omega_R(\tau_1)}{\dot{\Delta}_{\varepsilon}(\tau_1)}+\frac{\Omega_R^{\dagger}(\tau_2)\Omega_R(\tau_2)}{\dot{\Delta}_{\varepsilon}(\tau_2)}\}}\} \quad \text{A29}$$

and

$$\rho_{Vj}(t=\tau_3+t')=\mathrm{Re}\{\rho_{Vj}(\tau_c)e^{i[\omega_R^3(t-\tau_3)+\phi_3]-\frac{\pi}{\hbar}\{\frac{\Omega_R^{\dagger}(\tau_1)\Omega_R(\tau_1)}{\dot{\Delta}_{\varepsilon}(\tau_1)}+\frac{\Omega_R^{\dagger}(\tau_2)\Omega_R(\tau_2)}{\dot{\Delta}_{\varepsilon}(\tau_2)}+\frac{\Omega_R^{\dagger}(\tau_3)\Omega_R(\tau_3)}{\dot{\Delta}_{\varepsilon}(\tau_3)}\}}\} \quad \text{A30}$$

(Where, $\phi(\tau_2)=\phi_1+\phi_2$, $\phi(\tau_3)=\phi_1+\phi_2+\phi_3$)

The amplitude renormalization terms can also be written as a product of the contribution at each singularity. In fact, the exponents in these terms involve operator functions. When the operators involved are operators the commutator of which commutes with either; [A,[A,B]]= [B,[A,B]], the operator functions could be transformed using the Nakker-Cambell-Hausdorf relation [137];

$$e^{\chi(\hat{A}+\hat{B})} = e^{\chi\hat{B}} e^{\chi\hat{A}} e^{\frac{1}{2}\chi^2[\hat{A},\hat{B}]} \quad \text{A31}$$

In a special case when $\hat{A}$ and $\hat{B}$ commutes, this reduces to

$$e^{\chi(\hat{A}+\hat{B})} = e^{\chi\hat{B}} e^{\chi\hat{A}} \quad \text{A32}$$

Similarly,

$$e^{\chi[\hat{A}+\hat{B}+\hat{C}]} = e^{\chi\hat{C}} e^{\chi\hat{B}} e^{\chi\hat{A}} e^{(\frac{1}{2}\chi^2)\{[\hat{A},\hat{C}]+[\hat{B},\hat{C}]} e^{(\frac{1}{2}\chi^2)[\hat{A},\hat{B}]} \quad \text{A33}$$

For three operators that commute with each other,

$$e^{\chi[\hat{A}+\hat{B}+\hat{C}]} = e^{\chi\hat{C}} e^{\chi\hat{B}} e^{\chi\hat{A}} \quad \text{A34}$$

Accordingly,

$$e^{-\frac{\pi}{\hbar}[\frac{\Omega_R^\dagger(\tau_1)\Omega_R(\tau_1)}{\Delta_\varepsilon(\tau_1)}+\frac{\Omega_R^\dagger(\tau_2)\Omega_R(\tau_2)}{\Delta_\varepsilon(\tau_2)}]} = e^{-\frac{1}{\hbar}[\frac{\Omega_R^\dagger(\tau_2)\Omega_R(\tau_2)}{\Delta_\varepsilon(\tau_2)}]} e^{-\frac{1}{\hbar}[\frac{\Omega_R^\dagger(\tau_1)\Omega_R(\tau_1)}{\Delta_\varepsilon(\tau_1)}]} \times e^{-\frac{\pi^2}{2\hbar^2\Delta_\varepsilon(\tau_2)\Delta_\varepsilon(\tau_1)}[\hat{N}(\tau_1),\hat{N}(\tau_2)]} \quad \text{A35}$$

Where, the operator $\hat{N}$, here represents, photon number operator of the radiation field. In the temporal regime of the coherent absorption, the influence of the inter-band polarization is very small as compared to the action of the radiation field and hence the operator Ω_R could be considered to represent the action of the radiation field;

$$\hat{N}(\tau_i) = \Omega_R^\dagger(\tau_i)\Omega_R(\tau_i) \quad \text{A36}$$

Thus, the procedures followed in arriving to eq.A32 and eq.A33 can be used to put eqs. A28 −A29 and similarly expressions involving contributions from more singularity points.

B

Appendix

B. *Dyson series Expansion*

The exponential function to be approximated using the Dyson's series expansion is in the form

$$I = e^{\frac{i}{\hbar}\int_{t'}^{t} d\bar{t}\beta_{\ell,m}(\bar{t})} \qquad B1$$

With,

$$\beta_{\ell,m}(t) = -\left(e\rho_{\ell}(t)V_{XC,\ell}(t) - e\rho_{m}(t)V_{XC,m}(t)\right) \qquad B2$$

Proceeding on expanding this function,

$$e^{\frac{i}{\hbar}\int_{t'}^{t} d\bar{t}\beta_{\ell,m}(\bar{t})} = 1 + T\{\sum_{n=1}^{\infty} (\tfrac{i}{\hbar})^{n} \tfrac{1}{n!}\int_{t'}^{t} dt_1\beta_{\ell,m}(t_1)\int_{t'}^{t} dt_2\beta_{\ell,m}(t_2)....\int_{t'}^{t} dt_n\beta_{\ell,m}(t_n)\} \qquad B3$$

$$\begin{aligned} e^{\frac{i}{\hbar}\int_{t'}^{t} d\bar{t}\beta_{\ell,m}(\bar{t})} &= 1 + (\tfrac{i}{\hbar})^{1} T\{\int_{t'}^{t} dt_1\beta_{\ell,m}(t_1)\} + (\tfrac{i}{\hbar})^{2} \tfrac{1}{2!} T\{\int_{t'}^{t} dt_1\beta_{\ell,m}(t_1)\int_{t'}^{t} dt_2\beta_{\ell,m}(t_2)\} \\ &\quad + T\{\sum_{n=3}^{\infty} (\tfrac{i}{\hbar})^{n} \tfrac{1}{n!}\int_{t'}^{t} dt_1\beta_{\ell,m}(t_1)\int_{t'}^{t} dt_2\beta_{\ell,m}(t_2)....\int_{t'}^{t} dt_n\beta_{\ell,m}(t_n)\} \end{aligned} \qquad B4$$

Taking only up to second order,

$$e^{\frac{i}{\hbar}\int_{t'}^{t} d\bar{t}\beta_{\ell,m}(\bar{t})} = 1 + (\tfrac{i}{\hbar})\int_{t'}^{t} dt_1 \beta_{\ell,m}(t_1) + (\tfrac{i}{\hbar})^2 \tfrac{1}{2!} T\{\int_{t'}^{t} dt_1 \beta_{\ell,m}(t_1) \int_{t'}^{t} dt_2 \beta_{\ell,m}(t_2)\} \quad \text{B5}$$

Considering now the average of eq.B5,

$$< \exp(\tfrac{i}{\hbar}\int_{t'}^{t} d\bar{t}\beta_{\ell,m}(\bar{t})) > = 1 + (\tfrac{i}{\hbar})\int_{t'}^{t} dt_1 < \beta_{\ell,m}(t_1) >$$

$$+ (\tfrac{i}{\hbar})^2 \tfrac{1}{2!} < T\{\int_{t'}^{t} dt_1 \beta_{\ell,m}(t_1) \int_{t'}^{t} dt_2 \beta_{\ell,m}(t_2)\} > \quad \text{B6}$$

Case1

$$\left\langle \beta_{\ell,m}(t_1)\beta_{\ell,m}(t_2) \right\rangle = 0 \quad \text{B7}$$

$$< \exp(\tfrac{i}{\hbar}\int_{t'}^{t} d\bar{t}\beta_{\ell,m}(\bar{t})) > = 1 + \tfrac{i}{\hbar}\int_{t-\tau}^{t} dt_1 \left\langle \beta_{\ell,m}(t_1) \right\rangle \quad \text{B8}$$

$$< e^{\frac{i}{\hbar}\int_{t'}^{t} d\bar{t}\beta_{\ell,m}(\bar{t})} > = e^{\frac{i}{2\hbar}\left\langle \beta_{\ell,m}(\tau) \right\rangle \tau} \quad \text{B9}$$

$$\left\langle \beta_{\ell,m}(\tau) \right\rangle = \frac{1}{\tau}\int_{t-\tau}^{t+\tau} d\bar{t}\beta_{\ell,m}(\bar{t}) \quad \text{B10}$$

Case2

$$\left\langle \beta_{\ell,m}(t_1) \right\rangle = 0 \quad \text{B11a}$$

$$\left\langle \beta_{\ell,m}(t_1)\beta_{\ell,m}(t_2) \right\rangle = \left\langle \beta_{\ell,m}(t_1)\beta_{\ell,m}(t_1) \right\rangle \delta(t_1 - t_2) \quad \text{B11b}$$

$$< \exp(\frac{i}{\hbar}\int_{t'}^{t} d\bar{t}\beta_{\ell,m}(\bar{t})) >= 1 + (\frac{i}{\hbar})^2 \frac{1}{2!} < T\{\int_{t'}^{t} dt_1 \beta_{\ell,m}(t_1)\int_{t'}^{t} dt_2 \beta_{\ell,m}(t_2)\} > \quad \text{B12}$$

The integral term from the right hand side is evaluated giving

$$\begin{aligned} T\{\int_{t'}^{t} dt_1 \beta_{\ell,m}(t_1)\int_{t'}^{t} dt_2 \beta_{\ell,m}(t_2)\} &= \int_{t'}^{t} dt_1 \int_{t'}^{t_1} dt_2 T\{\beta_{\ell,m}(t_1)\beta_{\ell,m}(t_2)\} \\ &+ \int_{t'}^{t} dt_2 \int_{t'}^{t_2} dt_1 T\{\beta_{\ell,m}(t_1)\beta_{\ell,m}(t_2)\} \\ &= 2\int_{t'}^{t} dt_1 \int_{t'}^{t_1} dt_2 \beta_{\ell,m}(t_1)\beta_{\ell,m}(t_2) \end{aligned} \quad \text{B13}$$

$$< \exp[\frac{i}{\hbar}\int_{t'}^{t} d\bar{t}\beta_{l,m}(\bar{t})] >= 1 + 2(\frac{i}{\hbar})^2 \int_{t-\tau_c}^{t} dt_1 \int_{t-\tau_c}^{t} dt_2 \left\langle \beta_{l,m}(t_1)\beta_{l,m}(t_1)\right\rangle \delta(t_1 - t_2) \quad \text{B14}$$

$$< \exp[\frac{i}{\hbar}\int_{t'}^{t} d\bar{t}\beta_{\ell,m}(\bar{t})] >= 1 + 2(\frac{i}{\hbar})^2 \int_{t-\tau_c}^{t} dt_1 \left\langle \beta_{\ell,m}(t_1)\beta_{\ell,m}(t_1)\right\rangle \int_{t-\tau_c}^{t} dt_2 \frac{Sin\omega(t_1 - t_2)}{\pi\omega} \quad \text{B15}$$

$$< \exp[\frac{i}{\hbar}\int_{t'}^{t} d\bar{t}\beta_{\ell,m}(\bar{t})] >= 1 + 2(\frac{i}{\hbar})^2 \left\langle \beta_{\ell,m}(\tau_c)\beta_{\ell,m}(\tau_c)\right\rangle \frac{1}{\pi}\int_{-\infty}^{\infty} d\omega \frac{[1 - Cos\omega\tau_c]}{\omega^2} \quad \text{B16}$$

But,

$$\frac{1}{\pi}\int_{-\infty}^{\infty} dx \frac{[1 - Cosx]}{x^2} = 1 \quad \text{B17}$$

This leads eq.B.12 to be written as

$$< \exp[\frac{i}{\hbar}\int_{t'}^{t} d\bar{t}\beta_{\ell,m}(\bar{t})] >= e^{-\frac{2}{\hbar^2}\left\langle \beta_{\ell,m}(\tau_c)\beta_{\ell,m}(\tau_c)\right\rangle \tau_c} \quad \text{B18}$$

C

Appendix C

C. The Pole Approximation

The purpose here is to compute the integral of the form

$$I = \int_{o}^{t} d\tau e^{\frac{i}{\hbar}[\Delta_{\alpha n} + \langle \beta_{\alpha n}^{\sigma\sigma} \rangle]\tau} V_{\alpha,n}^{\sigma\sigma}(t) V_{\alpha n}^{*\sigma\sigma}(t-\tau)[n_{\alpha\sigma}(t-\tau) - n_{n\sigma}(t-\tau)] \qquad \text{C1}$$

The integral represents a term appearing in the current density expression in chapter 7. By introducing a term that decays exponentially as τ exceeds t, we can stretch the upper limit of the integral to infinity. After making this approximation, we then find

$$I = \int_{-\infty}^{\infty} \frac{d\omega_1}{2\pi} \int_{-\infty}^{\infty} d\tau e^{\frac{i}{\hbar}[\Delta_{\alpha n} + \langle \beta_{\alpha n}^{\sigma\sigma} \rangle]\tau} \frac{e^{i\omega_1[t-\tau]}}{[\omega_1 - i\eta]} \{V_{\alpha,n}^{\sigma\sigma}(t) V_{\alpha n}^{*\sigma\sigma}(t-\tau)[n_{\alpha\sigma}(t-\tau) - n_{n\sigma}(t-\tau)]\} \qquad \text{C2}$$

$$I = \int_{-\infty}^{\infty} \frac{d\omega_1}{2\pi} \frac{e^{i\omega_1 t}}{\omega_1 - \frac{1}{\hbar}[\Delta_{\alpha n} + \langle \beta_{\alpha n}^{\sigma\sigma} \rangle] - i\eta} V_{\alpha,n}^{\sigma\sigma}(t) V_{\alpha n}^{*\sigma\sigma}(\omega_1)[n_{\alpha\sigma} - n_{n\sigma}] \qquad \text{C3}$$

Of course, this last equation could also be evaluated upon using pole approximation. Taking now the Fourier transform of the integral in eq.C3 we find that

$$\Im(I) = \int_{-\infty}^{\infty} d\omega \int_{-\infty}^{\infty} \frac{d\omega_1}{2\pi} \frac{e^{-i(\omega-\omega_1)t}}{\omega_1 - \frac{1}{\hbar}[\Delta_{\alpha n} + \langle \beta_{\alpha n}^{\sigma\sigma} \rangle] - i\eta} V_{\alpha,n}^{\sigma\sigma}(t) V_{\alpha n}^{*\sigma\sigma}(\omega_1)[n_{\alpha\sigma}(\omega_1) - n_{n\sigma}(\omega_1)] \qquad \text{C4}$$

$$\Im(I) = \int_{-\infty}^{\infty} d\omega_1 \frac{\delta(\omega-\omega_1)}{\omega_1-\frac{1}{\hbar}[\Delta_{\alpha n}+\left\langle \beta_{\alpha n}^{\sigma\sigma} \right\rangle]-i\eta} V_{\alpha,n}^{\sigma\sigma}(\omega) V_{\alpha n}^{*\sigma\sigma}(\omega_1)[n_{\alpha\sigma}(\omega_1) - n_{n\sigma}(\omega_1)] \quad \text{C5}$$

$$I(\omega) = \frac{[n_{\alpha\sigma}(\omega)-n_{n\sigma}(\omega)]}{\omega-\frac{1}{\hbar}[\Delta_{\alpha n}+\left\langle \beta_{\alpha n}^{\sigma\sigma} \right\rangle]} V_{\alpha n}^{\sigma\sigma}(\omega) V_{\alpha n}^{*\sigma\sigma}(\omega) \quad \text{C6}$$

D

Appendix D

D. Solving for the Equal Time Limit Value of the Two Time Correlation Function.

The Dyson's equation for the two time correlation function, in the primed time coordinate is

$$[\frac{d}{dt} - \frac{i}{\hbar}(\varepsilon_m(t) - \varepsilon_\beta(t))]G^<_{\beta,m}(t,t) = -\frac{i}{\hbar}\Sigma^S_{\beta,m}(t)[G^<_{m,m}(t,t) - G^<_{\beta,\beta}(t,t)] - \frac{i}{\hbar}[\Sigma^S_{\beta,\ell}(t)G^<_{\ell m}(t,t) - G^<_{\beta,\ell}(t,t)\Sigma^S_{\ell m}(t)] \quad \text{D1}$$

Denoting respectively the upper filled levels and the lower empty level in the first material by $|V_j\rangle$ and $|c\rangle$, and the lower empty level in the second material by $|\alpha\rangle$ the corresponding equations of motion for the lesser Green functions representing the equal time limit correlations between these states could be constructed . The solutions determined for the off-diagonal, in energy basis, lesser Green functions from direct integrations of the equations of motion are

$$G^<_{V_J,\alpha}(t,t) = -\frac{i}{\hbar}\int_o^t dt' e^{\frac{i}{\hbar}\int_{t'}^{t} d\bar{t}(\varepsilon_\alpha(\bar{t}) - \varepsilon_{V_J}(\bar{t}))} \{\Sigma^S_{V_J,\alpha}(t')[G^<_{\alpha\alpha}(t',t') - G^<_{V_J,V_J}(t',t')] + [\Sigma^S_{V_J,c}(t')G^<_{c\alpha}(t',t') - G^<_{V_J,c}(t',t')\Sigma^S_{c\alpha}(t')]\} \quad \text{D2a}$$

$$G^{<}_{C,\alpha}(t,t) = -\frac{i}{\hbar}\int_{o}^{t} dt' e^{-\frac{i}{\hbar}\int_{t'}^{t} d\bar{t}(\varepsilon_c(\bar{t})-\varepsilon_\alpha(\bar{t}))} \{\Sigma^{S}_{c,\alpha}(t')[G^{<}_{\alpha\alpha}(t',t') - G^{<}_{c,c}(t',t')] + [\Sigma^{S}_{C,V_j}(t')G^{<}_{V_j\alpha}(t',t') - G^{<}_{CV_j}(t',t')\Sigma^{S}_{V_j\alpha}(t')]\} \quad \text{D2b}$$

$$G^{<}_{V_J,C}(t,t) = \frac{i}{\hbar}\int_{o}^{t} dt' e^{\frac{i}{\hbar}\int_{t'}^{t} d\bar{t}(\varepsilon_c(\bar{t})-\varepsilon_{V_J}(\bar{t}))} \{\Sigma^{S}_{V_J,C}(t')[G^{<}_{V_J,V_J}(t',t') - G^{<}_{C,C}(t',t')] + [G^{<}_{V_J,\alpha}(t',t')\Sigma^{S}_{\alpha,c}(t') - \Sigma^{S}_{V_J,\alpha}(t')G^{<}_{\alpha,C}(t',t')]\} \quad \text{D2c}$$

Where, the off-diagonal singular self energy matrix components $\Sigma^{S}_{c,\alpha}(t)$ and $\Sigma^{S}_{\alpha,c}(t)$ are Hermitian conjugate pairs representing the tunnel coupling between electrons at the excited states $|\alpha\rangle$ and $|c\rangle$in the two material regions. The other pairs are representing the couplings between the upper filled level in the material under direct radiation and the excited state in that same material, $\Sigma^{S}_{V_J,c}(t)$ and $\Sigma^{S}_{c,V_J}(t)$, and the excited state in the second material region $\Sigma^{S}_{V_J,\alpha}(t)$ and $\Sigma^{S}_{\alpha,V_J}(t)$. The inter-band state couplings are of course related with the modified Rabi oscillation, modified by the inter-band polarizations, as explained in chapter5. The coupling corresponding to the excitation of electron to the state $|C\rangle$ and hence the annihilation of photon at the transition frequency ω_{CV_j} is

$$\Sigma^{S}_{C,V_J}(t) = -\Omega_R(\omega_{cV},t)e^{-i[\omega_{CV}t+\varphi(t)]} \quad \text{D3}$$

Similarly the coupling to the excited state $|\alpha\rangle$ in the second material involving the annihilation of photon at the frequency $\omega_{\alpha V_j}$ is

$$\Sigma^{S}_{\alpha,V_J}(t) = -\Omega_R(\omega_{\alpha V}, t)e^{-i[\omega_{\alpha Vj}t+\varphi(t)]} \qquad \text{D4}$$

The integral equations in eq.D2, here too, are difficult to solve. We proceed in iterating for the expressions we require to develop the current density expression; $G^{<}_{C,\alpha}$ and $G^{<}_{V_J,\alpha}$. This is made until we found expressions that could be conveniently approximated based on physical reasons. When the expressions for $G^{<}_{C,\alpha}$ and $G^{<}_{V_J,C}$ from eq.D2b and eq.D2c are substituted in to eq.D2a, it gives

$$\begin{aligned}\left[\frac{\partial}{\partial t'} - \frac{i}{\hbar}\varepsilon_\alpha(r',t')\right]G^{<}_{n\alpha}(r,t;r',t') &= \frac{i}{\hbar}\delta(r-r')\delta(t-t') \\ &+ \frac{i}{\hbar}\sum_{m\neq\alpha}\int_{-\infty}^{t} d\bar{t}\,G^{r}_{nm}(r,t;r',\bar{t})\Sigma^{<}_{m\alpha}(r',\bar{t};r',t') \\ &+ \int_{-\infty}^{t} d\bar{t}\,G^{<}_{nm}(r,t;r',\bar{t})\Sigma^{a}_{m\alpha}(r',\bar{t};r',t')\end{aligned} \qquad \text{D5}$$

Since $\delta(r-r')=0$ for coupled atomic states in the two material regions, the equation reduces to the form

$$\begin{aligned}\left[\frac{\partial}{\partial t'} - \frac{i}{\hbar}\varepsilon_\alpha(t')\right]G^{<}_{n\alpha}(t,t') = +\frac{i}{\hbar}\sum_{m\neq\alpha}\{&\int_{-\infty}^{t} d\bar{t}\,G^{r}_{nm}(t,\bar{t})\Sigma^{<}_{m\alpha}(\bar{t},t') \\ &+ \int_{-\infty}^{t'} d\bar{t}\,G^{<}_{nm}(t,\bar{t})\Sigma^{a}_{m\alpha}(\bar{t},t')\}\end{aligned} \qquad \text{D6}$$

It could recalled from chapter 6 that

$$\Sigma^{a}_{m\alpha}(\bar{t},t') = \theta(t'-\bar{t})[\Sigma^{<}_{m\alpha}(\bar{t},t') - \Sigma^{>}_{m\alpha}(\bar{t},t')]$$

$$= \frac{1}{2}\Sigma^{S}_{m\alpha}(\bar{t})\delta(\bar{t}-t') + \bar{\theta}(t'-\bar{t})[\Sigma^{<}_{m\alpha}(\bar{t},t') - \Sigma^{>}_{m\alpha}(\bar{t},t')] \qquad \text{D7}$$

$$\bar{\theta}(t'-\bar{t}) = \begin{cases} 1, t' > \bar{t} \\ 0, t' \le \bar{t} \end{cases} \qquad \text{D8}$$

$$[\frac{\partial}{\partial t'} - \frac{i}{\hbar}\varepsilon_{\alpha}(t')]G^{<}_{n\alpha}(t,t') = \frac{i}{2\hbar}\sum_{m\neq\alpha}\{G^{<}_{nm}(t,t')\Sigma^{S}_{m\alpha}(t') + \Gamma_{n\alpha}(t,t') \qquad \text{D9}$$

Where, the term $\Gamma_{n\alpha}$ in eq.D9 is to represent the scattering contributions. We shall to notice also that all the non singular self energies are absorbed in this term.

For the coherent regime response we neglect the scattering effects since assumed very small. Solving eq.D9 based on this simplifying approximation finally results

$$G^{<}_{n\alpha}(t,t') = \frac{i}{2\hbar}\sum_{m\neq\alpha}\int_{t_o}^{t'} dt_1 e^{\frac{i}{\hbar}\int_{t_1}^{t'} d\bar{t}\,\varepsilon_{\alpha}(\bar{t})} G^{<}_{nm}(t,t_1)\Sigma^{s}_{m\alpha}(t_1) \qquad \text{D10}$$

The equal time limit correlation function $G^{<}_{n\alpha}(t,t)$ is then determined from eq.D10 by taking the limiting case as t' approaches t from the positive side;

$$G^{<}_{n\alpha}(t,t) = \lim_{t'\to t^{+}}\left(G^{<}_{n\alpha}(t,t')\right)$$

$$= \frac{i}{\hbar}\sum_{m\neq\alpha}\int_{t_o}^{t} dt_1 e^{\frac{i}{\hbar}\int_{t_1}^{t} d\bar{t}\,\varepsilon_{\alpha}(\bar{t})} G^{<}_{nm}(t,t_1)\Sigma^{s}_{m\alpha}(t_1) \qquad \text{D11}$$

The two time correlation function under the summation could be decoupled in to the equal time limit value and the retardation by using the Kadanoff-Bayem anstaz [58]

$$G^{<}_{nm}(t,t_1) = i\hbar\sum_{s}\left[G^{r}_{ns}(t,t_1)G^{<}_{sm}(t_1,t_1) - G^{<}_{ns}(t,t)G^{a}_{sm}(t,t_1)\right] \qquad \text{D12}$$

Substituting this expression for the off-diagonal, in time, correlation function in eq.D11 and using the fact that $G^{a}_{sm}(t,t_1) = 0$ for $t_1 < t$ one easily obtains

$$G^{<}_{n\alpha}(t,t) = -\frac{1}{2}\sum_{m,s\neq\alpha}\int_{t_o}^{t} dt_1 e^{\frac{i}{\hbar}\int_{t_1}^{t} d\bar{t}\,\varepsilon_{\alpha}(\bar{t})} G^{r}_{ns}(t,t_1)G^{<}_{sm}(t_1,t_1)\Sigma^{S}_{m\alpha}(t_1) \qquad \text{D13}$$

I hereby declare that this PhD dissertation is my original work and has not been presented for a degree in any other University and that all the sources of material used for the thesis have been duly acknowledged.

Name: Mekonnen Abebe

Signature: _____

This PhD dissertation has been submitted for examination with my approval as University advisor.

Name: Prof. P. Singh

Signature: _____

Place and date of submission:

Department of physics

Addis Ababa University

April 2011